ATMOSPHERIC PROCESSING OF AEROSOLS AT A SITE IN RURAL CANADA

by

Maheswar Rupakheti

submitted in partial fulfillment of the requirements
for the degree of Doctor of Philosophy

at

Dalhousie University
Halifax, Nova Scotia
April 2006

Your file Votre référence
ISBN: 978-0-494-19607-6
Our file Notre référence
ISBN: 978-0-494-19607-6

DALHOUSIE UNIVERSITY

To comply with the Canadian Privacy Act the National Library of Canada has requested that the following pages be removed from this copy of the thesis:

Preliminary Pages
- Examiners Signature Page (pii)
- Dalhousie Library Copyright Agreement (piii)

Appendices
- Copyright Releases (if applicable)

TABLE OF CONTENTS

LIST OF FIGURES

LIST OF TABLES

ABSTRACT

Aerosol physical properties and chemical composition and concurrently measured gas-phase species and meteorological data at a rural site in Egbert, about 70 km to the north of Toronto in southern Ontario, in the spring of 2003, were analyzed to gain insights into the properties of rural aerosols and the processes governing their changes. The properties of rural aerosol were compared with the same of urban aerosol measured at Toronto. The intercomparisons among co-located aerosol instruments showed reasonable agreement, given the upper cut-off size of different instruments were considered. Aerosol chemical composition measured with the aerosol mass spectrometer revealed that exceptionally high nitrate mass concentrations were observed at Egbert, and the organic material contributed, on average, the highest fraction to aerosol mass for the sampling period. The ammonium, nitrate, sulfate and the organics at both sites had a mass modal vacuum aerodynamic diameters around 400-500 nm, however, a small organic mass mode at 100-200 nm was occasionally observed at Egbert, when the site was exposed to fresh urban air masses. Organic material dominated the composition of urban aerosol. The total organic material had two modes centered at 400 nm and 150 nm, with a significant amount of organic mass in the small mode. At both sites, the small organic modes were composed of mainly hydrocarbon-like substances, indicating that the combustion related emissions were the likely sources of small organic particles, whereas the larger mode organic particles were composed of mainly oxygenated materials. The nitrate mass concentrations averaged diurnally exhibited higher values during dark hours and a minimum in the afternoon, whereas sulfate and the oxygenated organics were highest during the afternoon period, indicative of photochemical processing. Total organics in the aerosol from the north showed a gradual increase with increasing temperature, likely associated with increasing biogenic emissions. The oxygenated organic fraction increased rapidly within 48 hours of photochemical age, after which there was little change, while the mass of sulfate increased continuously with time, suggesting that the condensation of sulfates onto organic particles impeded the increase in oxygenated organic fraction. Thus, within 1-2 day of photochemical age, the ability of these particles to act as cloud condensation nuclei (CCN) is controlled by inorganic species such as sulfates.

LIST OF ABBREVIATIONS AND SYMBOLS

Acronyms

AAAR	American Association for Aerosol Research
AMS	Aerosol Mass Spectrometer
APS	Aerodynamic Particle Sizer
BWP	Beam Width Probe
CARE	Centre for Atmospheric Research Experiments
DMA	Differential Mobility Analyzer
GC-FID	Gas Chromatograph - Flame Ionization Detection
CE	Collection Efficiency (of the AMS)
CCN	Cloud Condensation Nucleus (Nuclei)
HOA	Hydrocarbon-like Organic Aerosol
IE	Ionization Efficiency
IPCC	Intergovernmental Panel on Climate Change
MS	Mass Spectrum (Spectra)
NMHC(s)	Non Methane Hydrocarbon Compound(s)
NR	Non-refractory
OOA	Oxygenated Organic Aerosol
PILS-IC	Particle-into-Liquid Sampler –Ion Chromatograph
$PM_{2.5}$ (PM_{10})	Particulate Mass of Particles with $D_a < 2.5$ μm (10 μm)
PSC	Polar Stratospheric Clouds
R&P	Rupprecht and Patashnick Incorporated
SMPS	Scanning Mobility Particle Sizer
TEOM	Tapered Element Oscillating Microbalance
ToF	Time-of-flight
TSI	Thermo System Incorporated
UCPC	Ultrafine Condensation Particle Counter
USEPA	United States Environment Protection Agency

Symbols/Units

amu	Atomic Mass Unit
D_a	Aerodynamic Diameter
D_m	Mobility Equivalent Diameter
D_p	Particle Physical Diameter
D_v	Volume Equivalent Diameter
D_{va}	Vacuum Aerodynamic Diameter
$g\ cm^{-3}$	gram per cubic centimeter
HNO_3	Nitric acid
m/z	mass-to-charge ratio
$\mu g\ m^{-3}$	microgram per cubic meter
μm	micrometer or micron (= 10^{-6} m)
NH_3	Ammonia
NH_4NO_3	Ammonium nitrate
nm	nanometer (= 10^{-9} m)
NO	Nitric oxide
NO_2	Nitrogen dioxide
NO_x	Nitrogen oxides ($NO+NO_2$)
N_2O_5	Dinitrogen pentoxide
O_3	Ozone
ppbv	part per billion by volume
SO_2	Sulfur dioxide
χ	Dynamic Shape Factor

ACKNOWLEDGEMENTS

I am greatly indebted to Prof. Ulrike Lohmann for supervising this research, continuous guidance, many stimulating thoughts and fruitful discussions, regardless of location and time, whether she was at Dalhousie University or at the Institute for Atmospheric and Climate Science, Swiss Federal Institute of Technology (ETH), Zurich, Switzerland. I would like to thank her for the support and the opportunity to carry out this interesting research project. I am thankful to the thesis examination committee members, Dr. W. Richard Leaitch of the Meteorological Service of Canada, Toronto, and Dr. Randall V. Martin of Department of Physics and Atmospheric Science, Dalhousie University and the external examiner, Prof. James Sloan from the University of Waterloo.

This work would not have been possible without cooperation and assistance of many people, in particular those who provided invaluable data and important suggestion during various stages of this study. Katherine Hayden, Dr. Peter Brickell, Dr. Desiree Toom-Sauntry, Dr. Jan W. Bottenheim, Gang Lu, Dr. Shao-Meng Li and Dr. Jeffrey R. Brook from the Meteorological Service of Canada, Environment Canada, Downsview, Ontario provided vital data and fruitful discussions. I am thankful to Drs. Douglas R. Worsnop and John T. Jayne of the Aerodyne Research Incorporated, Massachusetts, USA for the technical and scientific discussion on Aerosol Mass Spectrometer (AMS) and the analysis of the AMS measurements. Many thanks to Dr. Glen Lesins, Lisa Phenny, Dr. Junhua Zhang, Dr. Yiran Peng, Dr. Abdus Salam, Dr. Moses Iziomon, Betty Carlin, Dr. Julia Marshall, Pamela Lehr, Yanjie Cheng at the Department of Physics and Atmospheric Science. I am thankful to the staffs at the department, including Ann E. Murphy, Anne M. Jeferry, Barbara Guvin and Melissa MacDougall who provided enormous assistance. Thanks to Dr. James Allan at the University of Manchester Institute of Science and Technology (UMIST), UK for the AMS data analysis software.

I express my special thanks to Dr. W. Richard Leaitch, who has been a huge source of valuable data, pertinent suggestion and discussion during the entire study. He extended kind support to me during my visits to Egbert and Toronto. He put in enormous critical editorial effort on the manuscripts.

Dalhousie University provided the Dalhousie Graduate Fellowship to pursue PhD in Atmospheric Science. This work was partially supported by the Multiscale Air Quality Network (MAQNet) funded by the Canadian Foundation for Climate and Atmospheric Sciences (CFCAS). I acknowledge their support.

My mother and other family members have always been a constant source of inspiration and support to me. I heartily appreciate their support and love. I acknowledge and thank Nanu Thapa, my wife, who sacrificed hundreds of hours we could have shared together. I thank her for her love, support, encouragement and sacrifice.

Chapter 1

Introduction

1.1 Atmospheric Aerosols

Atmospheric aerosols are airborne solid and liquid particles that range in size from a few nanometers to tens of micrometers in diameter [*Baron and Willeke, 2001; Seinfeld and Pandis, 1998*]. Aerosol particles are abundant and ubiquitous in the atmosphere. They originate from diverse natural processes (e.g., weathering, sea spray, volcanoes, biogenic emissions and forest fires) and human activities (e.g., fossil fuel combustion, industrial manufacturing, construction works and biomass burning). The particles can be emitted directly from the sources (primary particles) or formed in the atmosphere *via* gas-to-particle conversion processes (secondary particles) involving gaseous precursors such as sulfur dioxide or nitrogen oxides or volatile organic compounds (VOCs) [*Finlayson-Pitts and Pitts, 2000; Seinfeld and Pandis, 1998*]. Gaseous species may condense onto existing particles, thereby increasing the mass of particles, or gases may nucleate to form new particles. Atmospheric aerosols are remarkably diverse in number, mass, size and chemical composition between locations (e.g., urban, rural, marine, desert, stratosphere) and times, reflecting the wide range of particle sources. The ambient particles can contain inorganic material such as sulfate, ammonium, nitrate, sodium, chloride, crustal elements, trace metals, water and carbonaceous material (organic compounds and elemental carbon) [*Finlayson-Pitts and Pitts, 2000; IPCC, 2001*].

In the atmosphere, aerosol particles are processed in a number of ways: condensation of gas-phase species with low vapor pressure on the pre-existing particles, coagulation with other particles, chemical reactions, activation to form fog and cloud droplets, or act as ice nuclei, thereby modifying their size and chemical composition [*Seinfeld and Pandis, 1998*]. Particles are eventually removed from the atmosphere *via* two routes: dry

deposition (gravitational settling and impaction on the surfaces) and wet deposition (incorporated into cloud droplets and rain out or wash out). The residence time of the tropospheric aerosols is relatively short, a few days to a few weeks, while the stratospheric particles can have a lifetime of several years [*Seinfeld and Pandis, 1998*].

Atmospheric aerosols have received increased attention over the past two decades as there is a growing body of evidence that they significantly influence many important phenomena, such as air quality degradation, visibility reduction, acid rain, atmospheric heterogeneous chemistry, the Earth's radiation budget, cloud properties, hydrological cycle, and regional and global climate change [*Ackerman et al., 2000; Albrecht, 1989; Andreae, 2001; Charlson et al., 1992; Hansen et al., 1997; Lohmann and Feichter, 2005; Ramanathan et al., 2001; Ravishankara, 1997*], as well as alleged association with adverse health effects [*e.g., Schwartz., 1993*]. Because of increase in anthropogenic emissions of aerosols and precursor gases that lead to formation of particles in the air, atmospheric aerosol loadings have undoubtedly increased since the pre-industrial era, and the anthropogenic aerosols have been implicated in many areas ranging from human health to climate change [*IPCC, 2001*].

1.2 Aerosol Size and Chemical Composition

Aerosol particles are classified generally into four groups (modes) based on their size: nucleation mode (diameter, $D_p < 0.01$ μm), Aitken mode ($0.01 < D_p < 0.1$ μm), accumulation mode ($0.1 < D_p < 1$ μm) and coarse mode ($D_p > 1$ μm) [*Baron and Willeke, 2001; Seinfeld and Pandis, 1998*]. One should note that the exact classification of particles as a function of size can vary depending on the instrumentation employed to measure particles as different instruments use different measurement principles and techniques. Particles smaller than 0.01 μm (i.e., 10 nm) are often referred to as ultrafine particles, smaller than 1 μm as fine particles, and larger than 1 μm as coarse particles. For the ambient air quality monitoring purpose, two commonly used terms are PM_{10} and $PM_{2.5}$, which refer to the bulk particulate mass concentrations of particles with diameters < 10 μm, and < 2.5 μm, respectively.

New particles are created through clustering (i.e., nucleation) of certain gas molecules such as sulfuric acid and water [e.g., *Kulmala, 2003*]. Nucleation mode particles are short-lived (~ minutes) as they grow rapidly to larger sizes by condensation of gases with a low-vapor pressure and by coagulation with other particles. Aitken particles arise from the growth of nucleation particles formed in the air, and sometimes they are primary particles (e.g., vehicular emissions). Their lifetime is short as they grow to accumulation mode particles by condensation of gaseous species or by coagulation. The other sources for accumulation mode particles are direct emissions from the incomplete combustion of fuels. Because of the processes governing their formation, much of the mass in this mode is contributed by the secondary components: some non-volatile species such as ammonium sulfate and certain organics and semivolatile species such as ammonium nitrate and some organics partitioned from the gas-phase [*Seinfeld and Pandis, 1998*]. As the bulk of surface area is contained in this mode, accumulation mode particles are most significant for condensation of gas-phase species and heterogeneous chemistry [*Finlayson-Pitts and Pitts, 2000; Seinfeld and Pandis, 1998*]. Because the slower random motion of larger particles reduces the coagulation rate with other aerosol particles or with hydrometeors, and because accumulation mode particles are too small to sediment at a significant rate, the removal by wet and dry deposition is least efficient in this mode, causing these particles to accumulate more than other sizes [*Seinfeld and Pandis, 1998*]. As the accumulation mode particles are made up of a significant amount of water-soluble species such as ammonium sulfate and ammonium nitrate, they act as efficient cloud condensation nuclei (CCN), and hence they are important for climate effect [*Finlayson-Pitts and Pitts, 2000; Seinfeld and Pandis, 1998*]. They are ultimately removed from the atmosphere mainly by scavenging by cloud droplets and subsequent rainout or direct wash out by raindrops. The nucleation and Aitken mode particles account for the majority of atmospheric particle numbers, but due to their small size, they account for only a small faction of the total mass. Mechanical processes (e.g. wind blown dust, bubble burst in the ocean, agricultural and construction activities) produce coarse particles. Biogenic particles such as pollen, spores and bacteria also contribute to the coarse mode. Their atmospheric residence times are reasonably short as they are more readily removed by dry deposition.

1.3 Aerosol Effects on Human Health

The ambient particulate matter is a significant health hazard at the high concentrations found in urban and industrial environments [*e.g., Dockery et al., 1993*]. In recent years, numerous studies epidemiological studies reported the associations between ambient PM_{10} and a significant increase in a range of respiratory symptoms and cardiovascular diseases and daily deaths respiratory conditions [*Dockery et al., 1993; Pope et al., 2002; Schwartz, 1994*]. *Schwartz et al. [1996]* reported an increase of 1.5% in total daily deaths for each 10 $\mu g\ m^{-3}$ increase in PM_{10} exposure. The fine particles ($D_a < 2.5\ \mu m$), also known as respirable particles, are potent to much greater danger of any adverse health effect as they can penetrate deeper into human lungs [*Donaldson et al., 1998; Schwartz et al., 1996*]. The USEPA (United States Environment Protection Agency) promulgated the first-ever standards for $PM_{2.5}$ in 1997 in order to consider the fine particles [*Finlayson-Pitts and Pitts, 2000*]. With the primary aim of assessing the ambient air quality, $PM_{2.5}$ mass concentrations are routinely monitored in many countries.

The PM_{10} or $PM_{2.5}$ or size-fractionated mass concentrations [*Dockery et al., 1993; Dreher et al., 1996; Pope et al., 2002*], number concentrations [*Donaldson et al., 1998; Penttinen et al., 2001*], surface area [*Moshammer and Neuberger, 2003; Zimmer, 2002*], and chemical composition [*Neuberger et al., 2004; Thurston et al., 1996*] have all been linked with adverse health effects. However, what makes fine particles toxic – whether it's the size, or number, or mass, or composition, or combination thereof, or a mixture of particles with gaseous pollutants - is still largely inconclusive [*Davidson et al., 2005; Harrison and Yin, 2000; Peters et al., 1997*].

1.4 Aerosol Effects on Atmosphere and Climate

The most noticeable effects of ambient particles are air quality deterioration and visibility reduction during the obnoxious smog events in big cities. Atmospheric particles provide sites for surface chemistry and heterogeneous reactions that can have a major impact on the gaseous and condensed-phase composition of the troposphere and stratosphere [*Jacob, 2000; Molina, 1991; Martin et al., 2003; Ravishankara, 1997*]. For example, stratospheric aerosols in the form of polar stratospheric clouds (PSC) as well as sulfate

aerosols from volcanic eruptions are pivotal in the catalytic destruction of ozone by facilitating the conversion of chlorine compounds from relatively unreactive to reactive forms [*Solomon et al., 1986; Solomon et al., 1993*].

Atmospheric aerosols affect the earth's radiation budget directly through scattering of solar radiation back to space and absorption of solar radiation that consequently reduce the amount of energy reaching the surface (cooling or negative radiative forcing) [*Charlson et al., 1992; Chýlek et al., 1995*]. The global mean direct radiative forcing is estimated to be -0.4 W m^{-2} for sulfate aerosols, -0.2 W m^{-2} for biomass burning aerosols, -0.1 W m^{-2} for fossil fuel organic carbon, +0.2 W m^{-2} for fossil fuel black carbon, and in the range -0.6 to +0.4 W m^{-2} for mineral dust aerosols [*IPCC, 2001*]. Indirectly, aerosol particles capable of acting as CCN modify the cloud microphysical properties and cloud lifetime (negative radiative forcing). For a given amount of cloud liquid water content, an increase in aerosol number concentrations leads to more but smaller cloud droplets that will in turn enhance the cloud albedo (first indirect effect) [*Twomey, 1974; Twomey et al., 1991*], and also prolong the cloud lifetime as the cloud droplets are less likely to coalesce into raindrops (second indirect effect) [*Albrecht, 1989*]. In addition, aerosols that absorb solar radiation (e.g. black carbon) warm the atmosphere locally. This may result in either evaporation of cloud or inhibit cloud formation in the clear region, reducing local cloud cover, and thus yielding a net warming (semi-direct effect) [*Hansen et al., 1997*]. In a recent review of aerosol indirect effects, *Lohmann and Feichter [2005]* summarize that climate model estimates of radiative perturbations at the top of atmosphere (TOA) ranges from -0.5 to -1.9 W m^{-2} due to first indirect effect, from -0.3 to -1.4 W m^{-2} due to second indirect effect, and from +0.1 to -0.5 W m^{-2} for the semi-direct effect. It is suggested that the atmospheric aerosols counteract the warming effects of increasing anthropogenic greenhouse gases by an uncertain, but potentially large, amount [*IPCC, 2001*; *Andreae et al., 2005*].

The consequence of increases in atmospheric aerosol burden is that it can influence cloud formation and abundance, suppress rainfall or snowfall downwind of the polluted regions and change the hydrological cycle [*Ackerman et al., 2000; Andreae, 2001; Lohmann et*

al., 2000; Lohmann and Feichter, 1997; Lohmann and Feichter, 2005; Peng et al., 2002; Ramanathan et al., 2001; Rosenfeld, 2000]. The optical properties and hence the radiative forcing of atmospheric aerosols are functions of aerosol chemical composition, size, shape and mixing states [*Lesins et al., 2002*]. Despite the recent substantial growth in knowledge on the importance of aerosols to climate, the uncertainties in the estimation of aerosol radiative forcing are significantly large at present because of inadequate knowledge on aerosol sources, anthropogenic contributions, mechanistic understanding of aerosol physiochemical properties, the processes that govern their formation, and the potential impacts [*IPCC 2001*].

1.5 Atmospheric Organic Aerosols

Organic material contributes a significant fraction (~10-90%) to the ambient fine particulate mass in urban, rural, remote or marine environments [*Andreae and Crutzen, 1997; Middlebrook et al., 1998; Randles et al., 2004; Saxena and Hildemann, 1996*]. A substantial fraction (~50-80%) of particulate organics is water soluble [*Decesari et al. 2000; Zappoli et al. 1999*]. Unlike inorganic constituents, the organic material in atmospheric particles is a complex mixture of many different organic compounds, both natural and anthropogenic, with a wide range of chemical and thermodynamic properties, for example, hydrophobic and hydrophilic compounds with a varying degree of solubility [*Murphy, 2005; Seinfeld and Pandis, 1998*]. In polluted environments, nitrogen oxides (NO_x), gas-phase volatile organic compounds (VOCs), and possibly particulate organics that provide surfaces for heterogeneous reactions significantly control O_3 chemistry, and thus influence air quality and chemical composition of atmosphere [*Martin et al., 2003; Seinfeld and Pandis, 1998*]. It is known more recently that organic aerosols have the potential to play an important, yet a poorly understood, role in climate.

Organic material may be internally mixed with inorganics in the particles. Internally mixed organic compounds may enhance or inhibit the hygroscopic growth of particles, which is determined by the available mass and solubility of organics in the particles, thereby altering the ability of particles to act as cloud condensation nuclei (CCN) [*Novakov and Penner, 1993; Saxena et al., 1995; Shulman et al., 1996*]. Surface-active

organics lower surface tension and thus affect aerosol activation, while slightly soluble organics (e.g., adipic acid) can lower surface tension, alter bulk hygroscopicity and delay the particle growth by gradual dissolution [*Abdul-Razzak and Ghan, 2005; Facchini et al., 1999; Lohmann et al., 2004; Randles et al., 2004; Shantz et al., 2003*]. The oxygenation of particulate organic material changes the chemical composition and physical properties of the particles, in particular oxidation increases the water solubility thereby making organic aerosols more active as CCN [e.g., *Saxena et al., 1995; Kotzick and Niessner, 1999*]. Recent observational studies combined with the Lagrangian air parcel models have shown that organic aerosols can increase the number of cloud droplets [*Decesari et al., 2003; Facchini et al., 1999; Lohmann and Leck, 2005; O'Dowd et al., 2004*]. Measurements made downwind of the Indian sub-continent, Eastern Asia, and northeastern U.S. showed that the increasing organic fraction of submicron particulate mass substantially decreases the relative humidity dependence of light scattering, $f_{\sigma sp}(RH)$ [*Quinn et al., 2005*]. Furthermore, relatively younger and more neutralized aerosols with higher organic mass fraction containing less oxidized organics lead to the lower values of $f_{\sigma sp}(RH)$, while relatively old and acidic aerosols with lower organic fraction, and a high degree of oxidation of existing organics lead to higher $f_{\sigma sp}(RH)$ [*Quinn et al., 2005*].

It is likely that the composition of particulate organics and organic fractions in the particles change with time as aerosols undergo a series of atmospheric processing since emission or formation in air. Aerosol aging and resultant chemical processing may change the organic composition, for example, the oxygenated organic fraction in the particles. However, our knowledge of organic sources, mass concentrations, size-resolved composition, transformation or evolution in the air and removal from the atmosphere, and the potential implications for climatic effects is largely inadequate. Thus, of particular interest are the origin, chemical composition and microphysics of the organic component of atmospheric aerosol with implications for heterogeneous chemistry, ability of particles to act as CCN, climate and health.

1.6 Recent Advances in Aerosol Measurements

In order to properly attribute potential particle sources and sinks, understand the processes that govern the particulate formation, as well as to understand and estimate their impacts, quantitative measurements of particle number concentrations, mass concentrations and chemical composition as a function of particle size with high temporal resolution are crucial [*IPCC, 2001; McMurry, 2000*]. The instrumentation to measure online aerosol bulk mass concentrations, total number concentrations and number size distributions has been available for several years, but the instruments capable of analyzing size-resolved chemical composition with time- and size-resolution many times higher than the traditional methods have become available only recently [*Flagan, 2001; Jayne et al., 2000; Orsini et al., 2003; Patashnick and Rupprecht, 1991; Stolzenburg and McMurrry, 1991; Stolzenburg and Hering, 2000*]. A traditional approach to determine the particle composition involves collection of aerosol samples on filters and performing subsequent off-line analysis. There are, however, intrinsic limitations with this: a poor time resolution (e.g. 6 - 24 h), limited size resolution (e.g. impactors with a few size selections), evaporative loss of semivolatile compounds and chemical transformation during sampling, transport, storage and analysis, biasing the results [*Baron and Willeke, 2001; McMurry, 2000; Seinfeld and Pandis, 1998*].

In recent years, considerable advances have been made in aerosol measurement techniques that analyze particles directly from the air. Aerosol mass spectrometry is one such technique that aims at real-time simultaneous measurements of aerosol particle size and chemical composition of single particles [*e.g., Prather et al. 1994; Thomson et al., 2000*] or ensemble of particles [*Jayne et al., 2000*]. Because of their sensitivities, high size resolution (~ nm) and high time resolution (~ min.), these mass spectrometers have revolutionized the aerosol chemical composition measurements. The mass spectrometers are, arguably, the most significant development in aerosol measurements in the past 20 years [*McMurry, 2000*]. One such instrument is the Aerodyne aerosol mass spectrometer (AMS). The AMS is capable of providing near-real-time quantitative data on chemically-speciated mass size distributions and mass concentrations of the non-refractory species (species that evaporate rapidly at temperatures < 550°C in vacuum) in ensembles of

submicron particles [*Jayne et al., 2000*]. The aerosol time-of-flight mass spectrometer (ATOFMS) measures online the chemical compositions of single particles with diameter > 200 nm [e.g., *Prather et al. 1994*], while the thermal desorption chemical ionization mass spectrometer (TDCIMS) can perform online measurement of molecular composition of ultrafine particles at a time resolution of 5-10 min [*Smith et al., 2004; Voisin et al., 2003*]. Other recent techniques for online particle chemical composition analysis include automated samplers that are directly coupled with ion chromatographs to detect specific chemical components, for example, a particle-into-liquid-sampler (PILS) [*Orsini et al., 2003; Weber et al., 2001*], whereas other instruments such as a ambient particle nitrate (or sulfate) analyzer make use of chemiluminescence analyzer [*Stolzenburg and Hering, 2000*]. These analytical techniques have contributed to a "paradigm shift" in atmospheric science: recognition of the global role of organic compounds, for instance, the organics are of comparable importance to sulfates [*Murphy et al., 1998; Murphy, 2005; Novakov et al., 1997*].

1.7 Motivation for the Study

The main atmospheric factors influencing the ambient aerosol particle concentrations and size distributions, such as emission strengths of particle sources, temperature, relative humidity, wind direction and wind speed, and mixing heights fluctuate on time scales that are substantially shorter than 24 hours. Many sources and sinks of atmospheric particles, specifically ultrafine particles, are highly dynamic, with time scales of 1-10 min [*Jaenicke, 1982*]. Therefore, online measurements with high time-resolution and size resolution are highly desirable. The new advances in aerosol instrumentation have provided unprecedented capabilities for the study of aerosol dynamics that may change over a few minutes to hours. The detail chemical composition and simultaneously measured aerosol physical properties, gas-phase species and meteorological parameters are expected to provide further insights into the processes governing aerosol formation aerosol physical, chemical and optical properties that are vital in estimating aerosol impacts on climate.

Southern Ontario experiences generally higher $PM_{2.5}$ mass concentrations than other regions in Canada, and $PM_{2.5}$ mass concentrations are typically higher during the summer months than in the winter months [*Vet et al. 2001*]. Carbonaceous species (organic carbons and elemental carbon) and nitrates are two major components of $PM_{2.5}$ followed by sulfate and ammonium in urban site of Toronto, whereas sulfate is somewhat larger at other sites (e.g. Egbert, a rural site), and relatively small amounts of soil dust, sea salt and road salts are present at all sites [Li et al. 1996, *Vet et al. 2001*]. The sulfate and nitrate fractions of $PM_{2.5}$ exhibit seasonal cycles, higher sulfate concentrations occur in summer and lower in winter, whereas nitrate shows opposite pattern [*Brook and Dann 1999; Vet et al. 2001*]. This is believed to be the colder temperatures in winter that favor partition of nitrates to particle phase, and less oxidants available in winter that would reduce heterogeneous and homogeneous SO_2 oxidation [*Tan et al. 2002*]. The previous studies utilized mostly the filter analysis of particulate composition, which suffers from inherent limitations such as coarse time resolution.

The previous aerosol studies in Egbert and Toronto have referred to the "unidentified or residual mass" in the filter analysis as carbonaceous materials [*Vet et al., 2001*]. This loose definition of carbonaceous material, and lack of appropriate measurements of particulate organic material, lead to uncertain estimate of the contribution of total organic material to the ambient particulate matter, and the nature of particulate organics, for example, the composition is still largely unknown. Therefore, the origin, atmospheric transformation, and physical and chemical composition of the organic component of atmospheric aerosol are of particular research interest.

In an attempt to understand variations of the mass, size, number and chemical composition of rural aerosol, and gain further insights into particle sources and processes governing their formation, atmospheric sampling was conducted during the spring of 2003 at a rural site in southern Ontario, Canada. In this study, the aerosol chemical composition was measured with the aerosol mass spectrometer (AMS) with a 15-min time resolution. The AMS measurements provided unprecedented detail of the aerosol composition at Egbert. These measurements provide the mass of particulate total organics

that volatilize at 500-600°C, they cannot quantitatively provide mass of water-soluble and water-insoluble organics.

The aim of the study is to increase our knowledge of the processes governing the aerosol mass and chemistry at a rural site in eastern North America. The main objectives of this study are,

- To evaluate the performance of the Aerodyne aerosol mass spectrometer (AMS) as a tool for quantitative measurement of the chemically-resolved mass concentrations and mass size distributions of the non-refractory fractions of submicron particles in the rural environment through intercomparison with the co-located semi-continuous and time-integrated aerosol measurements.
- To investigate the mechanisms and processes that control variations of aerosol particle number concentrations, mass concentrations and chemical composition, diurnal variations of the aerosol components, and closely examine the short-lived pollution episodes of hours to days.
- To understand the levels of organic aerosol mass concentrations, association between gas-phase organics and particulate organics, and to explore the nature of organic material in aerosol particles that have undergone various degree of atmospheric processing.

The spring time measurements in Egbert have revealed many interesting features in the physical properties and chemical composition of atmospheric aerosols at the site. The high particulate mass concentration events during the sampling periods were dominated by ammonium nitrate. The organic material contributes a significant fraction to submicron particles during both polluted periods and relatively clean periods. Therefore, among others, the factors that influence nitrate formation, origin and composition of organics and atmospheric processing of aerosols, in particular oxygenation of organic aerosol are investigated. Furthermore, the physical properties and chemical composition of the rural aerosol (i.e., at Egbert) are contrasted, whenever appropriate, with the same for the urban aerosol (i.e. at Toronto) approximately 100 km distant.

Chapter 2

Field Study and Methods

2.1 Atmospheric Measurements at a Rural Site in Egbert

Atmospheric sampling was conducted at a rural site in Egbert, southern Ontario, about 70 km north of Toronto in the spring of 2003. Ambient aerosol species and gas-phase species were measured continuously in real-time during a 43-day period of sampling (27 March - 8 May). The sampling site, the Centre for Atmospheric Research Experiments (CARE: 44.23N, 79.78W; 251 m asl), is located in an agricultural area. There are no major anthropogenic sources nearby the site. There is a highway at about 3 km to the east of sampling site that runs from south to north. This site experiences a wide range of pollution levels: relatively clean air arrives from northern Canada while more polluted air is advected from the urban and industrial areas of southern Ontario, and the mid-west and northeastern United States [*e.g., Brickell et al., 2003*]. This site, as it experiences the variety of air masses and the agricultural influence, represents a unique location, and thus provides the opportunity to investigate the physical and chemical properties of aerosols under various atmospheric conditions and air mass histories.

The previous studies at Egbert showed that the $PM_{2.5}$ mass concentrations at Egbert are typically higher during the summer months than in the winter months [*Vet et al., 2001*]. The filter-based chemical analysis shows that the carbonaceous species and sulfate constitute a large fraction of $PM_{2.5}$, followed by nitrate and ammonium, and soil dust as a relatively minor constituent [*Vet et al., 2001*]. The fraction of nitrate to $PM_{2.5}$ is higher in the wintertime aerosol and lower in summertime aerosol, whereas sulfate shows the opposite pattern [*Brook and Dann, 1999; Vet et al., 2001*]. However, those samplings were used 24-h averaging intervals, and thus were unable to capture the shorter-term variations in particle size and chemistry and their diurnal changes, which is crucial in

understanding the physical and chemical processes that govern particle formation and transformation.

The springtime measurements presented here provide more detail of the physical properties and chemical composition of the ambient aerosol. They are used to investigate the diurnal behavior of aerosol constituents and closely examine short-term episodes.

2.2 Instrumentation and Methods

Most of the aerosol instruments deployed during this field study were capable of operating continuously/semi-continuously and provided real-time or near-real-time information on various aerosol properties. The set of instruments deployed in this campaign, their measurement capabilities and sampling intervals are given in Table 2.1. The measurements included $PM_{2.5}$ mass concentrations, total aerosol number concentrations, number size distributions, aerosol chemical composition and mass size distributions of certain species. An Aerodyne aerosol mass spectrometer (AMS) [*Jayne et al., 2000*] was deployed during this campaign. The AMS measurements are central to this study. All instruments were operated concurrently in an air-conditioned building on the site. The sampling intakes were approximately 2 m above the roof and about 6 m above the ground. Ambient aerosols were sampled through a copper tube (ID = 0.8 cm) at a flowrate of approximately 20 l min^{-1} over a distance of about 7 m to various instruments. The inlet to the APS was different stainless steel tube with 6 inch diameter. It was used to bring in ambient air to the room and the samples were drawn isokinetically to the APS, and thus the particle loss due to impaction at the surface of the tube was minimized.

2.2.1 Particle Number Concentrations and Number Size Distributions

The total particle number concentrations of particles larger than 3 nm in diameter were measured with an ultrafine condensation particle counter (UCPC, TSI Model 3025). In a CPC, aerosol particles are first saturated with a vapor species such as water vapor or *n*-butanol, and subsequently cooled to induce a supersaturated condition so that the condensation of vapor species grows the particles to liquid droplets large enough to be detected by optical means [*Stolzenburg and McMurrry, 1991*]. Particle number size

distributions from 20 nm to 420 nm mobility diameters were measured with a scanning mobility particle sizer (SMPS, TSI Model 3070 with UCPC Model 3025). The electrical mobility diameter (D_m) is the diameter of a sphere with the same migration velocity in a constant electric field as the particle of interest [*Flagan, 2001*]. An aerodynamic particle sizer (APS, TSI Model 3321) measured the number size distributions of particles with aerodynamic diameters from about 0.5 μm to 20.5 μm. The aerodynamic diameter is the diameter of a sphere with standard density (ρ_0 = 1 g cm^{-3}) that settles at the same terminal velocity as the particle of interest [*Baron and Willeke, 2001*]. The SMPS was operated almost continuously from April 1 to May 7 and the APS was run from April 3 to May 8. The sheath air streams in both the SMPS and APS were dried.

Table 2.1 Summary of the instrumentation deployed during atmospheric sampling at the Center for Atmospheric Research Experiments (CARE), a rural site in Egbert, Ontario

Instrument	Measurements	Size Range	Sampling Intervals	Sampling Periods
UCPC	Total number concentration	D_p > 3 nm	15 min	3/27- 5/8
SMPS	Number size distribution	D_m = 20-420 nm	5-60 min	4/1-5/7
APS	Number size distribution	D_a = 0.5-20.5 μm	10 min	4/3-5/8
TEOM	$PM_{2.5}$ mass concentration	D_a < 2.5 μm	30 min	3/27- 5/8
R&P8400N	Nitrate mass in $PM_{2.5}$	D_a < 2.5 μm	15 min	4/17-4/30
AMS	Non-refractory ammonium, sulfate, nitrate, organics mass concentrations, and their mass size distributions	D_{va} ~ 20-1500 nm	15 min	3/27- 5/8
Filters	Ammonium, nitrate, sulfate, chloride, sodium, calcium, magnesium, potassium	D_a < 2.5 μm	24 h	4/1-5/8
GC-FID	NMHCs	-	20 min	3/27- 5/8

D_p: physical diameter, D_m: mobility diameter, D_a: aerodynamic diameter, D_{va}: vacuum aerodynamic diameter

2.2.2 Particulate Bulk Mass and Chemical Composition

The $PM_{2.5}$ mass concentration is continuously monitored at CARE with a tapered element oscillating microbalance (TEOM, Rupprecht and Patashnick, Model 1400a). The TEOM measures the $PM_{2.5}$ mass concentrations by recording the frequency changes of an oscillating filter due to increases in the mass of the particles deposited on the filter [*Patashnick and Rupprecht, 1991*]. The TEOM $PM_{2.5}$ mass concentration records were averaged over every 30 min during this study. In addition, an Aerodyne aerosol mass spectrometer (AMS, Aerodyne Research Inc.) was used to measure 15-min averaged mass size distributions and mass concentrations of non-refractory species (compounds that volatilize below 500°C) in submicron aerosols [*Jayne et al., 2000*]. A particle nitrate monitor (Rupprecht and Patashnick Model 8400N) was deployed for two weeks (April 17-30) to measure nitrate concentrations in $PM_{2.5}$ with a time resolution of 15 min. It utilizes a humidified impaction process to collect the ambient particles in an integrated collection and vaporization cell. The collected particles are flash vaporized and a chemiluminescence analyzer detects the NO_x evolved from the vaporization [*Stolzenburg and Hering, 2000*]. In addition to the continuous/semi-continuous mass measurements in real-time such as the TEOM measurements, the time-integrated filter samples were also collected. The 24-h filter samples are collected daily (8:00 am to 8:00 am) and analyzed for the chemical composition of $PM_{2.5}$.

2.2.3 Non-methane Hydrocarbon Compounds and Auxiliary Measurements

Gas phase mixing ratios of 37 non-methane hydrocarbon compounds (NMHCs) are routinely measured at CARE using a liquid nitrogen cooled glass bead pre-concentration trap and multi-column capillary gas chromatograph - flame ionization detection (GC-FID) system [*Brickell et al., 2003*]. This fully automated system measures 37 NMHCs (C_2-C_8) in 20-min samples at a frequency of 10-12 samples per day. The gas phase concentrations of NO, NO_y, and O_3 are also routinely monitored. Ammonia (NH_3) is measured from citric acid impregnated filters sampled for 24 h. Meteorological data (wind direction, wind speed, temperature, relative humidity, pressure, solar irradiance and precipitation) are collected at this site every 10 min.

2.2.4 Aerosol Mass Spectrometer (AMS)

General Description

The AMS provides near real-time measurements of mass concentrations of non-refractory (NR) species in submicron aerosol particles as well as their mass distributions as a function of vacuum aerodynamic diameter [*Jayne et al., 2000; Jimenez et al., 2003a; Jimenez et al., 2003b*]. The 'vacuum aerodynamic diameter' of a particle is the aerodynamic diameter of that particle in the free molecular flow regime, which is different from the 'classical aerodynamic diameter' that is measured in the continuum flow regime [*DeCarlo et. al., 2004; Jimenez et al., 2003b*]. As this study focuses on the field application of the AMS, only a brief description of the AMS is provided here. The design of the AMS, its operation, quantification methods and calibration procedure are given detail elsewhere [*Alfarra et al., 2004; Allan et al., 2003a; Allan et al., 2003b; Jayne et al., 2000; Jimenez et al., 2003a*].

The AMS consists of three main sections: a particle-sampling inlet, an aerodynamic particle sizing chamber and a particle composition analysis section, as illustrated in Figure 2.1.

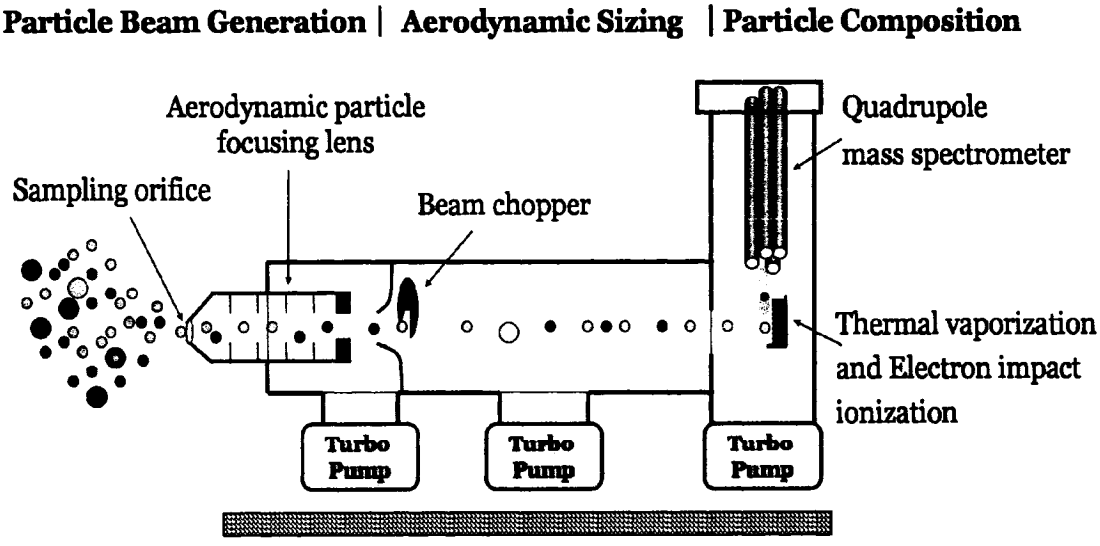

Figure 2.1 Schematic diagram of the Aerodyne Aerosol Mass Spectrometer (AMS), based on the description provided in *Jayne et al., 2000.*

Aerosol particles are introduced into the system through a 100 nm critical orifice at a flow rate of 1.5 cm^3 s^{-1}. The particle sampling lens or aerodynamic particle-focusing lens [*Liu et al., 1995a; Liu et al., 1995b*] brings nearly all submicron particles to the vacuum (~10^{-8} torr) in a narrow collimated beam, while the gaseous species are pumped out at various successive sections. The aerosol beam exiting the aerodynamic focusing lens can be modulated by a two-slit chopper wheel in such as way that the aerosol beam is either completely blocked ('beam blocked') or let to pass through freely ('beam open') or allowed to pass though in small pockets ('beam chopped'). Upon expansion into vacuum, particles acquire size-dependent velocities according to their inertia in the sizing chamber, where the particle-time-of-flight (TOF) is measured, and used to determine vacuum aerodynamic diameter (D_{va}). In the third section, particles hit a vaporizer (~500°C), where the non-refractory components flash vaporize, the vapor is ionized with electron impact (70 eV), and finally resultant positive ions are analyzed with a quadrupole mass spectrometer (QMA 422, Balzers, Liechtenstein).

Modes of Operation and Measurements

The AMS can be operated in two modes: mass spectrum (MS) mode and particle time-of-flight (TOF) mode. The mass spectra (mass-to-charge ratio, *m/z* 1-300 amu) of the ensemble of particles acquired during the MS mode operation are used to obtain ambient mass concentrations of non-refractory species such as ammonium, nitrate, sulfate, organics and chloride, without size information. In order to obtain a particulate mass spectrum, i.e., a spectrum free from the contributions of the gaseous species and the instrumental background, the mass spectrum in the 'beam closed' position is subtracted from the mass spectrum in the beam open position. One should note here that the mass concentration of "organics" is defined as the sum of all fragments after subtracting all the identified signals originating from ambient gas molecules, inorganic compounds, and instrumental artifacts such as sodium ions (Na+) from surface ionization on the vaporizer [*Allan et al. 2004a*]. In TOF mode, a set of pre-selected *m/z* is scanned as a function of particle TOF, from which the ensemble mass size distributions of non-refractory species as a function of vacuum aerodynamic diameter are derived. The vaporizer temperature for this AMS was set at about 500°C, which means that it was unable to detect refractory

components such as sea salt, black carbon and soil dust; however, it should be possible to see some non-refractory components internally mixed with refractory materials [*Jimenez et al., 2003a*].

The formulation for a quantitative computation of mass concentrations from the AMS measurements is described briefly here. The most recent quantification formulation for the mass concentrations, which is a revision and refinement of the quantification techniques described in the previous publications [*Jayne et al., 2000; Jimenez et al., 2003a; Allan et al. 2003a, Allan et al. 2003b*], is given in *Alfarra et al., [2004]*. The mass concentration of species i (C_i in $\mu g\ m^{-3}$) is determined using the following equation,

$$C_i = \frac{1}{CE_i}\frac{1}{RIE_i}\frac{MW_{NO_3}}{IE_{NO_3}}\frac{10^{12}}{Q N_A}\sum_{m/z} I_i^{m/z} \quad \ldots\ldots\ldots\ldots\ldots\ldots\ldots\ldots\ldots\ldots\ldots\ldots \quad (2.1)$$

where $I_i^{m/z}$ is the ion count rate (Hz) for a given fragment (m/z) of species i, Q is the sample flow rate (in $cm^3\ s^{-1}$), N_A is Avogadro's number, MW_{NO3} (62 g mol^{-1}) is the molecular weight of nitrate, and IE_{NO3} is the ionization efficiency for nitrate (i.e., number of ions detected per molecule vaporized). RIE_i is the relative ionization efficiency for species i, i.e., the ionization efficiency of species i relative to measured MW_{NO_3} / IE_{NO_3}, and CE_i is the particle collection efficiency at the vaporizer. The factor of 10^{12} is needed for unit conversion.

Particle Collection Efficiency

The AMS overall particle collection efficiency (OCE) depends on the particle transmission efficiency of the critical orifice and the aerodynamic lens (E_L), broadening of the particle beam as the non-spherical particles are poorly focused (E_S) and the degree of "bounce" of the particles off the vaporizer (E_B) [*Huffman et al., 2005; Jimenez, 2004*]. The inlet and aerodynamic focusing lens has a near 100% transmission efficiency for the particles within the range of 60 nm to 600 nm vacuum aerodynamic diameters, and reduced efficiencies for the particles in the range of ~20-60 nm and 600-1500 nm [*Liu et*

al., 1995a; Liu et al., 1995b; Jayne et al., 2000; Zhang et al., 2002]. A fraction of small particles is lost because the particles smaller than 60 nm are too small to be aerodynamically focused into the collimated beam as the majority of them tend to follow the gas streamlines. Likewise, a significant amount of mass in larger particles is not detected as the particles larger than 600 nm tend to impact on lens stages, with the loss being more pronounced for particles with larger aerodynamic diameters.

The collection efficiency (CE) of the particles by the vaporizer (oven), i.e., the particle collection at the vaporizer, is now believed to be determined largely by the degree of "bounce" of the particles off the oven [*Jimenez, 2004*] related to the morphology of the particle. The non-spherical particles are more likely to bounce off the oven. The particle beam width and shape-related collection efficiency (E_S) can be measured in real-time with a particle beam width probe (BWP) [*Huffman et al., 2005*]. However, the beam width probe was not installed in this AMS during this field campaign.

The average ambient relative humidity during this campaign was 71% (Standard deviation = 21%) with a median of 76% and 25th percentile of 54%. Inorganic species (ammonium, nitrates and sulfates) dominated the particle composition. Thus, most of the particles contained some hygroscopic component, and despite some warming of the aerosol as it entered the building housing the instruments, it is believed that many of the particles were at least slightly wet when sampled. Overall, the collection efficiency is poorly understood. Laboratory aerosols of ammonium nitrate and ammonium sulfate indicate collection efficiencies of 1 and 0.2, respectively. However, the complex mixtures of species such as nitrate, sulfate and organics found in the atmosphere do not necessarily mimic pure laboratory particles. In this study, a collection efficiency of unity for all species has been used as it is the simple and fundamental assumption, and the collection efficiency is not necessarily constant. The AMS particle collection efficiencies have been found close to 100% for the ambient particles at high relative humidities [*Alfarra et a., 2004, Allan et al., 2004b*]. Thus, based on what is known about the collection efficiency, a reasonable estimate for the uncertainty in the AMS measurements if the collection efficiency is less than unity is ±25%.

Besides the factors mentioned above, any change in the ionization efficiency (IE) with time introduces uncertainty in the AMS measurements. Calibrations of the absolute ionization efficiency with nearly monodisperse particles of ammonium nitrate (NH_4NO_3) were performed 2-3 times each week. The particles were generated by atomizing a solution of NH_4NO_3, drying the droplets and then size selecting the particles with a TSI Electrostatic classifier. The AMS IE was found to decrease by up to 15% between mass calibrations (2-3 days intervals), although some of this uncertainty could be related to the calibration aerosol. In this study, the most recent information on the ionization efficiencies of other species relative to NH_4NO_3, was used. The relative ionization efficiencies (REI), which is determined from the laboratory studies, are 1.1 for nitrate, 1.2 for sulfate, 1.3 for chloride, 3.5 for ammonium, and 1.4 for organics [*Alfarra et al., 2004; Allan et al., 2004a*].

Detection Limits

The AMS detection limits for the particle bound non-refractory species are estimated as three times the standard deviation of the 15 min (in this campaign) signals in the mass spectrum (MS) mode during periods with very low signals in the field campaign [*Allan et al., 2003a*]. The 15-min detection limits for ammonium, nitrate, sulfate, and organics for this campaign are estimated to be 0.015 $\mu g\ m^{-3}$, 0.006 $\mu g\ m^{-3}$, 0.006 $\mu g\ m^{-3}$ and 0.015 $\mu g\ m^{-3}$, respectively. This technique considers the uncertainties due to electronic noise and the ion counting statistics of the background [*Allan et al., 2003a, 2003b*]. *Zhang et al. [2005]* estimated the detection limits for the AMS measurements of mass concentrations based on the mass spectra of particle free (i.e., filtered) ambient air. They defined the detection limits of the species (e.g., ammonium, nitrate, nitrate, and organics) as 3 times the standard deviation of the corresponding species signals in the filtered air. The detection limits estimated by *Zhang et al. [2005]* were 2-3 times higher than the instrumental detection limits defined by *Allan et al. [2003a, 2003b]*.

2.2.5 Mass Estimation from the Number Size Distributions

In an effort to examine closure among some of the measurements, the particle number size distributions from the SMPS and APS measurements were converted to mass

concentrations. The number concentration in each size bin measured with the SMPS was converted to the mass concentration assuming that the particles were spheres (dynamic shape factor, χ = 1) with an average particle density (ρ_p) of 1.5 g cm^{-3} for the whole campaign, and thus the mobility equivalent diameter (D_m) was equal to the volume equivalent diameter (D_v) or the physical diameter (D_p). For the APS data, particles were assumed to be spheres with a standard particle density (i.e., ρ_0 = 1 g cm^{-3}). The particle densities based on the measurements of ammonium, sulfate, nitrate and organics mass concentrations using the AMS varied between 1.25 g cm^{-3} to 1.66 g cm^{-3}. The maximum uncertainty based on the variations in the relative amounts of each species in the particulate matter is estimated at ± 20% of the estimated mass concentrations. The mass concentrations from each instrument were averaged to a common interval of 1 hour in order to perform intercomparisons between mass loadings measured with three different techniques (AMS, SMPS and APS) that utilize different working principles.

It is noteworthy here that the particle aerodynamic diameter depends on the flow regime [*Baron and Willeke, 2001; Seinfeld and Pandis, 1998*]. The flow regime of the gas around a particle is determined by the Knudsen number ($Kn = 2\lambda / D_p$, where λ is the mean-free-path of the gas molecules that depends on the operational pressure of the instrument, and D_p is the particle physical diameter). The value of Kn <<1 indicates continuum flow, Kn >>1 indicates free molecular flow, and Kn = 0.4 to 20 is usually refereed to as transition regime between free molecular regime and continuum regime [*Baron and Willeke, 2001*]. The particle diameter measured with the APS is referred to as the (classical) aerodynamic diameter (D_a) as it is measured in the continuum flow regime. Therefore, the particle diameter measured with the AMS is referred to as vacuum aerodynamic diameter (D_{va}) as it is the aerodynamic diameter measured in the free molecular flow regime [*Jimenez et al., 2003b*]. The relationships between volume equivalent diameter (D_v) and vacuum aerodynamic diameter (D_{va}), and between classical aerodynamic diameter (D_a) and vacuum aerodynamic diameter (D_{va}) are given in equation (2.2) [*DeCarlo et al., 2004; Jimenez et al., 2003b*].

$$D_{va} = \frac{1}{\chi_v}\frac{\rho_p}{\rho_0} D_v, \text{ and } D_{va} = \sqrt{\frac{1}{\chi_v}\frac{\rho_p}{\rho_0}}\, D_a \quad \text{..... (2.2)}$$

where ρ_o = 1 g cm^{-3} and χ_v is the dynamic shape factor in the free molecular regime, χ_v accounts for particle asphericity (χ_v =1 for spherical particles). Equation (2.2) was utilized to transfer the number distributions measured with the SMPS and APS to the mass size distributions in vacuum aerodynamic diameter (D_{va}) space, and compared with the AMS derived mass size distributions. Hence, the SMPS and APS covered the size range from about 30 nm - 25.5 μm vacuum aerodynamic diameters.

2.3 Atmospheric Measurements at an Urban Site in Downtown Toronto

In this study, the physical properties and chemical composition of atmospheric aerosols of a rural area (i.e., Egbert) will be contrasted, whenever appropriate, with the same from an urban area approximately 100 km distant. The urban measurements were conducted from August 20 to September 25, 2003 (about 37 days) at the Wallberg Building of the University of Toronto (43.66N, 79.39W) located on College Street in downtown Toronto, Ontario [*Buset et al., 2005; Brökenhuzen et al., 2005*].. The aerosol measurement instruments included the aerosol mass spectrometer (AMS), among others, most of which were the same as in the Egbert campaign. The ambient measurements at the University of Toronto and some results have been previously described [*Buset et al., 2005; Brökenhuzen et al., 2005*]. The ambient particulate matter in Toronto originates from both local urban activities (e.g., fossil fuel combustion for transportation, industrial and residential uses) and the regional-scale transport of particles and precursor gases emitted from coal-fired power plants and urban activities in southern Ontario and mid-west and northeastern United States [*Vet et al., 2001*]. Agricultural activities in the vicinity of the city, which is normally associated with higher ammonia concentrations, also affect the aerosol loadings in Toronto. This region occasionally experiences smog episodes during summer months. It is estimated that about 1,700 premature deaths and 3,000-6,000 hospital admissions every year in Toronto are associated with air pollution [*Pengelly and Summerfreund, 2004*].

Chapter 3

Intercomparison of Co-located Instruments

In order to test the performance of the AMS and other instruments, the AMS measurements were compared with the measurements from the co-located instruments that included TEOM $PM_{2.5}$ mass concentrations, R&P particulate nitrate mass concentrations, estimated mass concentrations and mass distributions from the SMPS and APS number distributions, and particulate components from the 24-h filter measurements in Egbert.

3.1 Mass Size Distribution: AMS and SMPS+APS

Before the intercomparisons among instruments are presented, the time series of the aerosol component mass concentrations measured with the AMS at Egbert and at the University of Toronto in downtown Toronto are briefly discussed. Figure 3.1a shows the time series of ammonium, nitrate, sulfate and total organics mass concentrations measured with the AMS in Egbert from March 27 to May 8, 2003, and Figure 3.1b shows the time series of those species in downtown Toronto from August 20 to Sep 25, 2003. The particle chemical composition at Egbert varied considerably typically over a few hours. The episodes of the highest particle mass concentrations at Egbert were dominated by nitrate. The submicron particulate nitrate mass concentration as high as 16 $\mu g\ m^{-3}$ is exceptional. Ammonium and nitrate mass concentrations had the highest correlation ($r = 0.94$) among ammonium, nitrate, sulfate and organics mass concentrations. There are couples of sulfate and organic events as well. In Toronto, the organic material dominated the aerosol composition during the sampling period, except for the first two days that represents a regional smog episode in southern Ontario and a few sulfate events (Aug 29, Sep 13, 14, 22, 24) when sulfate was a prominent component. Nitrate mass concentrations were low during the entire campaign. The ammonium and sulfate were

likely in the form of ammonium sulfate as they were highly correlated (r=0.93). The total organic mass loadings are much higher at this urban site than a rural site in Egbert.

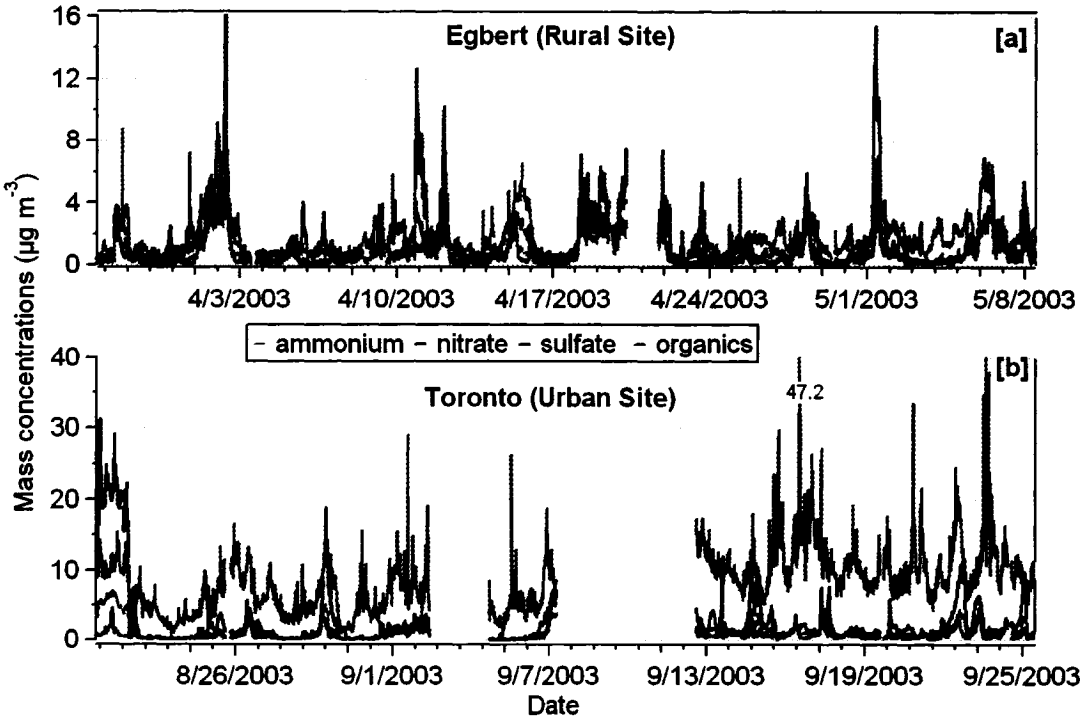

Figure 3.1 Time series of particulate ammonium, nitrate, sulfate, and organics mass concentrations of measured with the Aerosol Mass Spectrometer (AMS) (a) at CARE in Egbert from March 27 to May 8, 2003, and (b) at the University of Toronto in downtown Toronto from August 21 to September 25, 2003.

The number size distributions measured with the SMPS and APS were converted to mass size distributions as a function of vacuum aerodynamic diameter (D_{va}) as described in chapter 2. Figure 3.2 shows the average mass distributions of the AMS total mass concentrations - sum of ammonium, nitrate, sulfate and organics mass concentrations only - and the combined estimated masses from the SMPS and APS number distribution measurements. Only those periods when all three instruments were sampling are used to produce Figure 3.2; hence, it covers most of, but the entire sampling period. The SMPS+APS mass distribution indicates substantially more mass above 500 nm vacuum aerodynamic diameters than the AMS total mass distribution (mass modal D_{va} of about

725 nm and 450 nm respectively). A major reason for the absence of mass in the AMS measurements at the larger particle sizes is the reduced transmission efficiency of the AMS inlet system above 600 nm [*Allan et al., 2003b; Jayne et al., 2000*]. The estimated curve of transmission efficiency of the inlet lens [*Allan et al., 2003b; Jayne et al., 2000*] is also shown in Figure 3.2. The measured AMS mass concentration drop-off at the larger sizes follows closely the computed AMS lens transmission efficiency. The possible presence of refractory components, such as soil dust and black carbon, is another factor that will contribute to differences between the two measurements, since this AMS does not detect those components of the particulate matter. A third factor is the morphology of the particles. Non-spherical particles or those with an aggregate form may have a lower collection efficiency in the AMS. Differences in the particle density from the assumed 1.5 g cm^{-3} will introduce some uncertainty to this comparison: the maximum uncertainty based on the variations in the relative amounts of each species in the particulate matter is estimated at ± 20% of the estimated mass concentrations. Note that the AMS collection efficiency can be lower than unity for some particles.

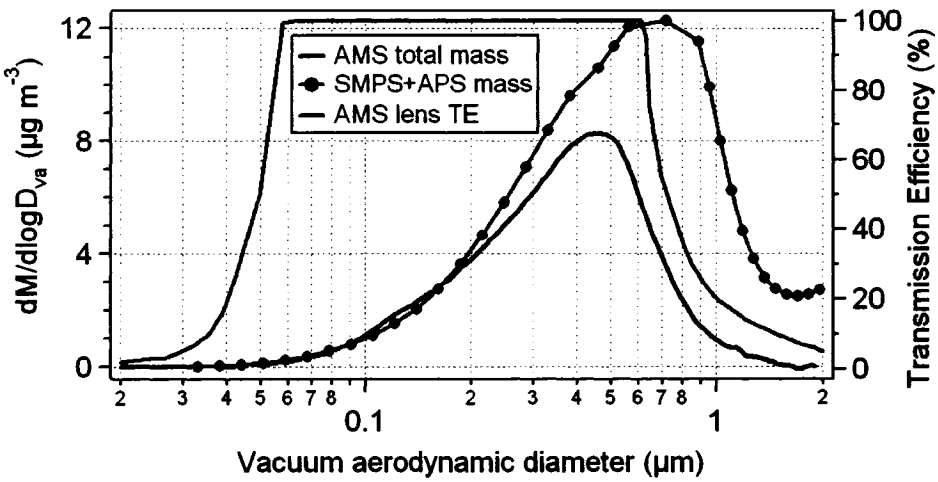

Figure 3.2 The average mass size distribution of AMS total mass (sum of ammonium, nitrate, sulfate and organics) and mass size distribution estimated from number size distributions from SMPS and APS, assuming that particles are spherical with a particle density of 1.5 g cm^{-3}. Estimated transmission efficiencies (TE) for the AMS inlet lens as a function of particle vacuum aerodynamic diameters [*Allan et al., 2003b; Jayne et al., 2000*] are also shown.

3.2 Mass Concentrations: AMS and SMPS+APS

Figure 3.3 shows the temporal variations of the hourly averaged AMS total mass concentrations, the $PM_{2.5}$ measured with the TEOM (TEOM $PM_{2.5}$), and the $PM_{2.5}$ mass concentrations estimated from the number size distributions (SMPS+APS $PM_{2.5}$). The AMS total mass concentration is the sum of only non-refractory ammonium, nitrate, sulfate and total organics mass concentrations The variations in the SMPS+APS $PM_{2.5}$ and the AMS total mass concentrations are similar, but the SMPS+APS $PM_{2.5}$ is higher than the AMS total mass concentrations, consistent with the comparison of the size distributions in Figure 3.2. The AMS total mass concentration is, on average, about 61% of the SMPS+APS $PM_{2.5}$ and 70% of the SMPS+APS PM_1. To demonstrate the role of the larger particles in the time series comparisons in Figure 3.3, the estimated mass concentrations of particles with aerodynamic diameter in 0.5 μm - 2.5 μm range from the APS number concentrations are included separately. Increases in the APS mass concentrations correspond well with increases in the difference between the SMPS+APS $PM_{2.5}$ and the AMS total mass concentrations.

The total of the potential refractory material (calcium, magnesium, potassium and sodium) from the ion analysis of the filter $PM_{2.5}$ ranges from 0.13 μg m^{-3} to 4.3 μg m^{-3}. The total refractory material in $PM_{2.5}$ was high during April 9-11 (~ 3.75 μg m^{-3}), 14-15 (~ 4.07 μg m^{-3}), 25-26 (3.32 μg m^{-3}), 27-28 (4.3 μg m^{-3}) and April 30-May 1 (3.42 μg m^{-3}), and low during April 18-20 (<2.15 μg m^{-3}). Contrasted with the differences between the AMS total mass concentrations and SMPS+APS $PM_{2.5}$ mass concentrations, these levels of refractory materials, without the corresponding anion mass, may contribute to some of the deviations. The difference between AMS total mass concentrations and SMPS+APS $PM_{2.5}$ is pronounced during April 18-20. In this case, the mass of the larger particles (D_a = 0.5-2.5 μm) reaches 24 μg m^{-3}, the total refractory material is less than 2.15 μg m^{-3}, and the AMS ammonium, nitrate and sulfate mass concentrations (24 h averages) are 35%-55% lower than the filter ammonium, nitrate and sulfate. Thus, during this period, the major source of disagreement appears to be the inability of the AMS to sample the larger non-refractory particles, and a small quantity of refractory material as a minor contributor. The difference between the SMPS+APS $PM_{2.5}$ and the AMS total

mass increases slightly during the afternoons when the relative humidity drops compared to the nights and early mornings. Relatively large changes in the relative humidity may influence the morphological structure of the particles. Lower relative humidity may lead to non-spherical particles that are more susceptible to bounce off the vaporizer.

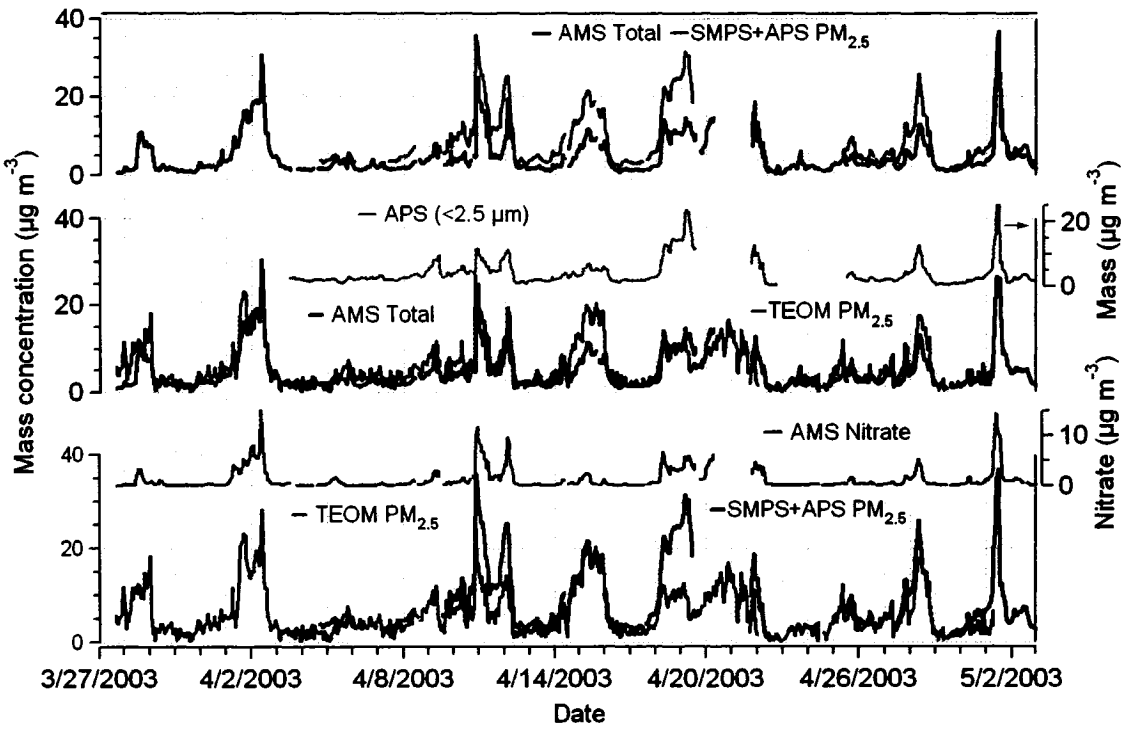

Figure 3.3 Intercomparison among hourly AMS total mass concentrations (i.e. the sum of only ammonium, nitrate, sulfate and organics mass concentrations), SMPS+APS $PM_{2.5}$ (estimated $PM_{2.5}$ mass concentrations from number distributions measured with the SMPS and APS) and TEOM $PM_{2.5}$ mass concentrations. The APS mass concentrations of particles with aerodynamic diameter in 0.5-2.5 μm range (APS<2.5 μm) and the nitrate mass concentrations measured with the AMS are also shown.

3.3 Mass Concentrations: AMS and TEOM

The AMS total mass concentrations and the TEOM $PM_{2.5}$ agree reasonably well. The AMS total mass concentrations is slightly lower than the TEOM $PM_{2.5}$ (on average, the AMS total mass is about 81% of TEOM $PM_{2.5}$). The TEOM $PM_{2.5}$ is notably higher than AMS total mass concentration on April 14-15. Some of the difference in the averages of the TEOM and the AMS stems from increases in particles larger than 0.6 μm, as

indicated by the APS, and some is due to the presence of refractory materials. During April 14-15, the SMPS+APS $PM_{2.5}$ and TEOM $PM_{2.5}$ agree well (the bottom plot). In this particular case, the mass concentrations of nitrate and the APS mass (i.e. < 2 μm) are relatively low. Refractory materials are relatively high, implying that a significant source of disagreement is due to materials that the AMS was unable to measure. This period coincides with lowest relative humidities (<50%) and highest temperatures (20-28°C) that persisted over nearly 2 days. Consequently, some of the particles may have been crystalline and subject to a lower collection efficiency in the AMS. This could account for some of the difference with the TEOM measurements.

The inability of the TEOM to report $PM_{2.5}$ correctly during nitrate events is evident. For example, during April 18-19, the TEOM $PM_{2.5}$ compares well with the AMS total mass, whereas there is a significant discrepancy of the SMPS+APS $PM_{2.5}$ with both the TEOM $PM_{2.5}$ and AMS total mass concentrations. The AMS indicates that there was a nitrate episode during April 18-19, the APS shows significant mass in the 0.5-2.5 μm aerodynamic diameter range and the filters indicate twice the nitrate of the AMS. Thus, it appears that, in this case, the filters and the APS measured the larger nitrate-dominated particles, whereas the AMS was unable to see entire nitrate due to drop off in transmission efficiency of the larger particles. Volatilization of semivolatile species, such as ammonium nitrate, in the TEOM inlet, maintained at 30°C, may explain the reduced mass indicated by the TEOM [*Allen et al., 1997*]. Such evaporative loss can be a concern when using the TEOM to monitor $PM_{2.5}$, in particular, in areas where other semivolatile species contribute significantly to the particulate matter.

3.4 Mass Concentrations: AMS and Filter Measurements

The $PM_{2.5}$ bulk chemical composition (nitrate, sulfate, ammonium, chloride, sodium, calcium, magnesium and potassium) was determined by analyzing daily filter samples collected for 24 h (8:00 am to 8:00 am). In order to perform statistical intercomparisons with the filter data, the AMS data were averaged to a common averaging interval of 24 h (8:00 am to 8:00 am). The AMS did not have complete 24 h coverage on all days due to calibrations and maintenance, so only days with AMS sampling of more than 16 h are

used. Figure 3.4 displays the time series of ammonium, nitrate and sulfate mass concentrations acquired by the two measurements. Included in Figure 3.4 are Ca^{++} and Na^{+} mass concentrations from the filter pack analysis of $PM_{2.5}$. Although the temporal variations of species from two measurements co-vary, the AMS measurement is frequently lower than filter measurements.

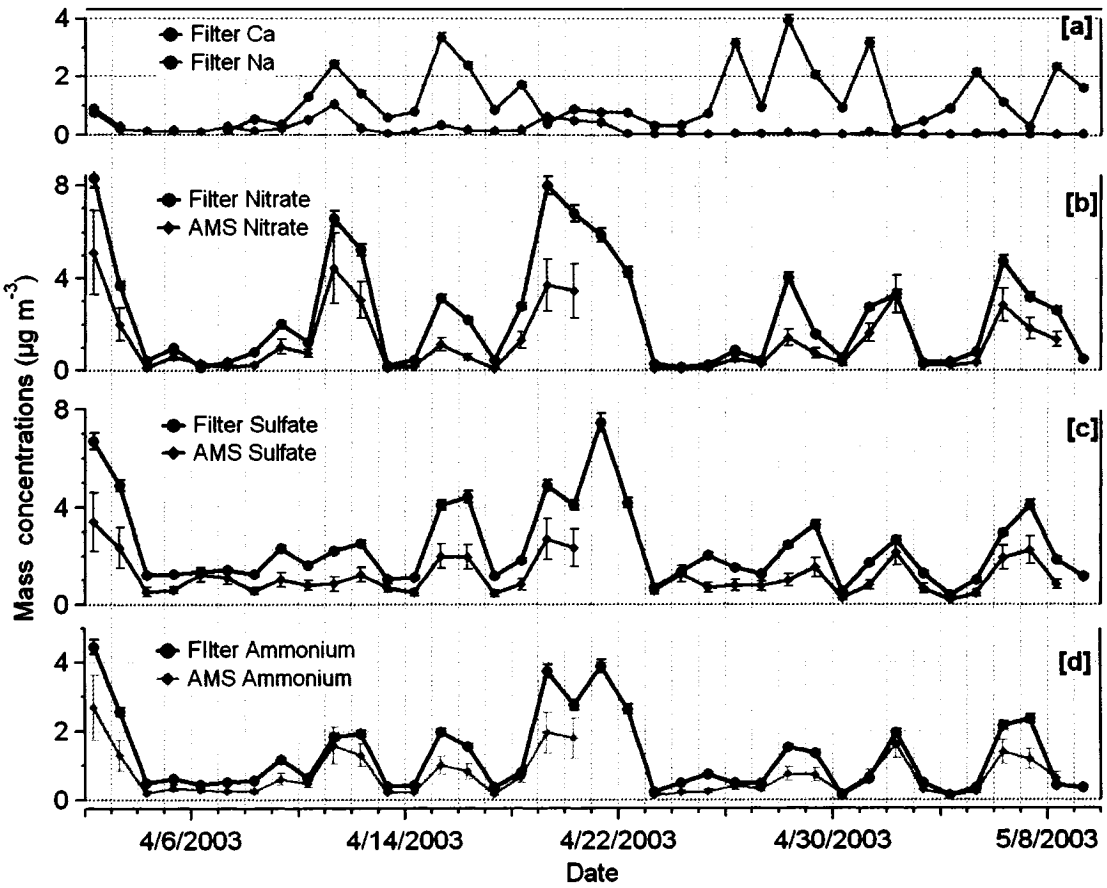

Figure 3.4 Time series of mass concentrations of (a) Ca^{++} and Na^{+} from the filter pack analysis of $PM_{2.5}$, (b) nitrate measured with the AMS and nitrate from $PM_{2.5}$, (c) sulfate measured with the AMS and sulfate from $PM_{2.5}$, (d) ammonium measured with the AMS and ammonium from $PM_{2.5}$, Both AMS and filter data are 24 h averages.

In Figure 3.4, the relative difference between the AMS and filter measurements generally tends to be higher when $PM_{2.5}$ Ca^{++} mass concentrations increase. The presence of calcium, which is derived mainly from crustal materials and primarily contained in

supermicron particles [*Seinfeld and Pandis, 1998*], may lead some anions, specifically nitrate, to be associated with larger and more alkaline mineral particles [*Finlayson-Pitts and Pitts, 2000*]. In addition, some submicron particles may contain some nitrate or sulfate associated with calcium, though the fraction is expected to be low. The AMS does not detect those refractory fractions.

Figure 3.5 shows scatter plots of AMS derived ammonium, sulfate and nitrate mass concentrations with those determined from the filter analyses. The AMS measurements account for about 57% of the filter ammonium (slope = 0.57, intercept = 0.04 $\mu g\ m^{-3}$ and $r^2 = 0.92$), 56% of the filter nitrate (slope = 0.56, intercept = -0.05 $\mu g\ m^{-3}$ and $r^2 = 0.92$) and 50% of the filter sulfate (slope = 0.50, intercept = 0.07 $\mu g\ m^{-3}$ and $r^2 = 0.89$). The nitrate measured by the AMS may include contributions from ammonium nitrate, sodium nitrate in road salt particles and nitrogen containing organic compounds that may not be measured in the filter analyses. Despite the lower slopes, all three comparisons correlate well. The most likely factor that contributes to the discrepancies between the measurements is the presence of larger particles that AMS samples with reduced transmission, collection and volatilization efficiencies as discussed earlier. There is also some chance of collecting particles larger than 2.5 $\mu m\ D_a$ by the filter system due to the uncertainty in the size cut-off of the inlet as well as oxidation and condensation processes that may occur on the filters [*Drewnick et al., 2004*].

Several factors lead to uncertainties in AMS measurements and filter measurements. Those factors for the AMS measurements include the transmission efficiency of the lens within and beyond the 60 nm to 600 nm size range, beam broadening, particle bounce and change in the IE with time. Therefore, based on what is known about the collection efficiency, a reasonable estimate for the uncertainty in the AMS measurements if the CE is less than unity is ±25%. The error bars in the AMS measurements in Figures 3.4 and 3.5 include these factors as well as a small contribution due to the detection limits (very small values for 24 h). The uncertainties in the filter measurements are due to flow rate change, analytical uncertainty, blank levels, volatilization, reaction and condensation on

filters, and sampling of some particles larger than 2.5 μm. A value of 5% is used to represent the uncertainty in the filter concentrations in Figures 3.4 and 3.5.

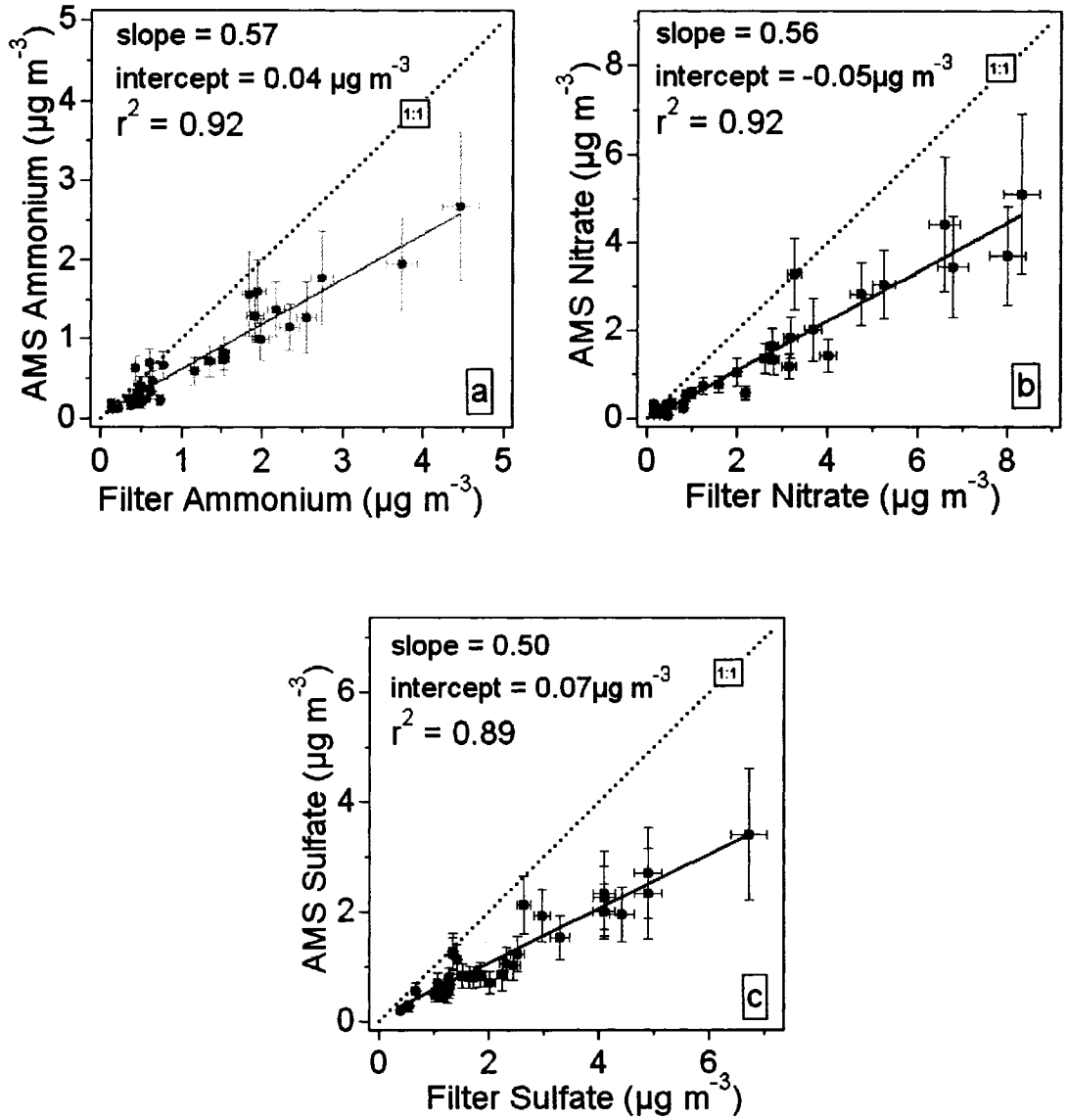

Figure 3.5 Intercomparison of 24 h averaged particulate ammonium, nitrate and sulfate mass concentrations measured with the aerosol mass spectrometer (AMS) and those from the filter pack analysis of $PM_{2.5}$. The error bars are explained in the text.

3.5 Nitrate Mass Concentrations: AMS and R&P 8400N

Automated semicontinuous measurements of the $PM_{2.5}$ nitrate concentrations were made with a R&P nitrate monitor (R&P8400N) from 17 April to 30 April. Figure 3.6 shows the correlation between the hourly averaged AMS and R&P8400N nitrate mass concentrations. The two measurements agree well, perhaps coincidently; the slope and intercept of this correlation plot are 0.98 and -0.08 μg m^{-3}, respectively, and r^2 is 0.92. During the two-week period the R&P8400N was used, the correlations among the AMS nitrate, R&P8400N nitrate and filter nitrate (all 24 h averages) indicate that the R&P8400N and the AMS recovered 49% and 46% of the filter nitrate, with r^2 values of 99% and 98%, respectively. The collection efficiency of the impactor in the R&P8400N is >95% for particles with aerodynamic diameters from 0.1 μm to 0.8 μm, the uncertainty is greater for particles > 0.8 μm [*Stolzenburg and Hering, 2000*]. The evaporative loss of the species such as ammonium nitrate has been estimated to be less than 6% [*Stolzenburg and Hering, 2000*]. Thus, the strong agreement between the AMS and R&P8400N may be coincidental and due to similarly poor collection efficiencies of both instruments for the larger particles.

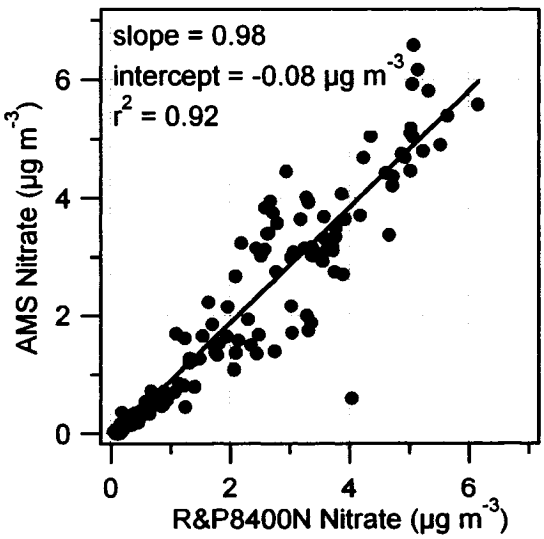

Figure 3.6 Intercomparison between particulate nitrate mass concentrations measured with the AMS and the nitrate in $PM_{2.5}$ measured with the R&P8400N particulate nitrate monitor. Both measurements were averaged to a common averaging interval of one hour.

Chapter 4

Ambient Aerosol in Egbert: General Properties

4.1 Local Meteorological Conditions

The average ambient temperature during the study was 5.3°C with a minimum of -11.8°C and a maximum of 28.3°C. The relative humidity varied between 19% and 100% (average = 71%). Wind speeds ranged from less than 1 m s^{-1} to as high as 14 m s^{-1} (average = 3.6 m s^{-1}). The frequency of local wind direction was highest for winds from the northwest (270°-360°), followed by the southeast (90°-180°), the southwest (180°-270°) and then the northeast (0°-90°). Nineteen days out of 43 days experienced either trace or moderate precipitation (9 days of rainfall, 3 days of snowfall and 7 days with a mix of both). There were trace amounts of snow on the ground until April 10. One morning (May 6) was foggy. Precipitation was observed between 8:00 am and 6:00 pm on only 5 days. The remaining 24 days were mostly sunny, and the solar irradiance reached as high as 970 W m^{-2}.

4.2 Mass Concentrations of Aerosol Components

Figure 4.1 illustrates time series of AMS derived ambient mass concentrations of ammonium, nitrate, sulfate and total organics in the submicron aerosols sampled at CARE from March 27 to May 8, 2003. Included in Figure 4.1 are 10 min average local wind directions, wind speeds, temperatures, relative humidities and 24 h averaged gas-phase ammonia (NH_3) concentrations. For the entire sampling period, the average mass concentrations of ammonium, nitrate, sulfate and the organics are 0.69 μg m^{-3}, 1.18 μg m^{-3}, 1.19 μg m^{-3}, and 1.73 μg m^{-3}, respectively. The summary statistics of various components during the measurement period is presented in Table 4.1. The minimum-maximum ranges of the percentage contribution of ammonium, nitrate, sulfate and

organic mass fractions to the total particulate mass, where the total is the sum of only these four components, are 0-30%, 0-60%, 3-82% and 14-87%, respectively, indicating that organic material constitutes a large fraction of the total fine aerosol mass. The averages (in %) of those fractions contributing to total mass are shown in Figure 4.2.

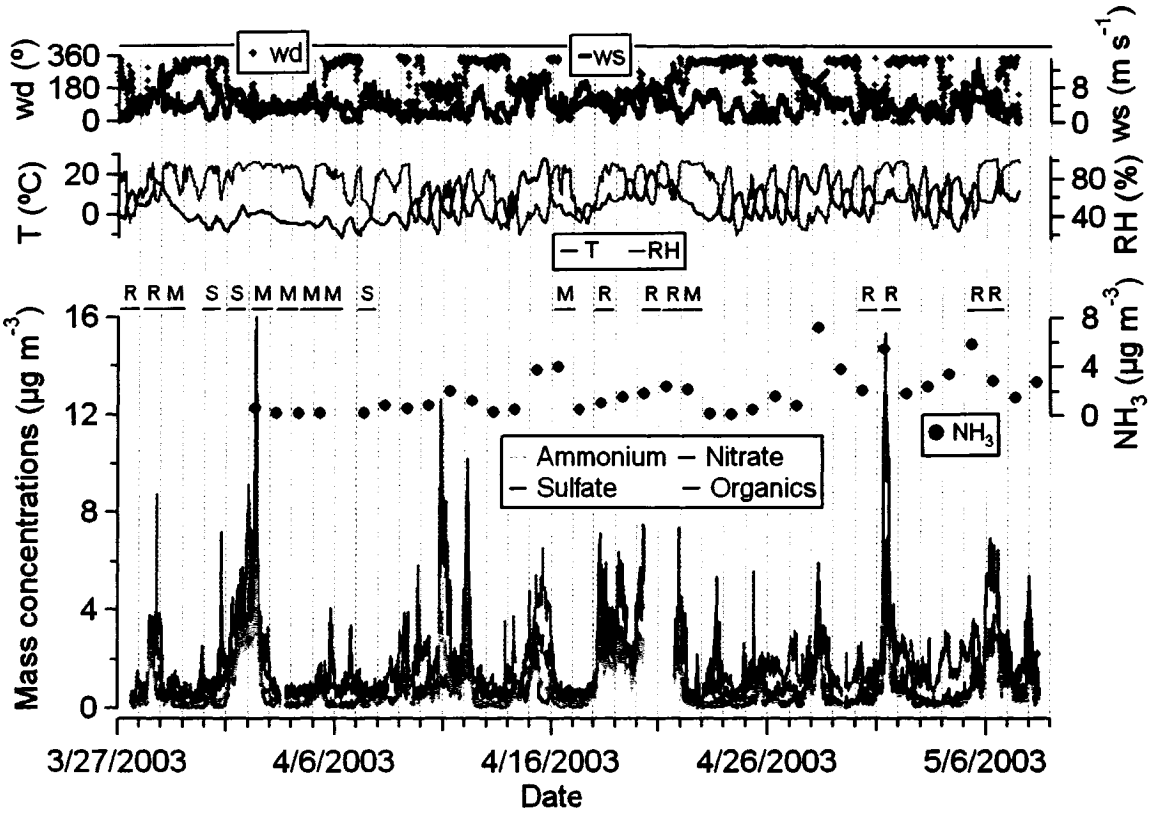

Figure 4.1 Time series of ammonium, nitrate, sulfate and organics mass concentrations of ambient submicron aerosols measured with the Aerosol Mass Spectrometer (AMS), together with ambient temperature (T), relative humidity (RH), wind speed (ws) and wind directions (wd) at CARE from March 27 to May 8, 2003. The chemical components are 15 min averages and the meteorological parameters are 10 min averages. The gas-phase concentrations of ammonia from filter pack analysis (24 h averages) are also shown. Days with precipitation are marked with S (snow), R (rain) and M (mix of snow and rain).

Typically, depending upon the histories of air masses arriving at the site, the particulate mass concentrations and particle composition varied considerably over a few hours. Higher fine particle mass concentrations were observed when the winds were southerly and the wind speeds were lower, implying that the urban/industrial emissions advected

from the city centers and industrial regions to the south of the site significantly influence the ambient particulate mass concentrations in Egbert. In general, the cleaner periods during this study were associated with air masses coming from north. Aerosol particles from the northwest were composed of mainly sulfate and organics. On a few occasions (e.g., March 31, April 5, 6 and 23), sulfate dominated the northerly aerosol but the events were short-lived. Those events correspond to the air masses that had passed over the Sudbury region (industrial area with nickel smelters noted for higher SO_2 emission) to the northwest. The episodes of the highest particle mass concentrations were dominated by nitrate. Higher nitrate mass concentrations occurred during dark hours, in particular early mornings with lower temperatures and higher relative humidities. This secondary aerosol component is prevalent in Egbert due to availability of free ammonia (NH_3) and its proximity to urban centers such as the city of Toronto that may result in transport of NO_x during southerly flows [*Vet et al., 2001*]. However, the nitrate peaks (Figure 4.1) with about 6 $\mu g\ m^{-3}$ to as high as 16 $\mu g\ m^{-3}$ of nitrate mass concentrations are exceptional, and mechanisms that lead to formation of such high particulate nitrate mass concentrations requires further investigation.

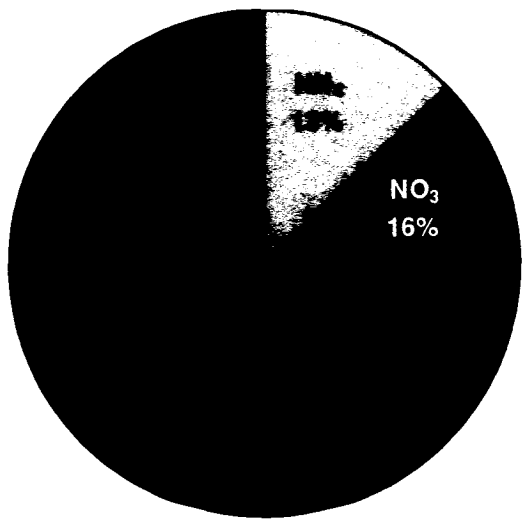

Figure 4.2 The averages of ammonium, nitrate, sulfate and total organic mass fractions contributing to total particulate mass measured with the Aerosol Mass Spectrometer (AMS) at Egbert from March 27 to May 8, 2003.

It is worth mentioning here that the previous aerosol studies at Egbert have referred to the "unidentified or residual mass" in the filter analysis as carbonaceous materials [*Vet et al., 2001*]. This loose definition of carbonaceous materials, and lack of appropriate measurements of particulate organic material, lead to uncertain estimate of the contribution of total organic material to the ambient particulate matter, and the nature of particulate organics, for example, the composition is still largely unknown. The AMS measurements provide the mass of particulate total organics, both water-soluble and water-insoluble, that volatilize at 500-600°C. Thus, it is a more accurate measurement of particulate total organic material. In this study, the aerosol components (ammonium, nitrate, sulfate, and total organic material) measured at CARE with the AMS show that the organic material contributes, on average, the highest fraction to particulate mass (Table 4.1) during the sampling period.

Table 4.1 Summary statistics of mass concentrations ($\mu g\ m^{-3}$) of chemical constituents in the ambient aerosols measured with the Aerosol Mass Spectrometer (AMS). The total mass is the sum of only ammonium, nitrate, sulfate and organics. Aerosol acidity is the ratio of molar concentrations of ammonium to sulfate and nitrate[i.e., $NH_4^+/(2SO_4^{--}+NO_3^-)$]. SD is one standard deviation.

Species[a]	Min.-Max.	Average (SD)	Median	5th percentile	95th percentile
Ammonium	<0.015 - 6.18	0.69 (0.82)	0.35	0.09	2.46
Nitrate	<0.006 - 16.15	1.18 (2.00)	0.32	0.03	5.42
Sulfate	0.04 - 7.20	1.19 (1.01)	0.77	0.23	3.25
Organics	0.14 - 9.39	1.73 (1.24)	1.39	0.49	4.20
Total	0.36 - 32.92	4.80 (4.54)	3.03	1.16	14.17
m/z 43[b]/Organics	0 – 42%	6% (2%)	6%	4%	9%
m/z 44/Organics	0 – 21%	7% (2%)	7%	3%	10%
m/z 57/Organics	0 – 27%	2% (1%)	1%	1%	3%
Aerosol Acidity	0.05 - 2.48	0.93 (0.28)	0.88	0.37	1.30

[a] Detection limits [estimated with a technique described in *Allan et al., 2003*] for ammonium, nitrate, sulfate and organics were 0.015 , 0.006, 0.006 and 0.015 $\mu g\ m^{-3}$, respectively. [b] *m/z* 43, *m/z* 44 and *m/z* 57 are organic fragments at *m/z* = 43, 44 and 57, respectively.

There is a tendency for ammonia to increase with time through the study period in correspondence with generally increasing temperatures and decreasing snow cover. Ammonia mass concentrations remained less than 1 $\mu g\ m^{-3}$ at temperatures less than 5°C. The detection limit for NH_3 was 0.15 $\mu g\ m^{-3}$ (95% confidence limit). At temperatures below approximately 12°C, the gas-phase ammonia correlated positively with the particulate ammonium and nitrate mass concentrations, then the correlations became negative with the ammonia tending to be higher at higher temperatures. This may reflect a difference in the partitioning between the gas-phase ammonia and the particle-phase ammonium with more ammonia in the gas phase at higher temperatures. Ammonium correlated negatively with sulfate for temperatures <5°C coincident with the sulfate dominated air masses from the northwest. The variance in NH_3 may also be a result of changes in the local source strength of NH_3 during the period; the ground was warming during the study period and the fields were starting to be prepared for planting. Ammonium nitrate is a reaction product of nitric acid with NH_3, which is temperature dependent and influenced by relative humidity [*Seinfeld and Pandis, 1998*]. Higher levels of ammonia in Egbert from agricultural activities and the cooler temperatures may favor its formation. The fog and haze droplets also appear to have influenced ammonium nitrate formation (e.g., May 6).

Among the mass concentrations of ammonium, nitrate, sulfate and organics, the strongest correlation is between ammonium and nitrate (correlation coefficient, r = 0.94; Figure 4.3). This indicates that the higher levels of NO_x often advected from urban areas, ammonia from agricultural emissions around the site, and low temperature often observed at the site favored the formation of ammonium nitrate. Ammonium is moderately correlated with organics (r = 0. 78) and sulfate (r = 0.76). The correlation between organics and nitrate (r = 0.73) is slightly higher than that between organics and sulfate (r = 0.60). The correlation coefficient between nitrate and sulfate is 0.57. The average molar ratio of measured ammonium to nitrate plus sulfate (i.e., $[NH_4^+ / (2SO_4^{--} + NO_3^-])$ is 0.93 (standard deviation = 0.28) and the median is 0.88 for the entire campaign.

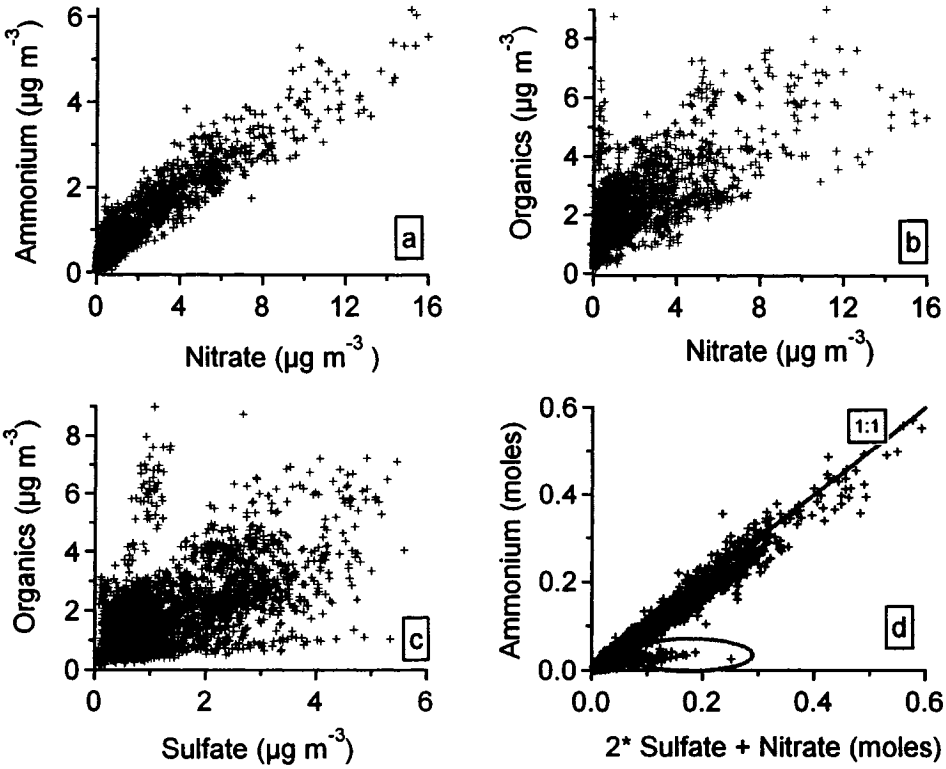

Figure 4.3 Correlations among aerosol components measured with the Aerosol Mass Spectrometer (AMS): (a) ammonium vs. nitrate, (b) organics vs. nitrate and (c) organics vs. sulfate. The acidity of the particles – the molar ratio of positive ions to negative ions $[NH_4^+/(2SO_4^{--}+NO_3^-]$ – is also displayed (d).

The smaller values of the ratio, some of them are noticeable and encircled at the bottom-left of the molar ratio plot in Figure 4.3, were observed mostly on the days with northwesterly winds when sulfate dominated the particles. This is consistent with reduced ammonia emissions in the colder North during that time. Although it may be implied from this that the aerosol was more acidic when the winds were from the north, the presence of refractory ions, undetected with the AMS, and organic acids in the particles leaves some uncertainty in trying to estimate aerosol acidity from these data.

4.3 Mass Size Distributions of Aerosol Components

Figure 4.4a shows the mass size distributions of ammonium, nitrate, sulfate and organic fractions of rural (Egbert) aerosol particles determined from the AMS measurements

averaged over the entire sampling period. Particulate inorganic species have similar unimodal mass distributions with modal vacuum aerodynamic diameters (D_{va}) between 475 nm and 500 nm. The particulate total organic material has two modes, a larger mode with a modal D_{va} close to that of the inorganics and a smaller mode peaked at about 150 nm. Most of the particle mass of the particles smaller than about 80 nm is organic. Thus, the average distribution is represented by smaller particles of mostly organics and larger particles more likely internal mixtures of organics, ammonium, sulfate and nitrate. The average distribution of species in this campaign is similar to that reported for the lower Fraser Valley, British Columbia, Canada [*Alfarra et. al., 2004*], indicative of an urban air mass that had undergone several hours of atmospheric processing. It also bears similarity to that measured at Trinidad Head, California when marine air mass influenced by continental emission was sampled [*Allan et al., 2004b*].

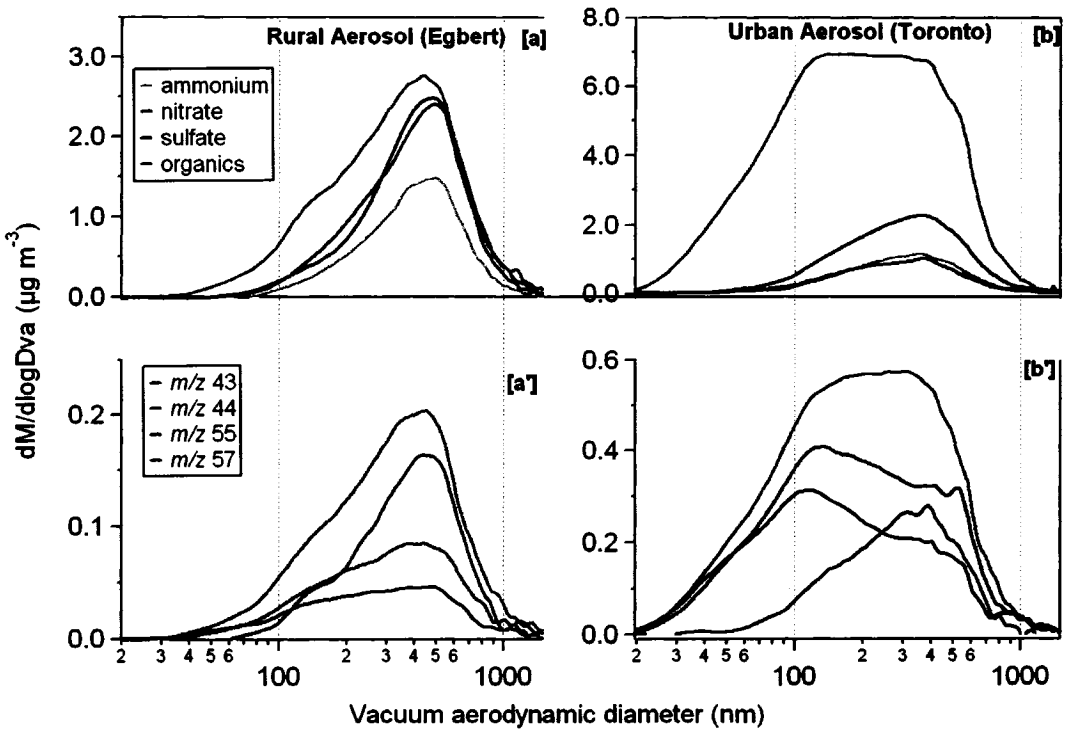

Figure 4.4 The average mass distributions of particulate ammonium, nitrate, sulfate and organics acquired by the Aerosol Mass Spectrometer at (a) a rural site near Egbert from March 27 to May 8, 2003, and (b) at an urban site in downtown Toronto from August 23 to Sep 25, 2003. The mass distributions of four key organic fragments are shown in (a') and (b').

In order to illustrate the difference in the mass distributions of aerosol components in the rural and urban aerosol, the average mass distributions of ammonium, nitrate, sulfate and total organics mass concentrations in urban aerosols acquired with the AMS in downtown Toronto are also displayed in Figure 4.4b. The first two days with smog were excluded while producing Figure 4.4b. There is a remarkable difference between the organic mass distributions in rural and urban environment. Organic material dominates the mass of urban aerosol. There is a significant particulate mass in the smaller particles, and the particles as small as 20 nm D_{va} are observed despite the reduced collection efficiencies of the AMS for smaller particles. The small particles are predominantly organic particles, and appear to be externally mixed with the inorganics. The mass modal diameters of the inorganic species are also smaller in urban aerosol.

The average distribution of species at this urban site is similar to that reported for other urban sites: for example, Urban Manchester and London, UK [*Allan et al. 2003a; Allan et al. 2003b*], Slocan Park in Lower Fraser Valley, British Columbia, Canada [*Alfarra et. al. 2004*], Queens, New York [*Drewnick et al. 2004b*], Pittsburgh, USA [*Zhang et al. 2005c*]. The increase in total particulate organic mass concentrations and small mode organics at this urban site was correlated with an increase in NO_x, suggesting that the likely source of the organics is traffic emissions. In previous urban studies, the organic mass distribution was found bimodal with a distinct smaller mode (modal $D_{va} < 200$ nm), attributed to local traffic emissions of hydrocarbon particles, while the larger mode contained some oxygenated organics [*Alfarra et. al., 2004; Allan et al., 2003a; Drewnick et al., 2004*]. The mass loading of small mode organic particles ($D_{va} < 200$ nm) in Egbert has positive correlations with several gas-phase NMHCs, including propene, ethylbenzene, toluene, benzene. This will be discussed later. The implication is that the small organic particles are most likely the result of primary emissions of organics from fuel combustion sources, and are probably transported from urban areas.

The average mass distributions of four key organic fragments at *m/z* 43, *m/z* 44, *m/z* 55 and *m/z* 57 are displayed in Figure 4.5a' and Figure 4.5b' for the rural aerosol and urban aerosol, respectively. The *m/z* 44 arises from oxygenated organics, *m/z* 57 from

hydrocarbons, whereas *m/z* 55 and *m/z* 43 receive contributions from both hydrocarbons and oxygenated organics [*Alfarra et al. 2004; Allan et al. 2003a; Allan et al. 2003b; Drewnick et al 2004a*]. The *m/z* 44 can be used as marker for the oxygenated organic aerosol (OOA), which tends to be higher in processed aerosols, and *m/z* 57 as an indicator for the hydrocarbon-like organic aerosol (HOA), which is generally higher in less processed aerosols [*Alfarra et al., 2004; Allan et al., 2004; Zhang et a., 2005a; Zhang et a., 2005b*]. The *m/z* 44 is preferentially higher in the larger mode for both sites whereas *m/z* 57 and *m/z* 55 are distinctly higher in the small mode for the urban site. Most of the particles smaller than about 100 nm showed a very small or no signature of oxygenated organics. This implies that the aerosol was more oxidized in the larger mode compared with the smaller mode. The mass distributions are suggestive of a dominance of hydrocarbon-like organics, most likely from fossil fuel combustion sources, mainly traffic in this downtown site. On average, the organic mass concentrations of the particles with $D_{va} < 200$ nm made up 50% of total organic mass of urban aerosol, in contrast to only 27% for the rural aerosol.

Although the mass distributions in Figure 4.4a provide an average picture for this springtime aerosol at CARE, they do not demonstrate the temporal variability of the aerosol mass size distributions during the study period. The mass distributions of organics and sulfate over shorter time intervals often showed significant mass below 100 nm. During the periods with higher particulate matter, often associated with southerly winds, organics showed distinct bimodal mass distribution and nitrate also tended to exhibit bimodal mass distribution coincident to organic modes. Nitrate may have condensed on the small organic particles during such events. Sulfate occasionally displayed a bimodal distribution during suspected particle nucleation and growth events.

4.4 Total Particle Number Concentrations

Figure 4.5a displays time series of the 15-min averaged total number concentrations of particles with diameter larger than 3 nm measured with the UCPC at CARE from March 27 to May 8, 2003. The total particle number concentrations (15-min averages) varied between 300 cm^{-3} and 25,000 cm^{-3} (average = 6,500 cm^{-3}, SD = 4,300 cm^{-3}, median =

6,000 cm^{-3}) during the entire sampling period. Aerosol number concentrations were dependent on the meteorological conditions and air mass histories.

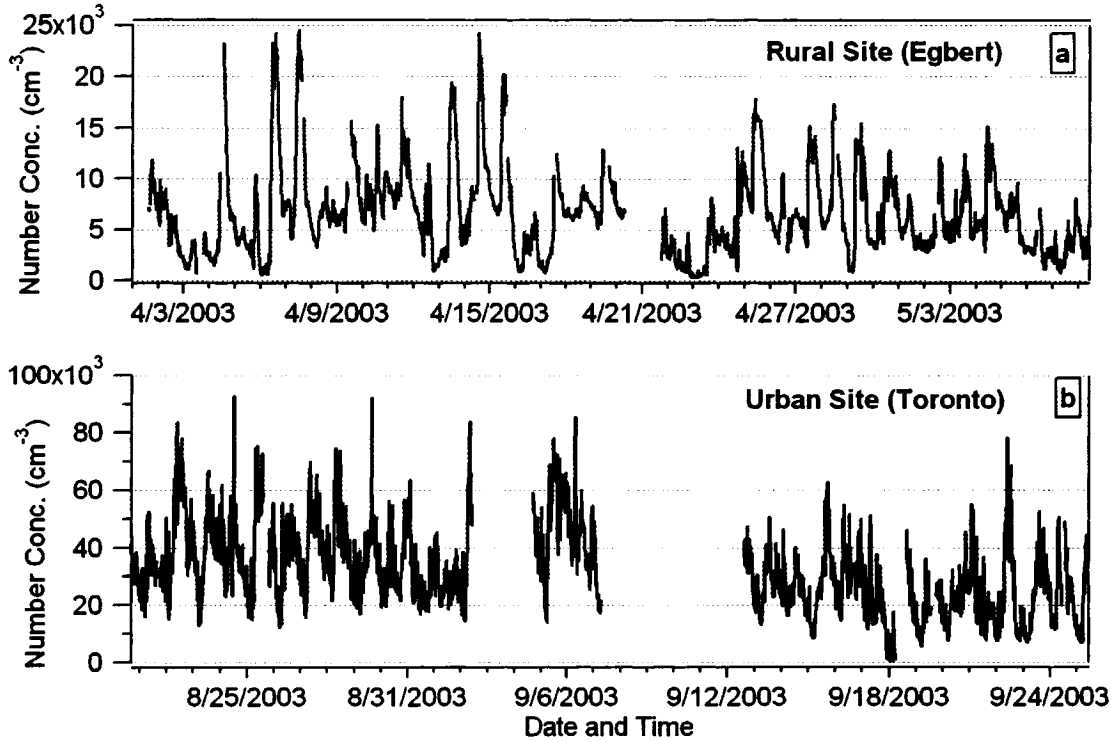

Figure 4.5 Time series of 15-min averaged particle total number concentrations (a) at a rural site in Egbert from March 27 to May 8, 2003), and (b) at an urban site in downtown Toronto from August 20- September 25, 2003.

There were several events with huge increases in aerosol total number concentrations during relatively clean periods regarding the mass concentrations, and coincided with sulfate-dominated aerosol composition. This massive excursion in particle number concentrations is probably due to small particles formed during recent nucleation events. Thus, the origin and composition of ultrafine particles, and their relationship to potential sources in the region is a subject of further investigation. This will be further explored, and discussed in next chapter. Furthermore, the particle total number concentrations sometimes increased moderately (~10,000-15,000 cm^{-3}) during southerly air trajectories, implying that the urban emissions were advected to the site.

Figure 4.5b shows the time series of total number concentrations measured with UCPC at an urban site in downtown Toronto. The measurements were carried out from Aug 20 to Sep 25, 2003. The total number concentrations in downtown Toronto varied between 100 cm^{-3} and 93,000 cm^{-3}, with an average value of 32,400 cm^{-3} (SD = 14,850 cm^{-3}) and median of 30,200 cm^{-3} for a period of 32 days. The number concentrations in downtown Toronto were 4-5 times higher than that in rural Egbert. There is a profound difference in total number concentrations at the rural site and the urban site. This reflects the severity of particulate pollution in downtown Toronto, and it may be a potential health hazard. In fact, *Thurston et al.,* [1994] reported the association between airborne fine particles and hospital admissions in Toronto. Higher levels of number concentrations in downtown Toronto were most likely due to huge amounts of particles emitted from the automobiles. College Street, where the sampling site was located, has a weekday daily traffic volume of ~ 33,000 vehicles and is representative of downtown Toronto traffic [*Tan et al., 2000*].

4.5 Diurnal Variations of Number Concentrations

The diurnal patterns in number concentrations at both sites were investigated. The diurnal pattern may provide information on the origin of particles, such as association between increase in total number concentrations and traffic emissions at the site. Figure 4.6a and Figure 4.6b display the diurnal variations in total particle number concentrations of the rural aerosol and the urban aerosol, respectively. There is a clear diurnal pattern in total particle concentrations in Egbert with the concentrations lower in night and early morning and higher in afternoon (12:00-15:00). Number concentrations gradually decrease from around 16:00 through the night to minima in the morning. This decrease in number concentrations may be due to increase in particle sinks (e.g., coagulation among particles or particle growth and gravitational settling) and a reduction in particle sources [*Seinfeld and Pandis, 1998*]. The diurnal variations in number concentrations closely follow the diurnal cycle of solar irradiance, indicating that the excursion in number concentrations in afternoon is likely due to new particles formation (nucleation) when photochemistry is intense [*e.g., Kulmala,, 2003; Zhang et al., 2005*].

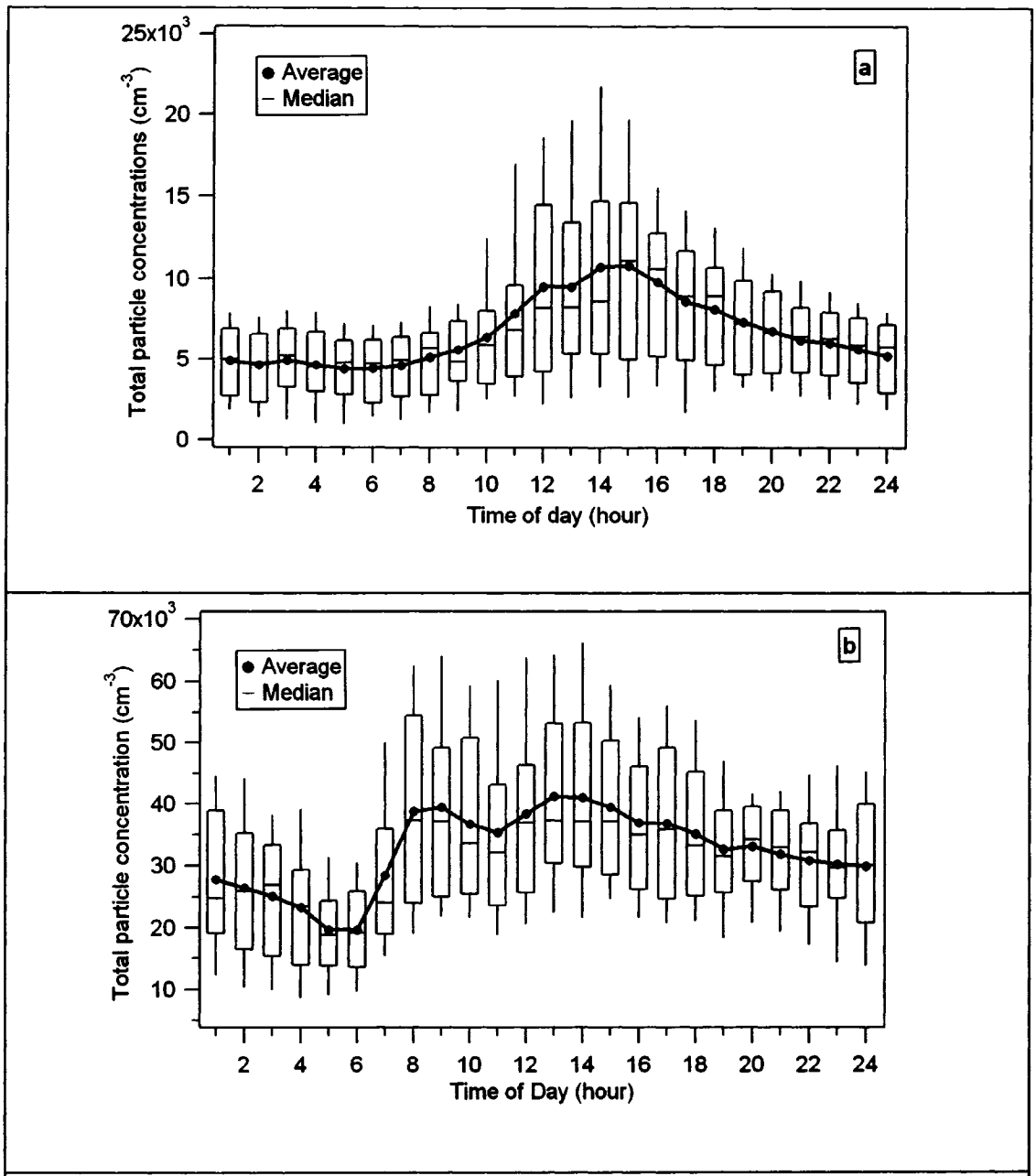

Figure 4.6 Diurnal variations of the total particle number concentrations for particles with diameters larger than 3 nm (a) in rural Egbert, and (b) in downtown Toronto. The top and bottom of the individual box represent the upper and lower quartiles, respectively, while the top and bottom of the whisker represent the 90th percentile and 10th percentile, respectively.

The diurnal pattern of number concentrations in Egbert is distinctly different from that at a site in downtown Toronto. The total particle number concentrations in Toronto also exhibit a clear diurnal pattern, with minima in early morning (5:00-6:00), a sharp increase during morning rush hours (7:00-9:00), higher and relatively constant levels in the

afternoon, and a gradual decrease through the night to the minima in the morning. This variation may reflect the change in traffic pattern at the site, and thus automobile emissions as the major source of ambient particles at the site. The additional increase in particle concentrations around noon may be due to new particle formation. Aerosol nucleation events have been observed in several polluted urban environments, for example, Pittsburgh [*Zhang et al., 2005, Stanier et al., 2005*]. One should note that, besides the changes in sources and sinks, mixing due to evolution of boundary layer influence the number concentrations.

4.6 Diurnal Variations of Aerosol Components

The 15-min averaged continuous measurements of aerosol chemical composition with the AMS, and extensive complement of other parameters such as aerosol number measurements and meteorological measurements provided unprecedented opportunity to study the diurnal variations of various aerosol components, and make inferences about the origin of various particulate species. Figure 4.7 displays box plots of the diurnal variations of particulate (a) nitrate, (b) sulfate, (c) ammonium and (d) organic mass concentrations acquired with the AMS for the entire study period.

There is a diurnal pattern in the nitrate mass concentrations in the means, medians, upper quartiles, and 90th percentiles with higher nitrate mass concentrations evident during early morning hours and minima in the afternoon. Ammonium nitrate formation is favored at lower temperatures [*e.g., Brook and Dann, 1999; Drewnick et al., 2004; Seinfield and Pandis, 1998*], which more often occurs during the nighttime. At night, the most significant mechanism that controls NH_4NO_3 formation is the conversion of NO_3 to N_2O_5, followed by homogeneous hydrolysis of N_2O_5 to form gaseous HNO_3, and heterogeneous hydrolysis of N_2O_5 on wet particle surfaces yielding particulate HNO_3 [*McLaren et al., 2004; Seinfield and Pandis, 1998*], i.e.,

$$NO_2 + O_3 \rightarrow NO_3 + O_2 \quad \text{---------- (4.1)}$$

$$NO_3 + NO_2 + M \leftrightarrow N_2O_5 + M \quad \text{---------- (4.2)}$$

$$N_2O_5(g)+H_2O(g)\rightarrow HNO_3(g) \quad \text{---------- (4.3)}$$

$$N_2O_5(p)+H_2O(p)\rightarrow HNO_3(p) \quad \text{---------- (4.4)}$$

The reaction (4.3) is considered to be very slow [*Atkinson et al., 2004; Seinfield and Pandis, 1998*]. The gaseous HNO_3 also condenses onto the particles, so does NH_3, and nitric acid on the particle reacts with NH_3 to produce NH_4NO_3 [*McLaren et al., 2004; Seinfield and Pandis, 1998*]. Higher relative humidity will favor the hydrolysis of N_2O_5 on wet aerosol surfaces. The nitrate diurnal pattern is qualitatively consistent with the diurnal variations of temperature and relative humidity. Because of its relatively high vapor pressure, ammonium nitrate shows stronger temperature dependence than most other constituents, such as ammonium sulfate and most of the oxygenated organics.

The sulfate means and upper quartiles show increased sulfate concentrations from just before noon until the late evening with minima in the morning hours (the median values peak in the late afternoon to early evening). The sulfate concentrations slightly increase with the daily increase in solar irradiance. This reflects increased photochemical production of sulfate during warm sunny afternoons [*e.g., Drewnick et al., 2004; Seinfield and Pandis, 1998*]. Lack of clear diurnal pattern in sulfate mass concentrations is suggestive of the regional scale production and transport of sulfates [*e.g., Drewnick et al., 2004*]. The lack of diurnal cycle in sulfate mass concentrations also reflects the fact that sulfate, unlike nitrate, does not partition into gas-phase [*Jimenez et al., 2003a*]. The different diurnal patterns of nitrate and sulfate not only indicate different formation mechanisms for the periods of higher concentrations of each, but they may also reflect a preference for the formation of NH_4NO_3 at lower sulfate concentrations [*Drewnick et al., 2004; Seinfield and Pandis, 1998*]. The diurnal pattern of ammonium mass concentrations tends to follow more closely that of nitrate, perhaps driven by the higher nitrate events. It is also influenced by sulfate around noon. Thus, its diurnal variation appears to be dictated by the combination of negative ion species, nitrate and sulfate. The total organic mass concentrations exhibit only a subtle diurnal variation with minimum around 4:00-5:00 pm (i.e., 17 h). This minimum is at about the same time that the sulfate

is maximized. Some key components of the particulate organics are considered in more detail in the next section.

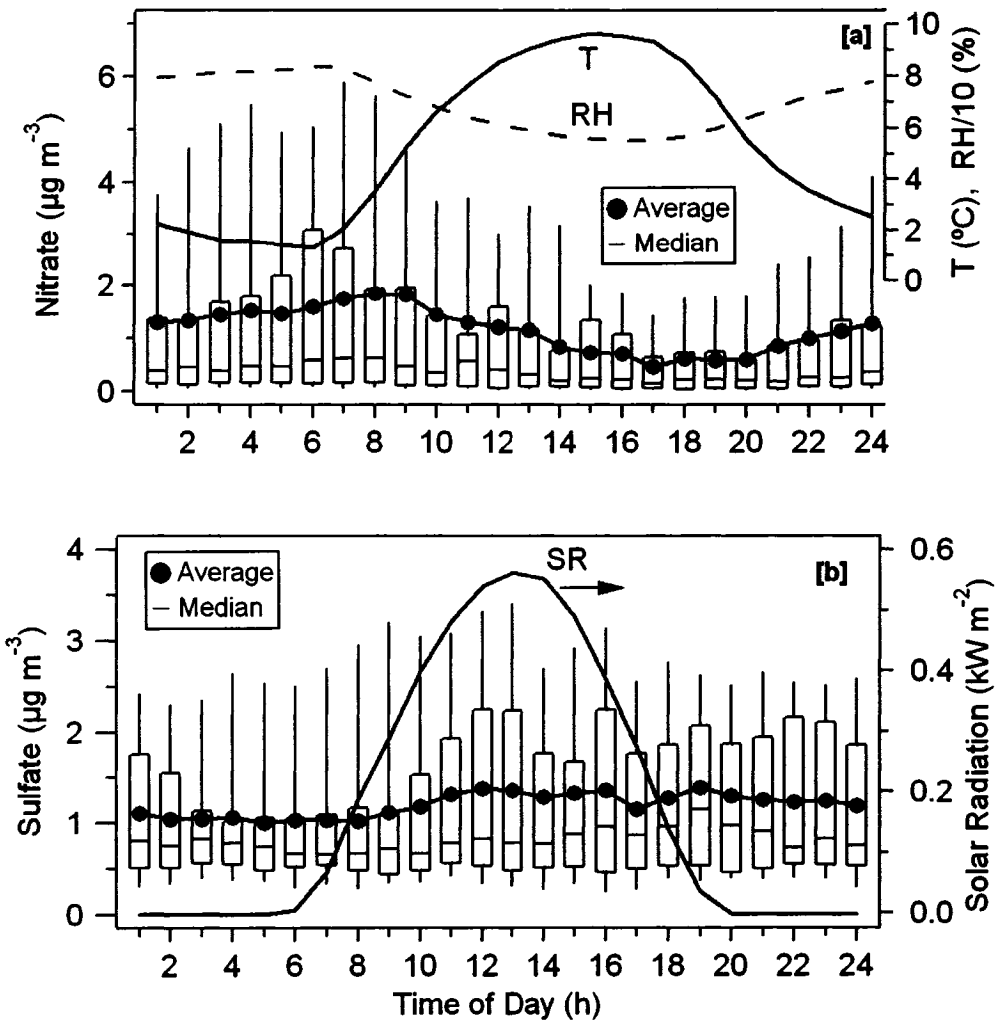

Figure 4.7 Diurnal variations of particulate (a) nitrate, (b) sulfate, (c) ammonium, and (d) organics mass concentrations measured with the AMS at Egbert, along with diurnal variations of ambient temperature (T), relative humidity (RH) and solar radiation (SR). The top and bottom of box represent the upper and lower quartiles, respectively. The top and bottom of the whisker represent 90th and 10th percentiles, respectively.

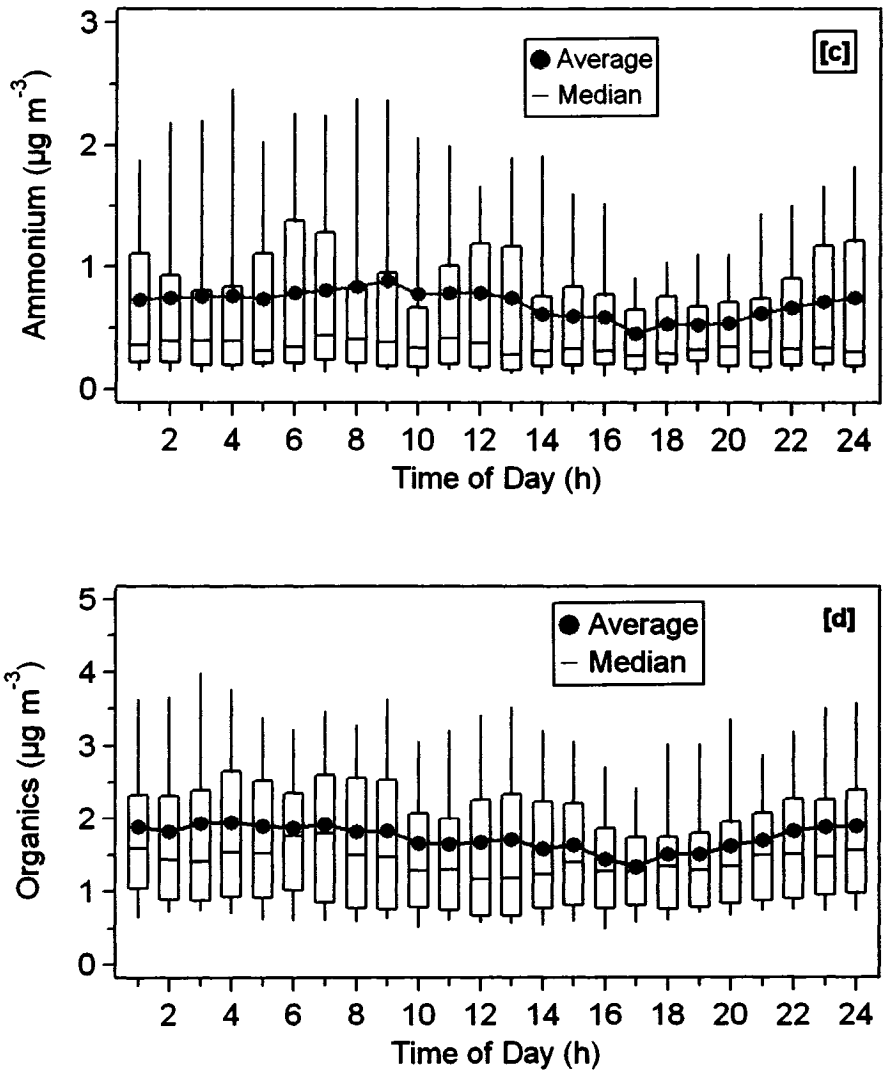

Figure 4.7 continued.

The diurnal patterns of ammonium, nitrate, sulfate and total organic mass concentrations at Toronto are also presented and compared with those at Egbert. Figure 4.8 shows the diurnal variations of particulate ammonium, nitrate, sulfate, and total organics mass concentrations measured with the AMS in downtown Toronto from August 22 to September 25. In order to avoid any bias due to an isolated smog event, the two days of smog episode at the beginning of the measurement were not included in these plots. Nitrate mass concentrations exhibit a clear diurnal cycle with higher nitrate

concentrations in the morning hours (8:00-10:00 am) and minima in the afternoon. The lower temperatures and higher relative humidities may favor the formation of ammonium nitrate during the nighttime or early morning hours. In contrast to 6:00 am -8:00 am peak in nitrate mass concentrations in Egbert, the nitrate mass concentrations peak around 8:00 am -11:00 am in Toronto. This pattern maybe associated with the increase in the morning traffic emissions under the shallow boundary layer accompanied by high relative humidities and lower temperatures that enhanced NH_4NO3 formation.

Sulfate mass concentrations do not exhibit a pronounced diurnal pattern, except for a subtle increase around noon and a gradual decrease during the night. The lack of diurnal pattern in sulfate mass concentrations, and sporadic increase in sulfate concentrations (Figure 3.1), imply that sulfate particles are produced and transported over the regional scale, rather than formed in-situ close to the site [*e.g. Drewnick et al., 2004a*]. It is also corroborated by the fact that the major SO_2 sources (mostly power plants) are located outside the city of Toronto i.e. in Southern Ontario and in the mid west United States [*Macfarlane et al., 2000*]. It is also possible that the clouds or fog influenced sulfate mass concentrations as a large portion of the total SO_2 oxidation can occur in the condensed phase [*Finlayson-Pitts and Pitts, 2000*]. Although there is no distinct diurnal pattern, ammonium mass concentrations slightly increase from around 8:00 am, maximize around 11:00 am, and remain higher until the late afternoon. The ammonium diurnal pattern follows more closely that of sulfate, but it is also influenced by nitrate in the morning. Total organic mass concentrations do not exhibit a significant diurnal change. This may reflect that the source strength of the organics (mostly traffic emissions) does not have a clear diurnal pattern. The nitrate, ammonium and total organics mass concentrations gradually increase from 6:00 am to 9:00 am, while increase in sulfate mass concentrations is subtle for the same period. However, at the same time, there is a huge increase in the total particle number concentrations (Figure 4.6). Black carbon concentrations increased during morning rush hours [*Buset et al., 2005*]. It is not surprising that change in mass concentrations is not visible in the overall mass of the organics because the small organic particles do not have enough mass to produce a substantial change to the overall organic mass.

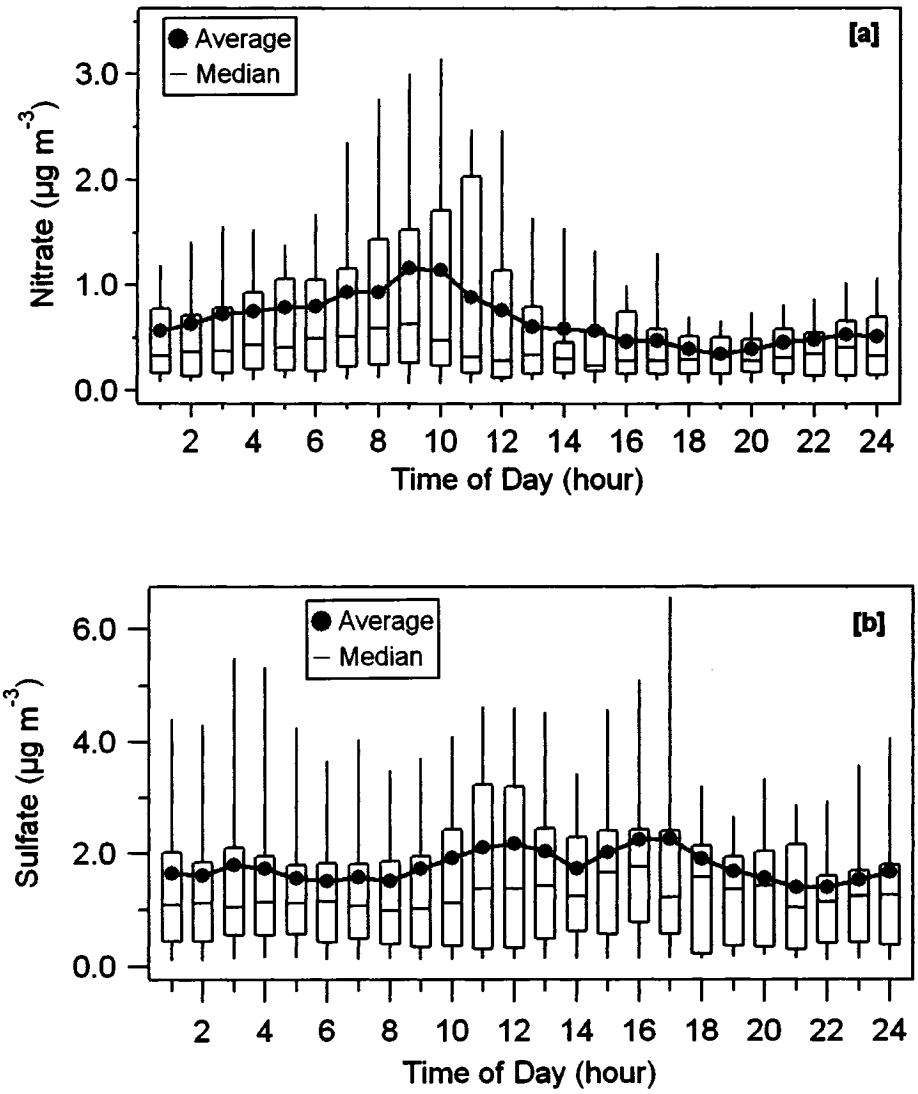

Figure 4.8 Diurnal variations of particulate (a) nitrate, (b) sulfate, (c) ammonium, and (d) organics mass concentrations measured with the AMS at the University of Toronto. In each box, The top and bottom of box represent the upper and lower quartiles, respectively. The top and bottom of the whisker represent 90th and 10th percentiles, respectively.

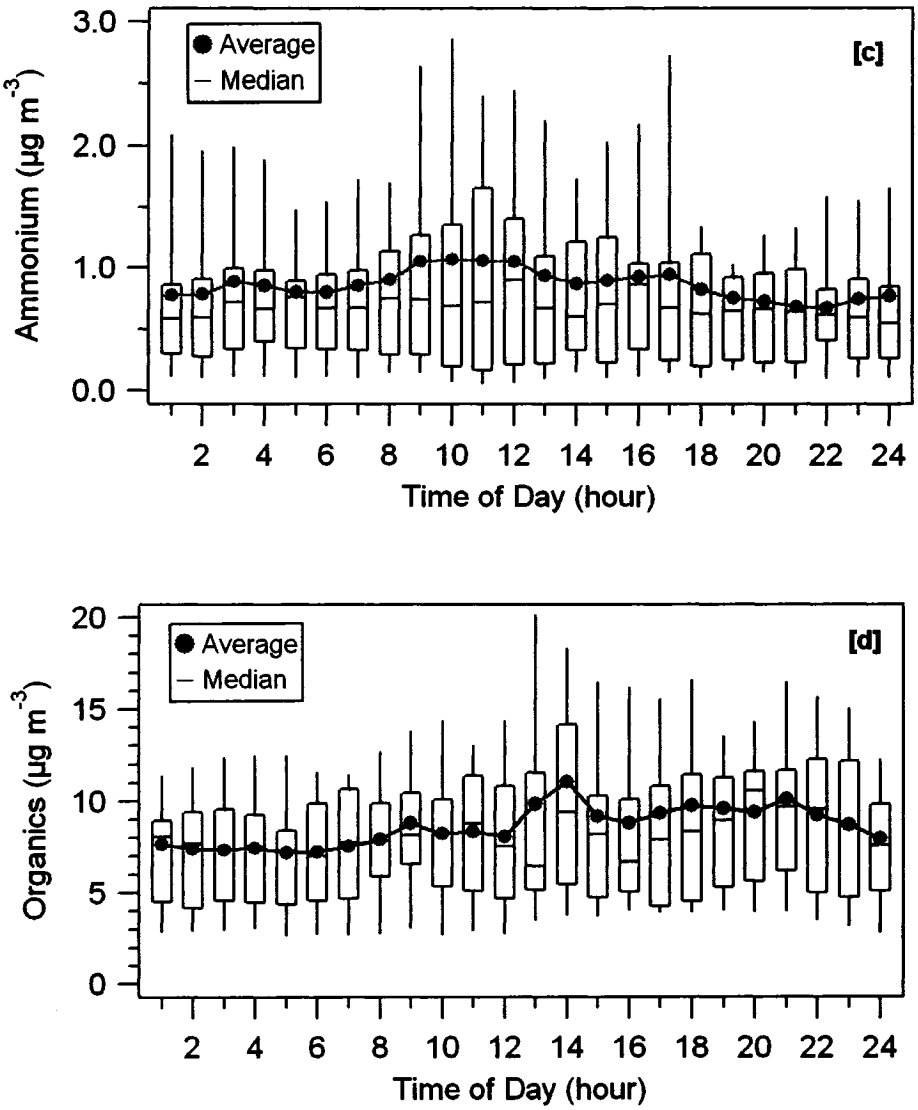

Figure 4.8 continued.

4.7 Diurnal Variations of Organic Components

Information about the general nature of particulate organics can be extracted by looking at the contributions of particular mass-to-charge ratios (*m/z*) to total organics. One should note that organic speciation into molecular levels is not possible with the AMS measurements, except identification of some types of organics present in the particles, such as the presence of oxygenated organics and hydrocarbon-like organics [*Allan et. al., 2003a, Allan et al., 2003b, Alfarra et al., 2004, Zhang et al., 2005a; Zhang et al., 2005b*].

Oxygenated organics such as di-carboxylic and poly-carboxylic acids produce intense peaks at *m/z* 44(COO^+) and 18(H_2O^+) in the AMS mass spectra due to decarboxylation of acids, while other oxygenated organics such aldehydes, ketones, alcohols and esters produce major peaks at *m/z* 43($C_2H_3O^+$), 55($C_3H_3O^+$), 29(CHO^+), 28(CO^+), and contribute minor fractions to *m/z* 44 and 18 [*Alfarra et al., 2004; Allan et al., 2003a, Allan et al., 2003b; Zhang et al., 2005a; Zhang et al., 2005b; Zhang et al., 2005c*]. The fragment *m/z* 57 (i.e., $C_4H_7^+$) arises typically from saturated hydrocarbon compounds chiefly from combustion sources, and the contribution of oxidized organics to *m/z* 57 is negligibly small [*Alfarra et al., 2004; Allan et al., 2003a; Allan et al., 2003b; Drewnick et al., 2004*]. The *m/z* 43 fragment also contains contributions from saturated hydrocarbon compounds ($C_3H_7^+$).

The previous studies have found a strong positive correlation between *m/z* 57 and particulate elemental carbon (EC), as well as gaseous CO and NO_x, all well-known markers for combustion exhaust [*Zhang et al., 2005a*]. The linear covariances of the ratio *m/z* 57/total organics with gas-phase organic species concentrations were strongly positive for several short-lived anthropogenic gaseous NMHCs concentrations such as ethylbenzene and toluene [*Allan et al., 2004*], and anti-correlated with oxidized organic compounds such as carbonyls [*Allan et al., 2004*]. In contrast, the ratio *m/z* 44/total organics was strongly correlated with gas-phase oxidized organic compounds such as carbonyls whose major sources are gas-phase oxidation, and anti-correlated with gas phase hydrocarbons with only direct emission as source [*Allan et al., 2004; Zhang et a., 2005a*]. In the urban Tokyo, the fragment *m/z* 44 measured with the AMS has been found strongly positively correlated with the water-soluble organic carbon (WSOC) measured with the PILS (particle-into-liquid sampler), the *m/z* 44 accounting for nearly 45% of WSOC for all seasons [*Kondo et al., 2006*]. Thus, the organic fragment *m/z* 44 can be used as marker for the particulate oxygenated organic aerosol (OOA), which tends to be higher in processed aerosols, and the fragment *m/z* 57 as an indicator for particulate hydrocarbon-like organic aerosol (HOA), which is generally higher in less processed

aerosols likely primary aerosol from relatively fresh emissions [*Alfarra et al., 2004; Allan et al., 2004; Zhang et a., 2005a; Zhang et a., 2005b*].

A few statistics of the fraction of particulate organics at *m/z* 43 (i.e., *m/z* 44/total organics), *m/z* 44 (i.e., *m/z* 44/total organics) and *m/z* 57 (i.e., *m/z* 57/total organics) during the entire sampling period are given in Table 4.1. The ratio *m/z* 44/total organics, which indicates the degree of oxygenation of particulate organics, was 0.07 (± 0.02) at Egbert, while it was 0.06 (± 0.02) at Toronto. The *m/z* 44/total organics ratios at other sites, for example, Langley (rural, 0.11), Sumas (semi-rural, 0.09) and Slocan Park (urban, 0.07) in Vancouver[1], Canada, Mexico City, Mexico (urban, 0.08), Pittsburgh, USA (aging urban pollution, 0.08), ACE Asia (East Asian continental outflow, 0.13), Jungfrauhoch, Switzerland (free troposphere, 0.14), indicate that *m/z* 44/total organics ratio for Egbert is similar to that of urban or aging urban aerosol. The correlations among gas-phase non-methane hydrocarbon compounds (NMHCs) and particulate oxygenated organic aerosols (OOA) and hydrocarbon-like organic aerosols (HOA) will be discussed in the next section.

The diurnal patterns of the fragments *m/z* 44 and *m/z* 57 are given in Figures 4.9a and 4.9b, respectively. The particulate hydrocarbons as represented by *m/z* 57 exhibit a diurnal pattern with slightly higher values during the nighttime and lower values in the afternoon. This may be due to increase in anthropogenic activities in the morning hours around the site, as well as increase in boundary layer mixing height in afternoon that dilutes the pollutants and decrease in mixing heights during night time and early morning that help accumulate pollutants. There is a highway at about 3 km to the east of the sampling site. In contrast, the particulate oxygenated organic represented by *m/z* 44 mass concentrations does not exhibit a clear diurnal pattern. The *m/z* 44 slightly increases around noon despite dilution due to increasing mixing height.

[1] The AMS data for Vancouver was provided by M.R. Alfarra provided, and the data for other sites were taken from a presentation by D.R. Worsnop at the Fifth AMS Users' Meeting at Georgia Institute of Technology Atlanta, October 8-12, 2004.

Lack of a clear diurnal pattern in *m/z* 44 mass concentrations suggests that the production and transport of (secondary) oxygenated organics take place over a regional scale. Since the sulfate mass concentration is higher in afternoon due to increased photochemical oxidation of SO_2 by OH to sulfate, and the fact that *m/z* 44 correlates well with sulfate (r = 0.63), some organics, may be both in the gas-phase and in the particle-phase, are also oxygenated during daytime when photochemistry is intense. However, *m/z* 44 correlates positively also with nitrate (r = 0.57), and nitrate mass concentration is higher during dark hours, it is possible that some organics are oxygenated during nighttime possibly due to nitrate chemistry.

Besides the chemistry, the diurnal evolution of the boundary layer mixing height influences the pollutant (absolute) mass concentrations. The fragment *m/z* 44 and total organics should dilute in the same fashion, and thus the ratio *m/z* 44/total organics experience minimum effect of dilution. The diurnal pattern of this ratio, i.e., the oxygenated fraction is shown in Figure 4.9c. Now, the oxygenated fraction in the organics exhibits a more pronounced diurnal pattern. The oxygenated fraction gradually increases from 8:00 am, maximizes about noon and remains elevated during the afternoon hours. Note that this ratio (*m/z* 44/total organics) may increase slightly in afternoon due to the lower mass concentrations of total organics. However, there is only little diurnal variation in the average mass concentration of total organics diurnally (Figure 4.7d). The pattern of *m/z* 44/total organics follows closely that of the solar irradiance, suggesting photochemical production of the oxygenated organics. The increase in *m/z* 44/total organics is also similar to that of sulfate, except that the rise in *m/z* 44/total organics appears to begin earlier than that of sulfate. Although the assessment of an earlier rise in *m/z* 44 must be considered cautiously, such a difference may indicate a more important role of the development of the boundary layer in the sulfate variation.

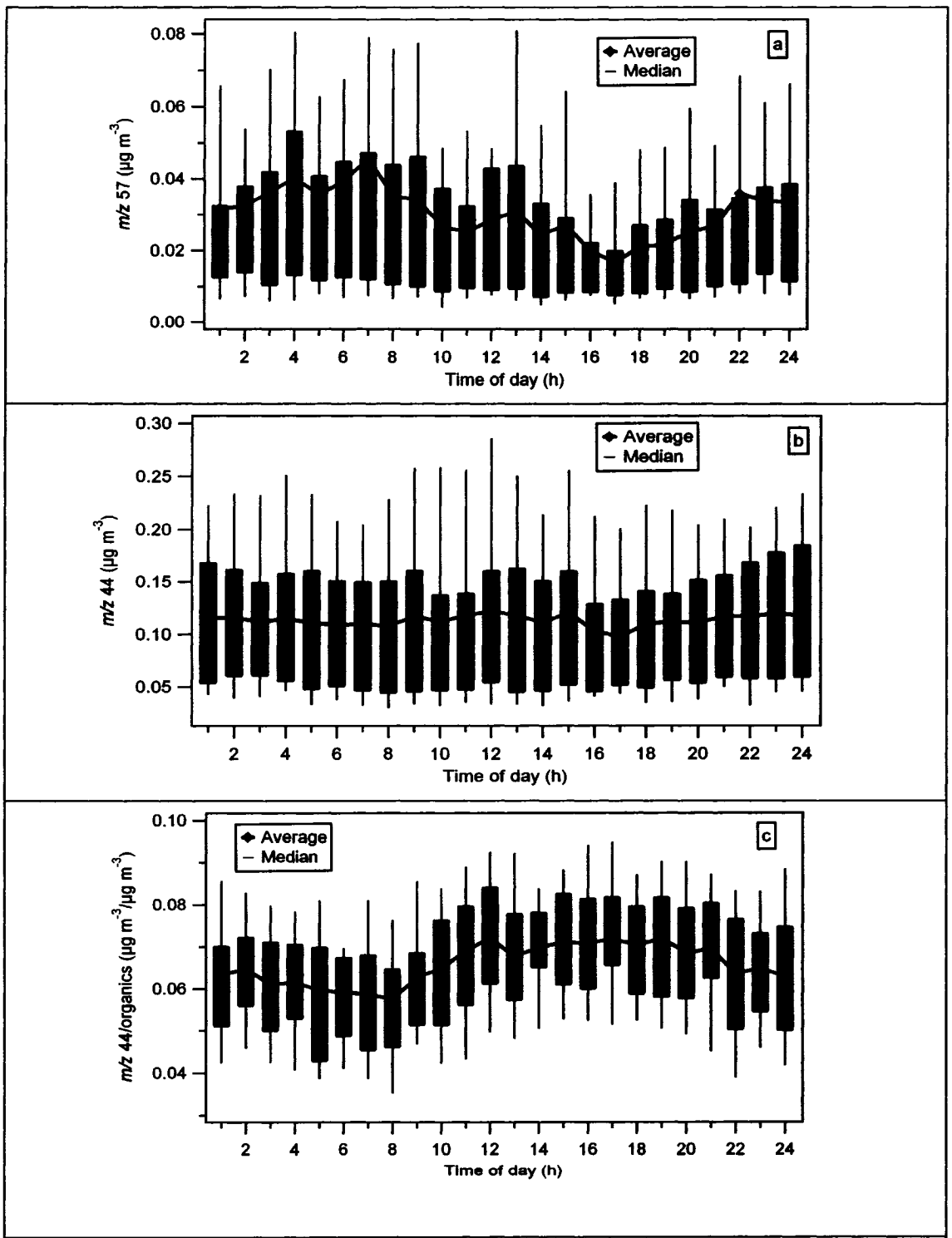

Figure 4.9 Diurnal patterns of particulate mass concentrations of (a) *m/z* 57 (a marker for hydrocarbon-like organics) and (b) *m/z* 44 (a marker for oxygenated organics), and (c) a fraction *m/z* 44/total organics for the entire sampling period. In each box, the top and bottom of box represent the upper and lower quartiles, respectively. The top and bottom of the whisker represent 90^{th} and 10^{th} percentiles, respectively.

As displayed in Figure 4.10, the averages of *m/z* 57/total organics ratios for the urban aerosol showed a slight increase during the morning rush hour, coincident with the increase in black carbon mass concentrations [*Buset et al., 2005*].

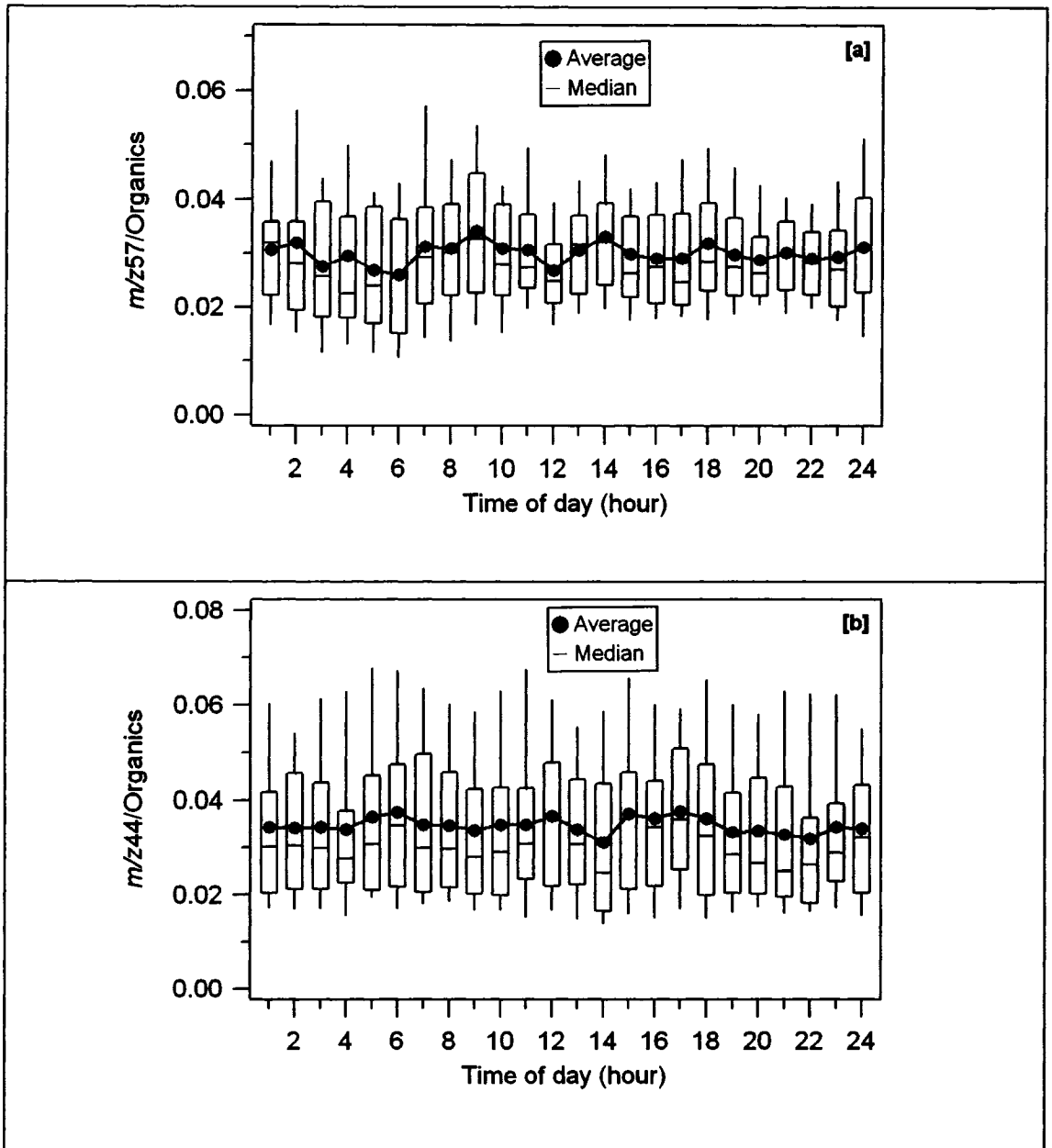

Figure 4.10 Diurnal patterns of fractions (a) *m/z* 57/total organics and (b) *m/z* 44 *m/z* 44/total organics for the entire sampling period (first 2 days excluded) in Toronto. In each box, the top and bottom of box represent the upper and lower quartiles, respectively. The top and bottom of the whisker represent 90th and 10th percentiles, respectively.

The averages of *m/z* 44/total organics ratios did not exhibit a clear diurnal pattern. The ratios *m/z* 57/organics and *m/z* 44/organics showed opposite patterns at least during the day, implying that the particulate hydrocarbons tend to be higher in the fresh emissions. The lack of diurnal patterns in the ratio *m/z* 44/total organics indicates that the atmospheric conditions were not conducive to secondary organic aerosol formation as the particles as well as gaseous pollutants were recently emitted. Highly oxygenated organics are of regional origin, and thus show little diurnal pattern [*Zhang et al., 2005b,c*].

4.8 Particulate Organics and Gas-phase NMHCs

As mentioned earlier, the previous studies found that the particulate organic fragment at *m/z* 57 measured with the AMS correlated significantly positively with particulate elemental carbon (EC), as well as gaseous CO and NO_x, all well-known markers for combustion exhaust [*Zhang et al., 2005a*]. Furthermore, the linear covariances of the ratio *m/z* 57/total organics with gas-phase organic species concentrations have been found strongly positive for several short-lived anthropogenic gaseous NMHCs concentrations such as ethylbenzene and toluene [*Allan et al., 2004*], and anti-correlated with oxidized organic compounds such as carbonyls [*Allan et al., 2004*]. In contrast, the ratio *m/z* 44/total organics was strongly correlated with gas-phase oxidized organic compounds such as carbonyls whose major sources are gas-phase oxidation, and anti-correlated with gas phase hydrocarbons with only direct emission as source [*Allan et al., 2004; Zhang et a., 2005a*]. This indicates that the particulate hydrocarbons are most likely emitted in the form of primary organic aerosols from fresh emissions such as traffic emissions, and the particulate oxygenated organics increase during periods of high aging in the gas-phase [*Alfarra et al., 2004; Allan et al., 2004; Zhang et a., 2005a*].

Time series and mass size distributions of these key organic fragments provide important information on the nature of organic aerosol such as the qualitative information on degree of atmospheric processing. Figure 4.11 shows the time series of the mass concentrations of total particulate organics, *m/z* 44 and *m/z* 57 as well as gas phase mixing ratios of some non-methane hydrocarbon compounds (NMHCs) and O_3 for the entire sampling period. Increases in total organic particulate matter coincide with increases in the various gas-

phase NMHCs. The traffic emissions are the major source of atmospheric NMHCs, such as ethane, benzene, toluene and ethylbenzene [*Seinfeld and Pandis, 1998*]. The atmospheric lifetime of ethylbenzene, propene, m-xylene, toluene and ethane due to reaction with OH is approximately 2.6 h, 6 h, 7 h, 2.4 days and 30 days, respectively, for an ambient OH concentration of 1.5×10^6 molecules cm^{-3} [*Seinfeld and Pandis, 1998*].

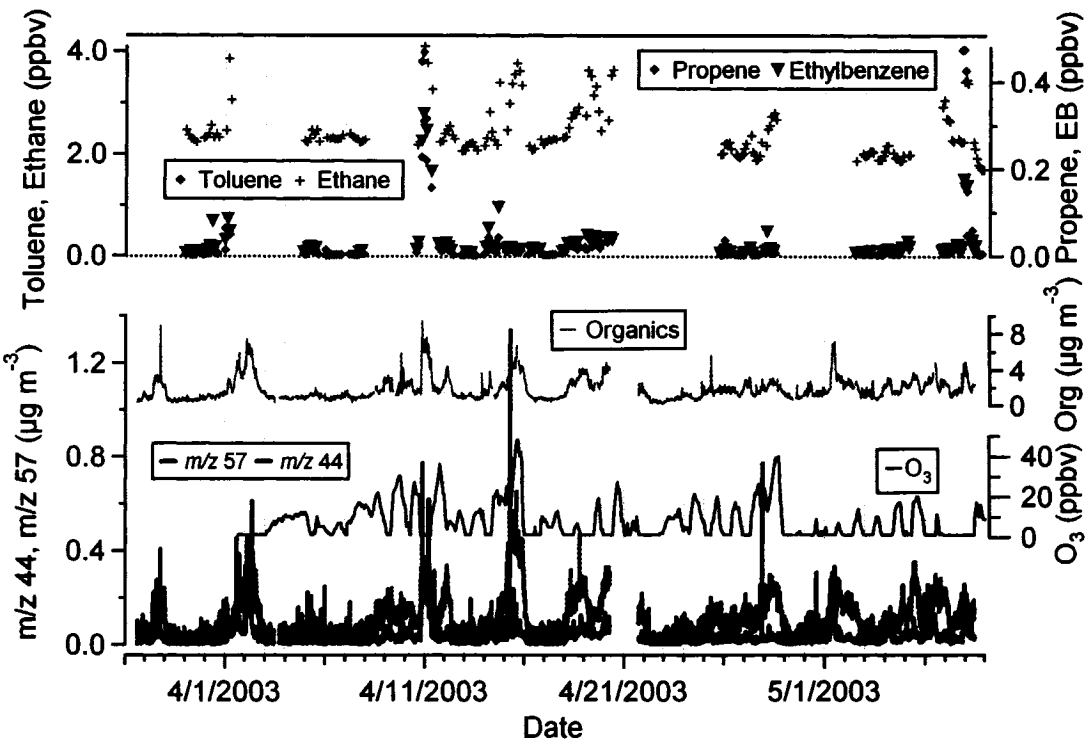

Figure 4.11 Time series of particulate total organics, and organics contributing to *m/z* 57 (an indicator for hydrocarbon-like organic aerosol, HOA) and *m/z* 44 (an indicator for oxygenated organic aerosol, OOA) reported by the AMS, and gas-phase mixing ratios of some select NMHCs and ozone. EB indicates ethylbenzene and 'Org.' indicates total organics.

There are several particulate hydrocarbon events (i.e., higher *m/z* 57). Those events tend to be shorter in duration than the periods with higher oxygenated organics (i.e., *m/z* 44) that tend to persist for several hours, sometimes 1-2 days. There is a hydrocarbon event over the night of April 10 through morning of April 11 with relatively high gas phase mixing ratios of several hydrocarbon compounds, including ethylbenzene, propene and toluene and very low O_3. This event and others with sharp increases in ethylbenzene,

propene and toluene coincide with higher *m/z* 57 relative to *m/z* 44 in the AMS time series. The April 10-11 increase of the *m/z* 57 mass concentration with higher NMHCs and lower O_3 (most likely due to titration by NO) suggests common emission sources, such as traffic, with relatively little chemical processing. Periods with higher *m/z* 44 (e.g., April 8-9, 15, 28) show no peaks in short-lived NMHCs (e.g., ethylbenzene, toluene) but peaks in ethane. The April 15 event is notable because the values of *m/z* 44, ethane and O_3 are highest during the sampling, as is the ratio of the *m/z* 44 mass concentrations to the total organic mass concentrations. Thus, the aerosol during this period is perhaps the most chemically processed of any during this study.

The organic mass loading in the small mode of the organics (< 200 nm) was occasionally significant at Egbert when urban air masses affected the site. In the previous urban studies, it has been found that the small organic mode, where present, correlated significantly with CO and NOx, both emitted primarily from the combustion sources, whereas the accumulation mode organics were much more strongly correlated with O_3 and PAN (peroxyacetyl nitrates) [*Alfarra et al., 2004, Allan et al., 2003a, Allan et al., 2003b*]. Figure 4.12 shows strong positive correlations between the mass concentrations of organics in small mode (<200 nm) and several gas-phase NMHCs, pointing to fossil fuel combustion-related emission as the source of the smaller organic particles [*Alfarra et al., 2004; Allan et al., 2003a; Drewnick et al., 2004*]. Figure 4.12 also includes correlations between the several NMHCs and the ratios of *m/z* 57 to total organics, as well as the ratios of *m/z* 44 to total organics. The strong positive correlations of the various NMHCs with *m/z* 57/total organics suggest common sources, whereas the anti-correlations with *m/z* 44/total organics indicate further oxidation of hydrocarbons as the aerosol is processed.

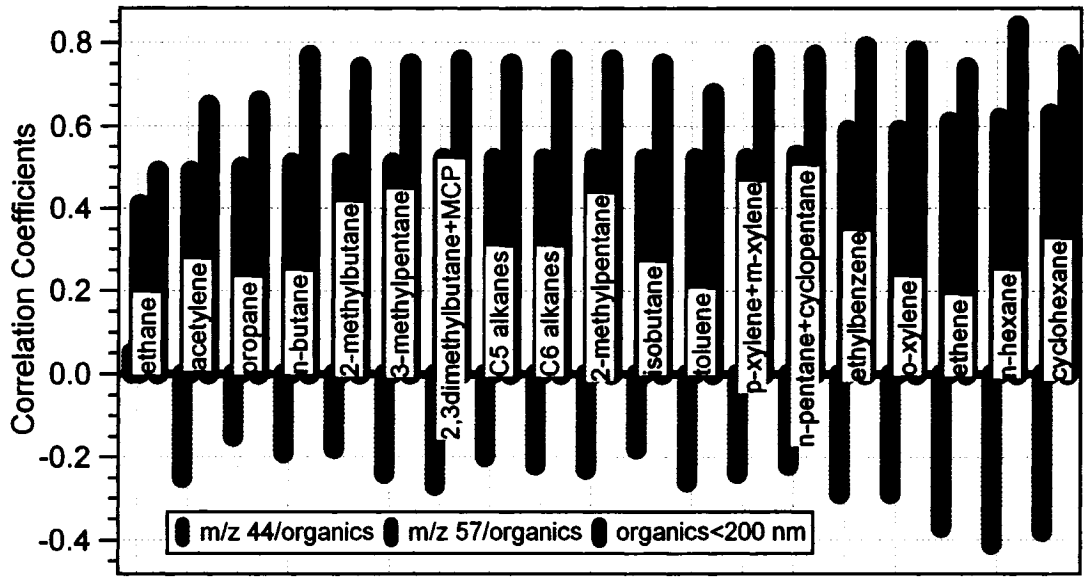

Figure 4.12 Correlations between the mass concentrations of organics in small particles (<200nm) and mixing ratios of the gas-phase non-methane hydrocarbon compounds. The correlations between those NMHCs and particulate *m/z* 57/organics and *m/z* 44/organics are also included.

4.9 Two Case Studies: Contrasting Relatively Less Processed aerosol with Aged Aerosol

Two periods are selected for more detailed examination of the size distributions of total organics and some key organic fragments, as well as inorganic components during these periods:

- Event 1 (April 10, 7:45 pm - April 11, 11:00 am) with higher nitrate and organics, and lower sulfate.
- Event 2 (April 15, 10:00 am - 9:00 pm) with higher organics and sulfate, and lower nitrate.

Event 1 and event 2 also mark the higher levels of particulate hydrocarbons and highest oxygenated organics, respectively.

4.9.1 Event 1 - April 10, 7:45 pm - April 11, 11:00 am

The average ambient temperature and relative humidity during this event were 3.5°C (min = -1.3°C, max. = 13°C) and 60% (min = 40%, max = 78%), respectively. The total particle number concentrations (>3 nm) were in the range of 6,000 - 10,800 cm^{-3}. The mixing ratios of several NHMCs increased. Particulate nitrate makes the largest contribution to the fine particle mass fraction followed by organics, ammonium and very low sulfate (Figure 4.1, Figure 4.13a). During this and other nitrate events, the O_3 concentrations drop near zero. It is likely that O_3 was titrated by NO ($NO + O_3 \rightarrow NO_2$) near the source and advected to the site as such. Being overnight, there was no significant production source to replenish the O_3. Lower temperatures, relatively higher levels of NH_3 and remarkably low concentrations of sulfate perhaps created environment favorable for NH_4NO_3 formation. Figure 4.13a illustrates that nitrate and ammonium both have dominant mass distributions at a modal vacuum aerodynamic diameter of ~ 225 nm.

According to Figure 4.13a, the nitrate was more coincident with the smaller organic particles, suggesting that NH_4NO_3 may have condensed onto pre-existing organic particles. The sulfate is also unimodal peaked about 500 nm. Organics have a distinct mode at about 200 nm D_{va}, a bit smaller than the nitrate peak and a second mode coincident with the sulfate peak and a secondary peak in the nitrate mass. Assuming that the available particulate ammonium neutralizes all sulfates before neutralizing nitrate it is found that there is excess nitrate in the size range between 170 nm to 350 nm, coinciding with the organic mass distribution peak. There are at least two possible explanations for this: 1) the unneutralized nitrate is due to the absorption of HNO_3 or N_2O_5 by the aqueous particles, or 2) the excess nitrate is from organic nitrates.

The particles smaller than 100 nm appear to be mainly externally mixed organics. The presence of the high small particle mass during this event and the elevated levels of short-lived anthropogenic NMHC, such as ethylbenzene, propene, toluene among others [*Seinfeld and Pandis, 1998*], indicate that the sampling site was indeed impacted by relatively recent anthropogenic emissions. Figure 4.13a also includes the back trajectories of the air mass that arrived at the site at 4:00 am on April 11 at two heights (250 m and

1000 m). It manifests the anthropogenically influenced aerosol, as the air mass appears to have come from northern Canada to near Toronto and then looped to the north arriving at the Egbert site after spending significant time over urban areas. The back trajectory was computed from the HYSPLIT4 (Hybrid Single Particle Lagrangian Integrated Trajectories) model [*Draxler and Rolph,* 2000] with EDAS (Eta Data Assimilation System) data as meteorological inputs (*www.arl.noaa.gov/hysplit.html*).

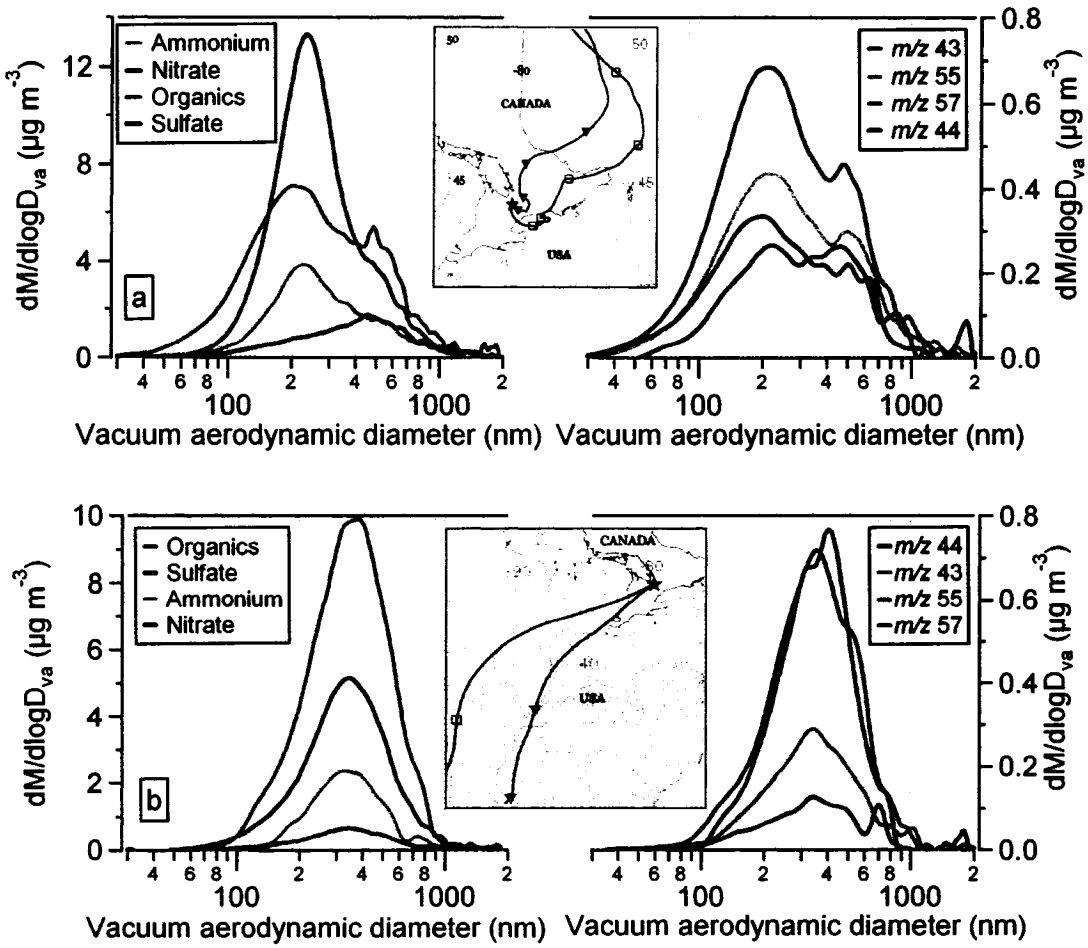

Figure 4.13 Mass size distributions of particulate ammonium, nitrate, sulfate, and organics during the two different events on (a) April 10-11 and (b) April 15 as described in the text. Mass distributions of selected key organic mass fragments are also included. Typical air mass back trajectories (red: 250 m and blue: 1000 m, and two marks along trajectory represent 24 h interval) for these events are also displayed.

Figure 4.13a also includes the mass distributions of some key organic fragments, *m/z* 44 (oxygenated organics), *m/z* 57 and *m/z* 55 (typically hydrocarbons), and *m/z* 43 (both). The fragment *m/z* 44 is bimodally distributed with a relatively higher concentration in the larger mode whereas the other three fragments are preferentially higher in the small mode. Particles smaller than ~80 nm appear to be externally mixed organic particles containing mostly hydrocarbons. This implies that the aerosol is more oxidized in the larger mode compared with the smaller mode.

The trajectory analysis and the chemical size distribution data suggest the following explanation for the presence of the two major modes in the aerosol. There is no major local anthropogenic source, other than agricultural activities. Ammonia emission is also low in northern regions due to cold temperatures. Most of the sulfate and organics in the larger mode at about 500 nm were, therefore, very likely present earlier in the history of this air parcel before it reached southern Ontario. Then, anthropogenic sources in the vicinity of Toronto were responsible for the addition of smaller primary organic particles and NO_x that eventually, in the presence of local NH_3 as well as increased relative humidity, led to relatively local formation of the nitrates in both the smaller and larger modes. Since the smaller organic aerosols were present in the urban outflow, the nitrate condensed on those particles because those particles provided a large surface area.

4.9.2 Event 2 - April 15, 10:00 am - 9:00 pm

The ambient air was relatively warmer and drier during this event than during event 1 with an average temperature of 25.6°C (min. = 18.3 °C, max. = 28.3°C) and an average relative humidity of 38% (min = 32%, max = 58%). The total particle number concentration varied between 7,600 and 20,000 cm^{-3} and the O_3 concentration remained higher throughout the event. Only NMHCs with longer atmospheric lifetime (e.g. ethane, propane) were measured. The organics make the largest contribution to the submicron mass followed by sulfate and ammonium (Figure 4.13b). Nitrate is relatively low. The warmer temperatures and lower relative humidities appear to be unfavorable condition for particulate nitrate formation; the warmer temperatures on April 14 and 15 preferred the gas-phase particle-phase partitioning towards ammonia. The back trajectories show

that the air mass passed over urban and industrial regions to the southwest before arriving at the site.

The particulate organics, sulfate, ammonium and nitrate were most likely internally mixed as these four constituents exhibit very similar unimodal mass distributions with modal diameters around 350 nm (Figure 4.13b). In both an absolute and relative sense, the fraction of oxygenated organics in the particles (*m/z* 44) is much higher than during event 1, and *m/z* 57 remains very low during this event, indicating that the aerosol arriving at Egbert was much more chemically processed during this event than the previous one.

Chapter 5

Aerosols from the North and the South

5.1 Data Classification: Aerosols from the North and the South

The data set is classified into groups: aerosol from the north and aerosol from the south. The purpose of classifying the data into two categories is to investigate the physical properties and chemical composition of atmospheric aerosols in two different conditions, and get insights into the possible sources and processes governing their formation and transformation. Of particular interest are exceptionally high nitrate mass concentrations observed in Egbert when the site is exposed to relatively fresh urban emissions advected by southerly flows, and the sources and nature of particulate organics during northerly flows, which were mostly associated with clean air from the north (Figure 5.1).

The data set is classified into two groups based on three parameters:

a. local wind direction,
b. gas-phase NO mixing ratios measured at the site (i.e., at CARE), and
c. air mass back trajectories.

The local wind direction is used simply to separate winds from the north, where there are fewer local and regional sources, versus winds from the south with more significant sources particularly on the regional scale. As gas-phase NO_x ($NO + NO_2$) measurements at CARE were not available for the study period, gas-phase NO mixing ratio was used as an identifier for the polluted air mass with relatively recent (anthropogenic) emissions arriving at the site. The increases in NO mixing ratios were associated with increases in several gas-phase NMHCs mixing ratios, including those of anthropogenic origin, such as toluene, n-butane, ethylbenzene, acetylene. The air mass back trajectories arriving at

three heights (250 m, 500 m and 1000 m above the ground) at the site at a given hour were computed with the HYSPLIT4 (HYbrid Single Particle Lagrangian Integrated Trajectories) model [*Draxler and Ralph, 2000*] using EDAS (Eta data assimilation system) data as meteorological inputs (www.arl.noaa.gov/hysplit.html). In addition to the separation into two groups, air trajectories were used to explore the origins and histories of air masses, and to estimate approximate transport time from the major pollution sources (e.g., cities). The classification was carried out as described below.

5.1.1 Aerosol from the South

A data point is classified as one associated with a southerly air mass if one of the following criteria is satisfied.

a. local wind direction and air mass trajectories fall entirely within 90° and 270° (i.e., southerly), the NO mixing ratio exceeds 1.0 ppb.
b. the air mass originates in the south (i.e., south to the site), passes over urban areas although it approaches the site from the north (wind sectors 0-90° and 180-360°), or the air mass originates in the northern regions but passes over the urban areas to the south or east, and finally approaches the site locally from south (90-180°), and both cases accompanied by increase in NO mixing ratios above 1.0 ppb.

Thus, the 'aerosol from the south' classified in this fashion is associated with the air masses advected from urban and industrial areas of southern Ontario and Quebec (e.g., Toronto, Ottawa, Montreal), and the mid-west and northeastern United States (e.g., Ohio Valley, New York etc.), and mostly represents the pollution events observed at Egbert.

5.1.2 Aerosol from the North

The aerosol observations were classified as 'aerosol from the north' that satisfy the following conditions,

a. local wind direction: within wind sectors 0-90° and 270-360° (i.e., northerly), the air trajectory falls entirely within those wind sectors, and the NO mixing ratios $\leq$ 1.0 ppb

b. periods with precipitation or right after precipitation with low NO mixing ratios are also considered as clean periods.

The northwesterly air trajectories sometimes passed directly over the Sudbury region, an industrial area with nickel smelters noted for higher SO_2 emission, about 300 km to the northwest. This resulted in sharp but brief rises in sulfate mass concentrations at Egbert. These are classified as 'aerosol from the north with Sudbury influence'. The physical and chemical characteristics of aerosols during Sudbury influence are described later.

Figure 5.1 shows the time series of particulate ammonium, nitrate, sulfate and total organic mass concentrations for the southerly flows and northerly flows. Included in Figure 5.1 are time series of local wind direction (WD), ambient temperature (T), relative humidity (RH), mixing ratios of NO and toluene. In Figure 5.1e, the letter 'S' represents the periods with higher sulfate mass concentrations, which are associated with air trajectories that passed directly over the Sudbury region. Likewise, 'p' represents periods with daily precipitation ≥ 4.5 mm, and 'H' represents the periods when a high-pressure system developed in the Canadian Arctic and moved south, likely bringing the Arctic air masses to the sampling site at Egbert. The nitrate events and sulfate events were clearly separated into two groups; nitrate events were associated with southerly winds, while sulfate events were associated with winds from the north. Figure 5.2 contrasts the average particulate composition between clean and polluted periods. The averages of ammonium, nitrate, sulfate and organic mass fractions contributing to total particulate mass for the aerosol from the north (direct influence of Sudbury emissions excluded) were 12%, 8%, 34% and 46%, respectively. In contrast, the averages of those fractions in the aerosol from the south were 14%, 25%, 21% and 40% for ammonium, nitrate, sulfate and organics, respectively, indicating that organic material contributes a large fraction to total particulate mass in both cases, and contribution of nitrate was significantly higher in the aerosol from the south. The ratio of the molar concentrations of particulate ammonium to sulfate and nitrate [i.e., $a = NH_4^+ / (2SO_4^{--} + NO_3^-)$], which was used as a measure of aerosol acidity, indicates that the aerosols from the north were slightly more acidic [average a = 0.82 (SD = 0.33), median a = 0.81] than aerosols from the south [average a

= 0.93 (SD = 0.17), median a = 0.92]. The origin of high organic mass concentrations in aerosols from the north, and relatively clean periods, is of particular interest. Likewise, the formation exceptionally high nitrate mass concentrations associated with southerly wind requires further investigation.

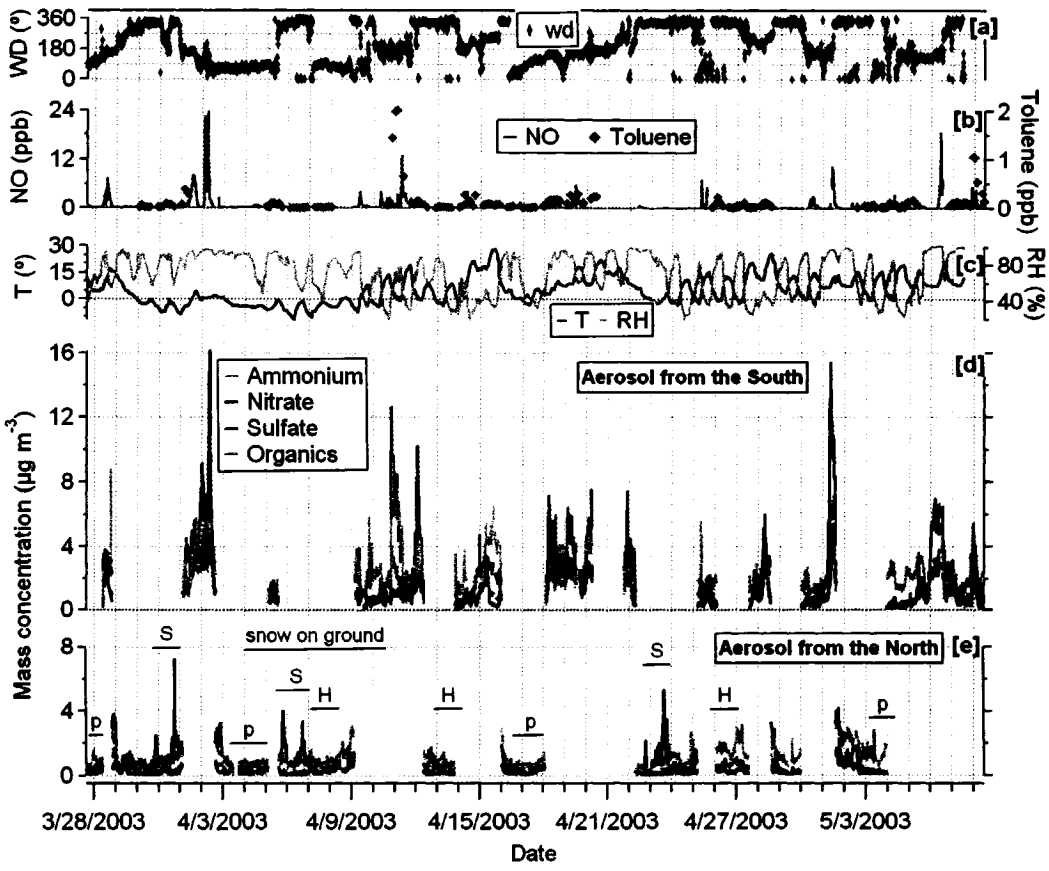

Figure 5.1 Time series of (a) local wind direction (WD), (b) mixing ratios of gas-phase NO and toluene, (c) ambient temperature (T), ambient relative humidity (RH), and particulate ammonium, nitrate, sulfate and total organic mass concentrations measured with the AMS for (d) southerly flows and (e) northerly flows during the sampling period. See the text for the meaning of letters 'S', 'H' and 'p'.

As will be discussed later, the effects of atmospheric processing of the aerosol particles were studied with the use of photochemical ages of air masses that arrived at the site. The photochemical age of the aerosol particle composition was estimated from the gas-phase mixing ratios of two anthropogenic NMHCs, benzene and toluene [*de Gouw et al.*,

2005; McFiggans et al., 2005; Roberts et al., 1984]. The photochemical age of the air masses from the south (mostly polluted urban/industrial emissions) ranged between about 1 h and 105 h, while that for the northerly air masses were between 48 h and 140 h, implying that the aerosols in the clean air were more processed.

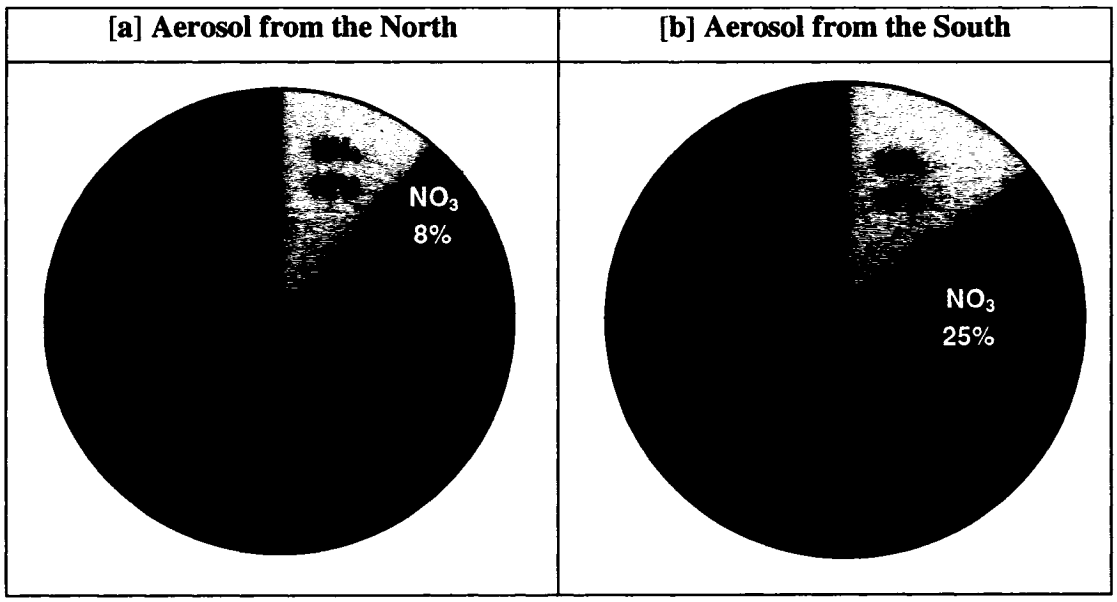

Figure 5.2 The averages of ammonium, nitrate, sulfate and total organic mass fractions contributing to total particulate mass measured with the aerosol mass spectrometer (AMS) at CARE for (a) aerosol from the north and (b) aerosol from the south during the sampling period.

5.2 Aerosol from the North

There is a gradual increase in particulate organic mass concentrations of the aerosol from the north after April 22. This trend is demonstrated in Figure 5.3. This gradual but noticeable increase in organics in the aerosol from the north (i.e., clean periods) exhibits a unique trend. Is this gradual increase in organics associated with increases in biogenic emissions? Biogenic organic emissions from trees and grass, and from soil may have been enhanced by increases in ambient temperature, solar radiation, loss of snow cover on the ground, and possibly decay of organic materials on the ground. Although the influence of anthropogenic emissions has been removed as much as possible with the aforementioned classification scheme, anthropogenic organics must still contribute some fraction to the particulate organics.

Figure 5.3 show time series of total particulate organic mass concentrations for the aerosols from the north, which are associated with the clean periods. Included in the figure are time series of ambient temperature for the entire sampling period and gas-phase NH_3 concentrations from the filter pack analysis for those days with northerly air masses. The solid black line in each panel represents the trend line that parameter. It is evident that all three parameters show increasing trend with time.

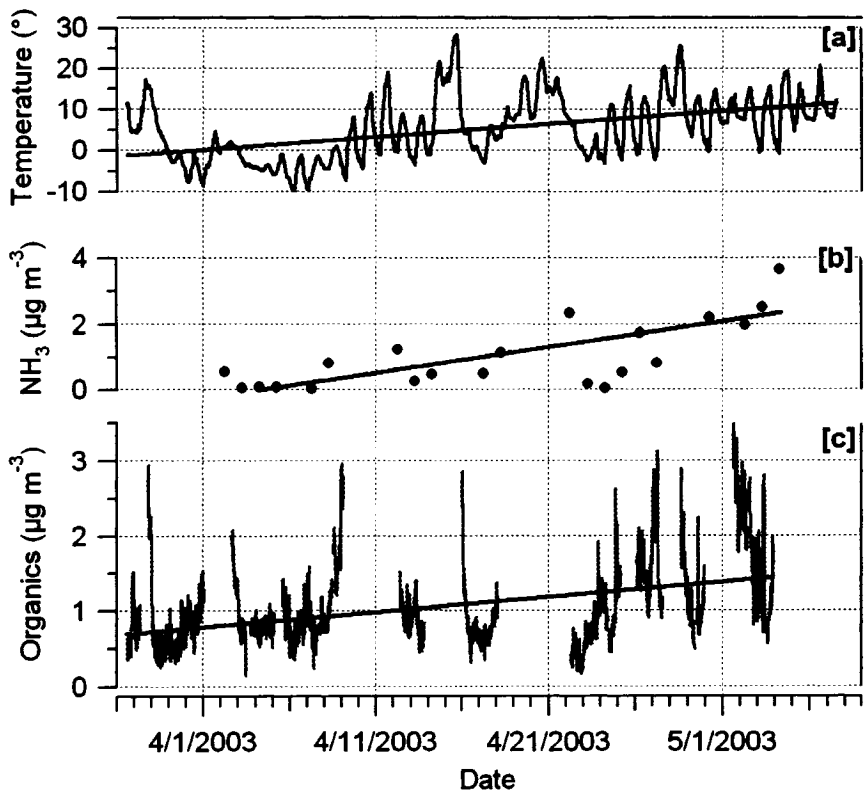

Figure 5.3 Time series of (a) ambient temperature for the entire sampling period, (b) gas-phase NH_3 concentrations from the filter pack analysis for the days with northerly air masses, and (c) total particulate organic mass concentrations for aerosol from the north. The solid black line in each panel represents the trend line.

Therefore, it is likely that the increase in ambient temperature enhanced the microbial activities in the soil and hence the emission of ammonia and organics. *Bigg* [2001] discuss the role of melting snow on the ground in modulating the emissions from the soil

of the aerosol precursors from decomposition of organic material. The process requires liquid water, which means that the strongest contribution would be when the snow cover is melting. Higher gas-phase NH_3 concentrations may be associated to agricultural activities as well. The increase in particulate total organics may also be associated with emissions of reactive biogenic hydrocarbons from growing trees, grass and microbes in the soil, augmented by higher temperatures. Isoprene, which is a reactive hydrocarbon and a marker for biogenic species [*Seinfeld and Pandis, 1998*], was observed above detection limit only for a few hours on fours days (April 10-11, 19-20 and May 7-8) during entire sampling period. Those days had experienced southerly winds, and probably carried the aerosols originated in the southern US with biogenic organic contributions. During the northerly flows, there might have been contributions of biogenic emissions from the conifer trees, such as terpene oxidation products to the particulate organics. No other gas-phase or particulate species that can be used as a marker for biogenic emissions was measured in this study. Thus, it is possible that the increase in total particle organic in the aerosol from the north is due partly to microbes in the soil, and partly due to trees and grass. However, it was not possible estimate the contribution of each, as no markers were measured. The solar irradiance also exhibited an increasing trend with time, and so did the *m/z* 44 (an indicator for particulate oxygenated organics), indicating that the photochemical oxygenation of particulate organics increased with increasing solar intensity. Furthermore, the organic mass concentrations due to particles smaller than 200 nm and larger than 200 nm increased at the same rate, indicating that the change had no size preference, i.e., there was no evidence for an effect on particle size.

5.2.1 Average Mass Distributions

Figure 5.4 shows the mass distributions of particulate ammonium, nitrate, sulfate and organics measured with the AMS averaged over all periods with aerosol from the north, as identified above, except the periods with direct influence of Sudbury emissions. All four species have unimodal mass distribution with modal vacuum aerodynamic diameter around 450 nm. The contribution of organic material is larger or comparable to sulfate, and that of nitrate is noticeably low. The molar ratios of observed ammonium, nitrate and

sulfate [i.e., $NH_4^+/(2\ SO_4^{--} + NO_3^-)$] varied between about 0.8 to 0.5 for aerosol particles with diameters between about 180 nm to 1000 nm, indicating that aerosol particles were acidic; specifically particles within 400 nm to 600 nm were most acidic.

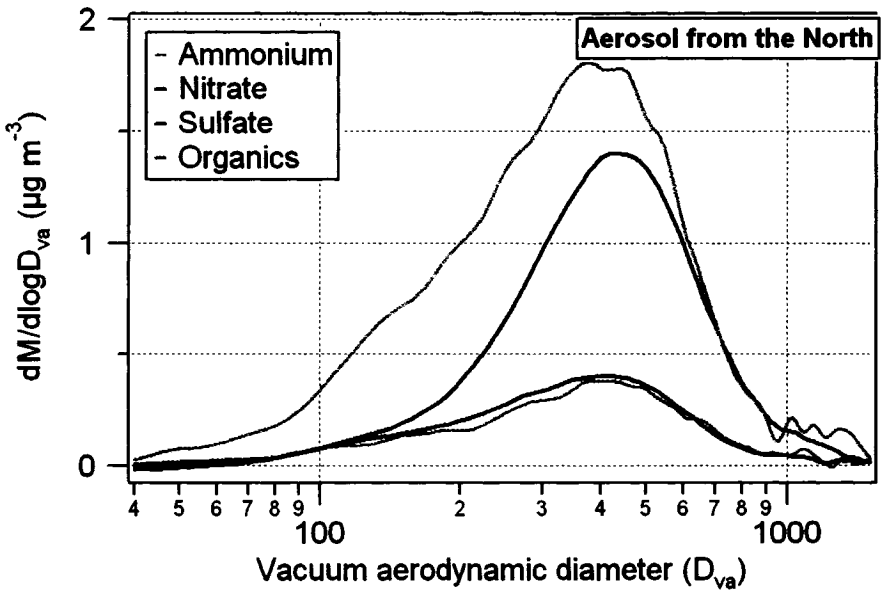

Figure 5.4 Average mass distributions of particulate ammonium, nitrate, sulfate, and organics measured with the AMS for the periods with the aerosol from the north as identified above. The periods with direct influence of Sudbury emissions were excluded.

5.2.2 Sudbury Influence

There were at least three periods (March 30-31, April 5-6, and April 22-23) with high sulfate mass concentrations, the events were short-lived though, during which the air trajectories had passed directly over the Sudbury region. Aerosol composition was dominated by sulfate, but organic material was also considerably high (Figure 5.1 and Figure 5.6). As an example, the back trajectories of the air masses that arrived at the site at three different heights (red: 100 m, blue: 500 m and green: 1000 m above ground) at 9:00 pm on March 30 are shown in Figure 5.5. The air trajectories directly passed over Sudbury area before arriving at the site.

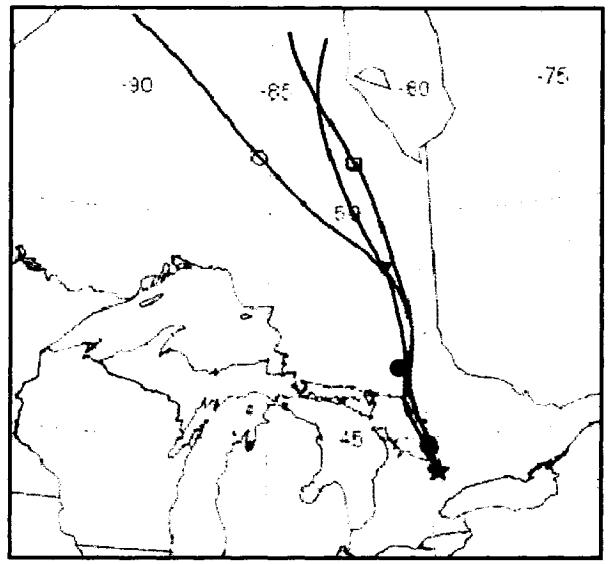

Figure 5.5 The back trajectories of the air masses that arrived at the site at three different heights (red: 100 m, blue: 500 m, and green: 1000 m above ground) at 9:00 pm on March 30. The two marks along the trajectory represents 24 h interval. The red dot indicates the Sudbury area.

Figure 5.6a shows the average mass distributions of ammonium, nitrate, sulfate and total organics as a function of particle vacuum aerodynamic diameters (D_{va}) for three sulfate events. Sulfate displayed a bimodal mass distribution with a primary mode at around 400 nm and a secondary mode centered at about 125 nm that was clearly discernable from the more dominant peak. There was a significant amount of organics, and nitrate was very low. Ammonium had bimodal mass distribution coincident to sulfate. However, aerosol particles were acidic as the molar ratios of particulate ammonium to nitrate and sulfate remained below 0.6 for the whole size range, and specifically, particles smaller than about 250 nm were most acidic as the ratio was between 0.1 and 0.5. This implies that the aerosol particles were composed primarily of sulfuric acid, if not pure sulfuric acid. The small mode sulfate particles probably originated from the nucleation of sulfuric acid while air masses were transported to the site.

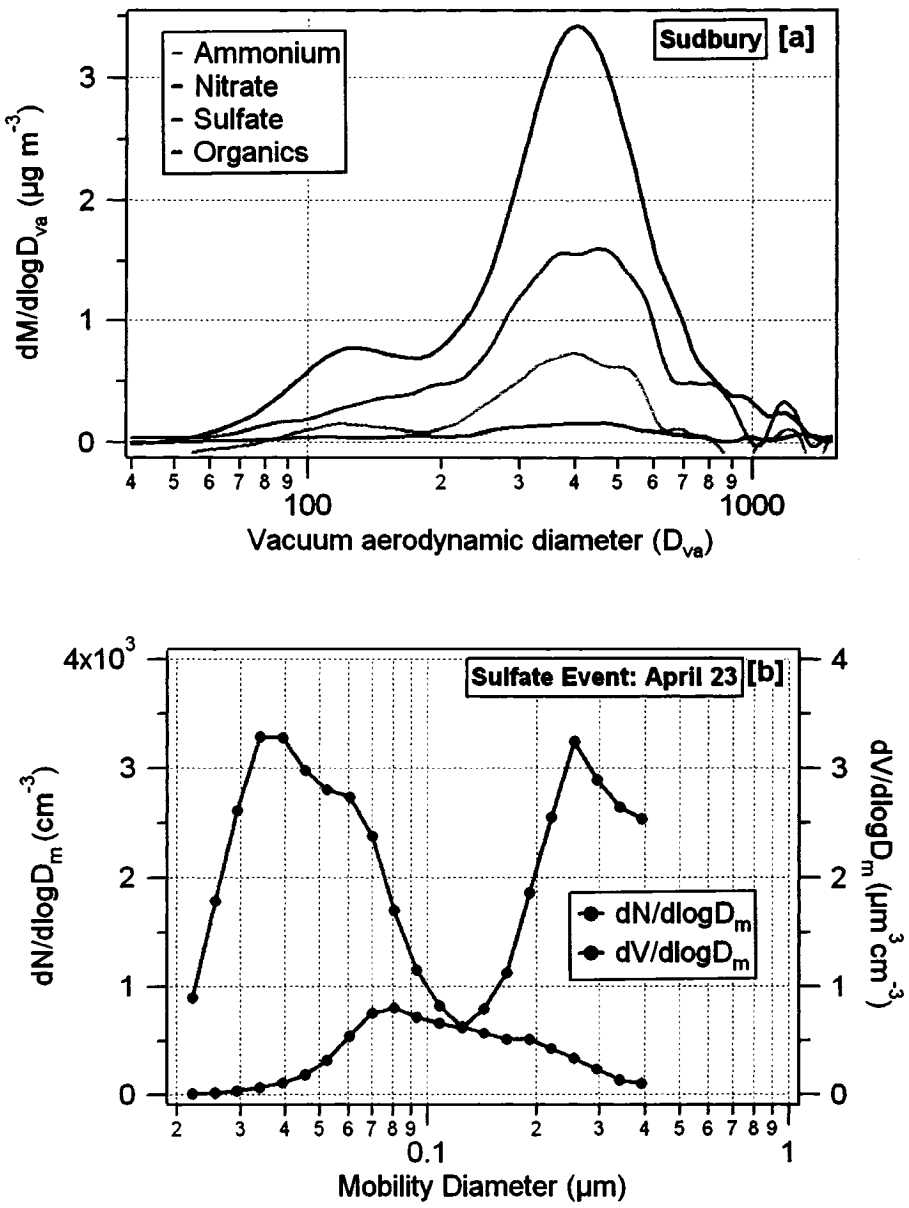

Figure 5.6 (a) Average mass size distributions of particulate ammonium, nitrate, sulfate and organics during the periods with direct influence of Sudbury emissions. The mass distributions were averaged over three events as identified in the text, and (b) Number size distribution and volume distribution of particles during a sulfate event on April 23, 2003.

Figure 5.6b displays the number distributions and the volume distributions of particles with mobility diameter (D_m) between about 20 nm and 420 nm measured with the SMPS during the sulfate event on April 23. The volume distribution resembles the mass

distributions measured with AMS shown in Figure 5.6a, with small mode around 80 nm D_m (D_{va} ~120 nm) and larger mode around 300 nm D_m (D_{va} ~120 nm).

5.2.3 High Pressure in the Arctic

The high-pressure systems developed in the Canadian Arctic and moved southwards during April 6-7, April 13-14, and April 26-27. It was likely that air masses came from Arctic during those three days, i.e., April 7, April 13 and April 26. Figure 5.7 shows the back trajectories of the air masses that arrived at the site at three different heights (red: 100 m, blue: 500 m and green: 1000 m above ground) at 11:00 am on April 13.

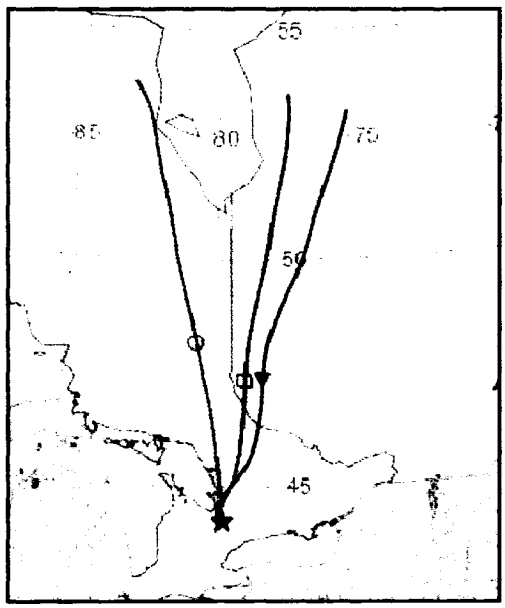

Figure 5.7 The back trajectories of air masses that arrived at the site at three different heights (red: 100 m, blue: 500 m, and green: 1000 m above ground) at 11:00 am on April 13. The two pallets along the trajectories represent 24 h interval.

The average size distributions of ammonium, nitrate, sulfate and organics averaged over all three events are shown in Figure 5.8. Particulate organic material is comparable or higher than the particulate sulfate. All four species have unimodal mass distributions with modal diameter around 400-500 nm D_{va}, except a shoulder of organic mass distribution centered at around 150 nm, implying that the aerosol was aged and four species were

likely internally mixed. The mass distributions of four species during three individual events resembled the average distribution shown in Figure 5.8. The individual mass distributions from the three Arctic air masses are very similar as shown in the small standard deviation.

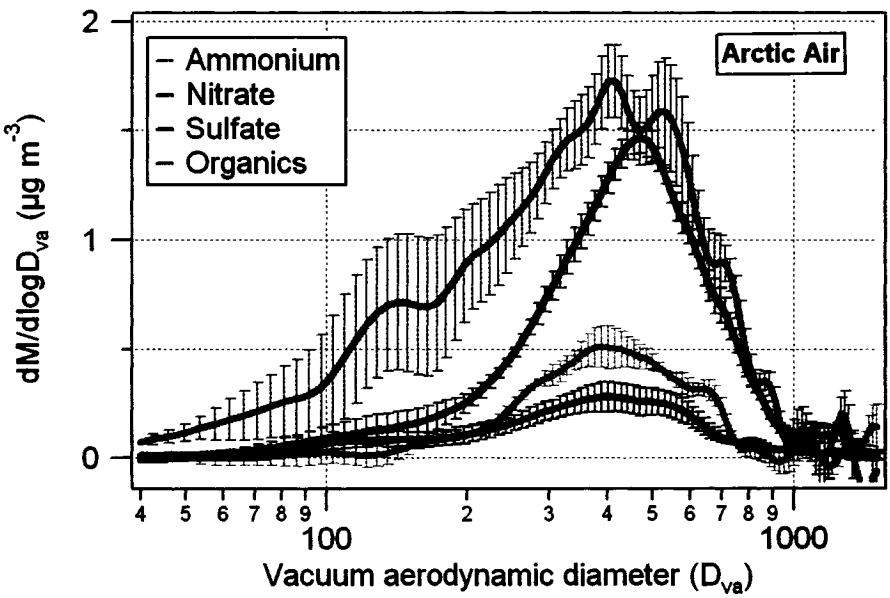

Figure 5.8 The average size distributions of particulate ammonium, nitrate, sulfate, and organics during the periods with air masses likely from Arctic. The error bars represent one standard deviation.

5.3 Aerosol from the South: Formation of High Particulate Nitrate

Figure 5.1 shows that the higher mass concentrations events at Egbert are due primarily to high nitrate mass concentrations, and Figure 5.2 indicates the organic material as a major fraction of total fine particulate mass followed by nitrate, sulfate and ammonium. What are the factors that control or enhance nitrate formation at Egbert; the proximity to the sources of gaseous precursors, temperature, relative humidity (e.g., the colder and wetter winter/spring), availability of NH_3, which is mostly of agricultural origin? Does the presence of organic aerosols play any role? The mechanisms of high nitrate formation at Egbert are not fully understood.

First, the observed mass distributions are analyzed. Figure 5.9a shows the average mass distributions of ammonium, nitrate, sulfate and organics measured with the AMS at Egbert averaged over all the periods with aerosol from the south as identified above. The mass distribution of each species is skewed towards the smaller sizes. Organic mass distribution exhibits a shoulder centered at around 125 nm D_{va}, otherwise all four species have a mode around 450 to 550 nm D_{va}. The aerosol particles smaller than 650 nm D_{va} were slightly acidic ($a < 0.9$), while particles larger than 650 nm were more acidic.

The average mass distributions of those four species averaged over four major nitrate episodes (April 1-2, 10-12 and May 1), as shown in Figure 5.9b, are remarkably different. Nitrate, organics, and ammonium exhibit bimodal distribution with modes with a small mode around 150-175 nm D_{va}, and a larger mode around 500 nm D_{va}, while the sulfate is unimodal with peak around 575 nm D_{va}. For average mass distributions during high nitrate cases, the observed ammonium, nitrate and sulfate indicate that the available particulate ammonium was enough to neutralize sulfate and nitrate in the particles smaller than 650 nm, while the larger particles were slightly acidic ($a < 0.8$). The nitrate events on April 1-2 and April 10-12 coincided with higher $PM_{2.5}$ sodium mass concentrations (~ 0.5-1 $\mu g\ m^{-3}$, 24-h averages), while sodium concentration was about 0.1$\mu g\ m^{-3}$ during the third nitrate event (May 1). For the first two nitrate events, the average aerosol acidity for particles larger than 650 nm was about 0.7 only, whereas it was 0.9 for the nitrate event on May 1. The molar ratios of Na^+ to Cl^- from the filter analysis of $PM_{2.5}$ indicate that the ratio was > 2 during first two nitrate events, in contrast to ~ 1 for the third nitrate event. This indicates that the excess nitrate in the larger particles during the first two events may be attributable to $NaNO_3$, which is apparently a reaction of product of HNO_3 with road salt aerosols. One should note that the NaCl particles mostly reside in supermicron size [*Seinfeld and Pandis, 1998*], and only a small fraction may contribute to submicron particles. As $NaNO_3$ has a melting point of 350°C [*CRC, 2000*], the AMS is likely to detect some $NaNO_3$ [*Allan et al, 2004*]. In addition to sodium nitrate, the nitrogen-containing organics may contribute to the excess nitrate, and the event 1 described in chapter 4 indicates such possibility.

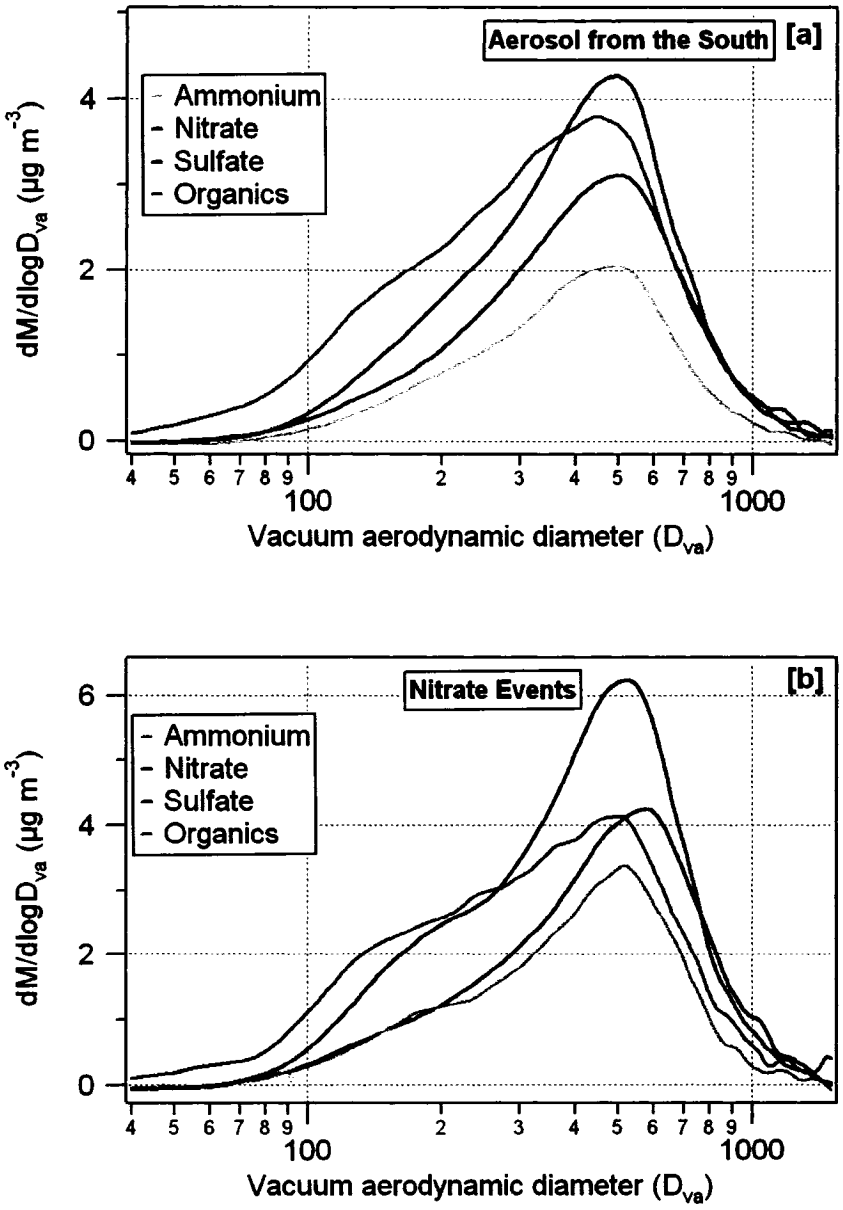

Figure 5.9 The average size distributions of particulate ammonium, nitrate, sulfate, and organics measured with the AMS averaged over (a) all periods with aerosol from the south, and (b) four major nitrate episodes (April 1-2, 10-12 and May 1).

The oxides of nitrogen NO and NO_2, which together referred to as NO_x, are the main ingredients for nitrate formation. The sources of NO_x are fossil fuel combustion, biomass burning and soil release. NO_x is emitted primarily as NO but during the day NO rapidly establishes an equilibrium with NO_2 [*Seinfeld and Pandis, 1998*]. The reactive nitrogen

species, including NOx, is of great importance for atmospheric photochemistry as they regulate the production of O_3 as well as particulate nitrate [*Seinfeld and Pandis, 1998; Vrekoussis et al., 2006*]. During daytime, the principal sink for NO_x is the reaction with OH radicals [*McLaren et al., 2004; Seinfeld and Pandis, 1998; Vrekoussis et al., 2006*].

$$NO_2 + OH + M \rightarrow HNO_3 + M \qquad \text{---------- (5.1)}$$

During nighttime, the most significant mechanism that controls NH_4NO_3 formation is the conversion of NO_3 to N_2O_5, followed by homogeneous hydrolysis of N_2O_5 to form gaseous HNO_3, and heterogeneous hydrolysis of N_2O_5 on wet particle surfaces yielding particulate HNO_3 [*Atkinson et al., 2004; McLaren et al., 2004; Seinfield and Pandis, 1998*]. The reactions are described in chapter 4. The gaseous HNO_3 also condenses onto the particles, so does NH_3, and HNO_3 on the particle reacts with NH_3 to produce NH_4NO_3 [*McLaren et al., 2004; Seinfield and Pandis, 1998*]. The reaction of N_2O_5 with water is efficient on wet aerosol surfaces, and the higher relative humidities will favor the hydrolysis of N_2O_5. The homogeneous reactions of NO_3 with biogenic hydrocarbons ($NO_3 + R \rightarrow HNO_3$ + organic products) may be important during nighttime depending upon the availability of biogenic hydrocarbons [*Geyer et al., 2001*], whereas the heterogeneous loss of NO_3 is considered minor and negligible [*Geyer et al., 2001; Heintz et al., 1996*]. Therefore, the nighttime accumulation mode nitrate at Egbert can be attributed to formation of particulate nitrate, either locally at the site or upwind locations and transported to the site, under appropriate environmental conditions (lower temperature and higher relative humidity), as well as availability of gaseous NH_3 from agricultural activities and nitrogen oxides from urban emissions. As the pre-existing small organic particles in the urban plumes provided high surface areas, it was most likely gaseous HNO_3 condensed on those particles, and hence the mass distribution of particulate nitrate resembled that of total organics. Because a number of gas-phase reactive nitrogen species (e.g., NO_2, NO_3, N_2O_5, HNO_3, NO_y) were not measured during this study, it severely limited the further analysis of the significance of various mechanisms described above.

5.4 Evolution of Composition with Photochemical Age

Atmospheric aerosols undergo a series of physical processing and a wide range of chemical reactions since emission or formation in the air. The inorganic components interact with the organic component in the particles, and likely form internal mixture as particles age. This may change the chemical composition of particles, size distributions organic composition and the organic fraction in the particles (e.g., the fraction of oxygenated organics in the particles). The two cases studies presented in chapter 4 demonstrated that the size distributions and composition of particles for the relatively recent emissions, which had evidence of less processing, were distinctly different from those for the aged aerosols. Atmospheric evolution of particulate organics is poorly understood. It is crucial to understand the composition and microphysics of the organic component of the atmospheric aerosol in refining our knowledge on the origins of organic aerosols and their implications for heterogeneous chemistry, ability of particles to act as CCN, and climate. The oxygenation of particulate organic material changes the chemical composition and physical properties of the particles, in particular oxidation increases the water solubility thereby making organic aerosols more active as CCN [e.g., *Saxena et al., 1995; Kotzick and Niessner, 1999*]. The photochemical oxygenation of particulate organics is of interest. In this study, the aerosol composition measurements made with the AMS and gas-phase non-methane hydrocarbon compounds (NMHCs) measured with a gas chromatograph-flame ionization detection (GC-FID) system [*Brickell et al., 2003*] were analyzed to study the atmospheric evolution of aerosol particles, in particular oxygenated organic component, with the photochemical age [*Roberts et al., 1984*]. The photochemical age of the aerosol particle composition was estimated from the ratios of two anthropogenic NMHCs, benzene and toluene [*de Gouw et al., 2005; McFiggans et al., 2005; Roberts et al., 1984*].

5.4.1 Estimation of Photochemical Age

Effect of Dilution

As described in the previous studies [*Kleinmann et al., 1996; McKeen et al., 1996; McKeen and Liu, 1993*], the change in concentration of a hydrocarbon X with mixing ratio [X] can be approximated as,

$$\frac{d[X]}{dt} = -L_X[X] - M([X] - [X^B]) \qquad \text{---------- (5.2)}$$

where L_x is the rate of loss of hydrocarbon X due to reaction with OH (i.e. $L_x = k_x$ [OH]), k_x is the reaction rate constant), M is a mixing coefficient that takes into account all the dilution processes when source air mixes with background air, and $[X_B]$ is the background mixing ratio of X. Assuming that L_x and M are constant, and background mixing ratio $[X^B] = 0$, the solution of equation (5.2) is

$$[X] = [X]_0 \, e^{-(L_X - M)t} \qquad \text{---------- (5.3)}$$

where $[X]_0$ is the initial mixing ratio of X, i.e., at the source.

For a pair of hydrocarbons X and Y, we can deduce an equation that relates concentrations of X and Y, i.e.,

$$\ln[X] = \frac{(M + L_X)}{(M + L_Y)} \ln[Y] + \ln C \qquad \text{---------- (5.4)}$$

where C is a constant dependant on the initial mixing ratios $[X]_0$ and $[Y]_0$. The slope is

$$m = \frac{(M + L_X)}{(M + L_Y)} \qquad \text{---------- (5.5)}$$

which yields

$$\frac{M}{L_X} = \frac{(1 - m\, k_Y / k_X)}{(m - 1)} \qquad \text{---------- (5.6)}$$

Thus, the slope of ln[X] versus ln[Y] plot can be used to estimate a relative measure of the contributions of chemical reaction and dilution to the loss of a hydrocarbon

[*Kleinmann et al., 1996; McKeen and Liu, 1993*]. In an effort to assess the importance of dilution, a pair of hydrocarbons, propane and iso-butane, are used for which the background concentrations can be approximate as zero [*Kleinmann et al., 1996*]. Gas-phase mixing ratios of 37 NMHCs were measured at CARE with a liquid nitrogen cooled glass bead pre-concentration trap and multi-column capillary gas chromatograph-flame ionization detection (GC-FID) system [*Brickell et al., 2003*]. Figure 5.10 shows the iso-butane and propane data from both groups, aerosols from the north and the south, separately applied to equation (5.4). The linear least square fits to ln[iso-butane] and ln[propane] data yielded a slope of 1.71(±0.07) with a r^2 value of 0.86 for the aerosol from the south, and a slope of 1.62(±0.09) with a r^2 value of 0.77 for aerosol from the north. Using the rate constants for the reactions of iso-butane and propane with OH at an average temperature of 278K [*Seinfeld and Pandis, 1998; Finlayson-Pitts and Pitts, 2000*] and the slopes of lines from Figure 5.10, the equation (5.5) yielded $M/L_{isobutane}$ = 0.18(±0.06) [or, $M/(M+L_{isobutane})$ = 15%(±2%)] for aerosol from the south, and $M/L_{isobutane}$ = 0.28(±0.12) [or, $M/(M+ L_{isobutane})$ = 21%(±3%)] for aerosol from the north. The change in reaction constants with temperatures was not considered while estimating M/L ratios. These ratios may be different for different hydrocarbons, and depend on the reference hydrocarbon, for example, propane in this study. Nevertheless, these predictions indicate that the dilution was not as important as reactions with OH in determining the concentrations of iso-butane and other hydrocarbons that react as rapidly as iso-butane. *McKeen et al. [1996]* obtained a value of $M/L_{isobutane}$ = 1.14 [or, $M/(M+L_{isobutane})$ = 53%], which was obtained from regression of iso-butane versus propane, in their analysis of hydrocarbon data collected over the Pacific Ocean downwind of the Asian continent. They found that the dilution estimates were fairly insensitive to the existence of nonzero background hydrocarbon concentrations. Likewise, from the hydrocarbon data collected over southern Nova Scotia, Canada, *Kleinmann et al. [1996]* obtained $M/L_{isobutane}$ = 0.72 [or, $M/(M+L_{isobutane})$ = 42%] for the iso-butane versus propane regression. This implies that the role of dilution was more significant during those two studies.

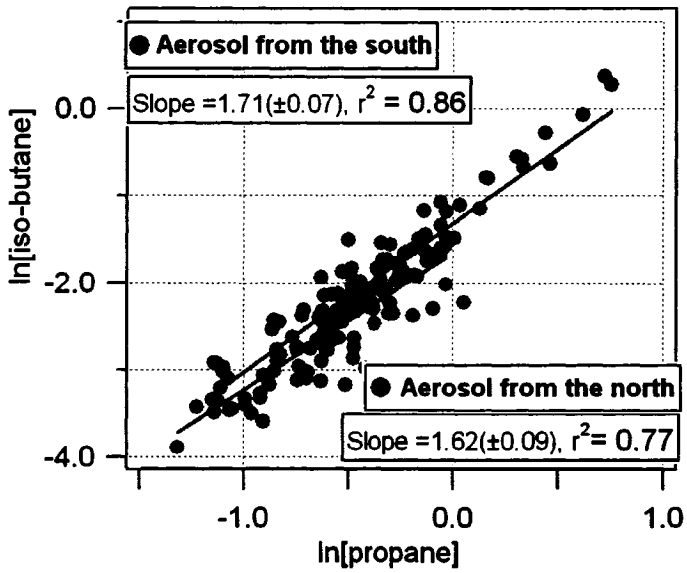

Figure 5.10 The ln-ln plot of iso-butane versus propane mixing ratios observed at Egbert during the polluted and clean periods.

Photochemical Age of Air Mass

The change in the logarithm of the ratio of hydrocarbons with time, for example, ln([toluene]/[benzene]), which changes monotonically with time, can be used as a marker for the degree of processing an air mass has undergone [*Kleinmann et al., 1996; McKeen and Liu, 1993; Roberts et al., 1984*]. In this study, atmospheric mixing ratios of toluene, $[X_T]$, and benzene, $[X_B]$, were highly correlated (correlation coefficient, r = 0.87). The photochemical age, t, of the sampled air mass was estimated from the ratio between observed mixing ratios of toluene and benzene, as described in previous studies [*de Gouw et al., 2005; McFiggans et al., 2005; Roberts et al., 1984*]. In other words, $[X_T]$ and $[X_B]$ were substituted in equation (5.2) and rearranged to get the following equation for the photochemical age,

$$t = \frac{1}{[OH](k_T - k_B)}\left[\ln\left(\frac{[X_T]}{[X_B]}\bigg|_{t=0}\right) - \ln\left(\frac{[X_T]}{[X_B]}\right)\right] \quad \ldots\ldots\ldots\ldots\ldots \quad (5.6)$$

where, k_T and k_B are the rate coefficients for the reaction of hydroxyl radical (OH) with toluene and benzene, respectively. The rate coefficients are temperature dependant [*Seinfeld and Pandis, 1998*]. Thus, a range of k_B (= 1.22-1.40 x 10^{-12} cm^3 $molecule^{-1}$ s^{-1}) and k_T (= 5.88-7.02 x 10^{-12} cm^3 $molecule^{-1}$ s-1) was estimated [*Seinfeld and Pandis, 1998*] for a wide range of ambient temperature measured at the site (T_{min} = -11.3°C, T_{max} = 27.9°C) during sampling period, and those values were used in equation (1). The air mass may be subjected to different temperatures during its history, and it is not possible to include that temperature variation in equation (1). [OH] is the 24-h average mixing ratio of hydroxyl radical. The OH mixing ratio was not measured during this experiment. Thus, the 24-h average values of OH mixing ratios at Egbert were estimated with the ECHAM GCM [*Lohmann et al., 1999*], and the values are 1.54 x 10^6 molecules cm^{-3}, 1.41 x 10^6 molecules cm^{-3}, and 1.37 x 10^6 molecules cm^{-3} for the month of March, April and May of 2003, respectively. The emission ratio ($|[X_T]/[X_B]|_{t=0}$ = 3.0±0.5) was estimated from the toluene and benzene mixing ratios in the air masses that came directly from urban areas with the signature of minimum oxidation processes. The photochemical age in this work, thus, represents the aging time relative to the minimum oxidation periods rather than the absolute age. The emission ratio has been assumed to be same for both the aerosol from the south and aerosol from the north.

Hydrocarbon compounds are largely removed by reactions with OH [*Roberts et al., 1984; Seinfeld and Pandis, 1998*]. The atmospheric mixing and dilution of air masses, reactions with halogens, which is a major sink for hydrocarbons in marine environment, with O_3 and nitrate, may also influence the hydrocarbon mixing ratios, and hence the photochemical age estimated on the basis of reaction with OH only may be different from the actual photochemical age [*Ehhalt et al., 1998; Finlayson-Pitts, 1993; McKeen and Liu, 1993*]. As shown earlier the dilution was not as important as reactions with OH. The halogen chemistry is assumed insignificant at this continental site. The reactions with O_3 and nitrate were not considered here, which may introduce some error in estimated photochemical age.

5.4.2 Change in Size Distributions with Photochemical Age

The change in aerosol composition with increasing photochemical age was investigated. The upper panels in Figure 5.11 show the average mass distributions of ammonium, nitrate, sulfate and total organics in the particles associated with air masses that had photochemical ages between (a) 0 h to 24 h, (b) 24 h to 48 h, and (c) 72 h to 96 h. The size distributions for first two intervals were chosen from the periods with aerosol from the South, and the third interval was taken from the periods with aerosol from the north. The bottom panels show the average mass distributions of two key organic fragments *m/z* 44 (a representative of the oxygenated organics) and *m/z* 57 (a representative for hydrocarbon-like organics) for the same photochemical age as indicated in corresponding upper panels.

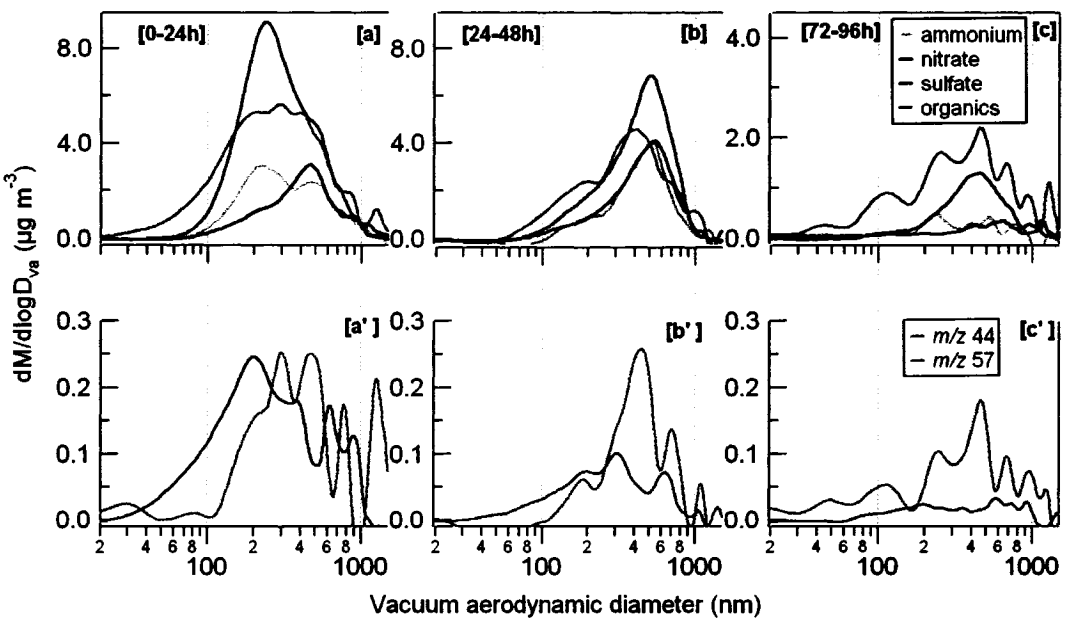

Figure 5.11 Average mass distributions of particulate ammonium, nitrate, sulfate, and total organics, and two key organic fragments, *m/z* 44 and *m/z* 57, for the photochemical age of mass between (a) 0 to 24 h, (b) 24 h to 48 h, and (c) 48 h to 96 h. The first two were from periods with aerosol from the south and the last one from the periods with aerosol from the north.

For the photochemical age of 0-24 hours, total organic mass distribution (Figure 5.11a), appears to be a combination of two modes, one mode at ~190 nm D_{va} and a second mode ~425 nm $D_{va,}$. Figure 5.11a' shows that *m/z* 57 is much higher than *m/z* 44 in the smaller

mode organics coupled with little or no inorganic species associated with the particles smaller than 80 nm. This indicates that the fresh aerosols contain mainly hydrocarbon-like substances and some oxidized in the smaller mode compared with the larger mode that contains mainly highly oxygenated organics. Those small hydrocarbon-like organic particles are most likely hydrophobic or less hygroscopic. Nitrate has a unimodal mass distribution with a mode coincident with the smaller organic mode, suggesting that HNO_3 may have condensed onto pre-existing small organic particles containing some inorganics such as sulfate. The presence of some sulfate on the particles likely retained some water, which might aid N_2O_5 hydrolysis. Sulfate mass distribution has a mode at ~ 450 nm, coincident with the organics in the larger mode, and there is less sulfate associated with the smaller mode. Ammonium mass distribution is bimodal, which is apparently the effect of nitrate and sulfate mass distributions. The *m/z* 57 is higher than *m/z* 44 in the smaller mode organics, indicating that the aerosol is composed of more hydrocarbon-like organics (mostly aliphatic organics) and less oxidized organics in the smaller mode compared with the larger mode. Figure 5.11b demonstrates that the smaller organic mode becomes less evident in next 24 hours. The mass distributions of the inorganics (ammonium, nitrate and sulfate) are unimodal (modal D_{va} ~500-550 nm). Over several hours of processing, the higher surface areas associated with the more numerous smaller particles nearer to the source regions promote the condensation of gas-phase secondary organics and inorganic species on small organic particles, thereby increasing their sizes and composition. It is evident in Figure 5.11b' that particulate hydrocarbon significantly decreases, and larger organic particles contain larger fraction of oxygenated organics. The particulate oxygenated organics may also increase due to oxidation of hydrocarbon-like material on the particle surface. For the photochemical age of 72-96 hours, the aerosol particles are composed of mainly organics and sulfate, and very low nitrate. Particulate organics are mostly oxygenated organics and a small fraction of hydrocarbons is present. Though there is a significant amount of mass in the small organic mode, the small organic particles contain significant amounts of oxygenated organics for the highly processed organics, in contrast to the small particles in relatively fresh emissions, as seen in Figure 4.4b (urban aerosol), which are composed mainly of less processed hydrocarbon-like substances.

Thus, this analysis also demonstrated that the size distributions of particulate organics and organic composition undergo a significant change with increasing photochemical age, i.e., with higher degree of processing. In addition, particulate nitrate formation appears be to relatively local.

5.4.3 Oxygenation of Organics with Photochemical Age

The evolution of aerosol composition, in particular the oxygenation of organic aerosol with photochemical age is further investigated. It is likely that the air masses from different source regions are exposed to differing degree of photochemical transformation. Therefore, the change in aerosol composition as a function of photochemical age is first investigated separately for the aerosol from the south and aerosol from the north.

Figure 5.12a shows how the particulate oxygenated organic fraction (represented by *m/z* 44/total organics) and the hydrocarbon-like organic fraction (represented by *m/z* 57/total organics) observed at Egbert evolved with increasing photochemical age of air mass for the aerosol from the south. The large blue dots and red triangles, connected with lines, represent the average value of *m/z* 44/organics and *m/z* 57/organics, respectively, for each 24-h time bins of photochemical age, and the vertical bar represents one standard deviation for each bin. The particulate hydrocarbon fraction decreases most rapidly during the first 24 hours of photochemical processing, gradually over next 12 hours, and thereafter remains relatively constant. In contrast, the oxygenated fraction increases rapidly during the first 48 hours after which little change is seen in the average. The trend of two fractions, in particular a little or no change after 48 is intriguing. Over time, the gas-phase secondary organic and inorganic species condense on the small organic particles, thereby increasing the oxygenated organic fraction. It may also increase due to oxidation of hydrocarbon-like materials on/in the particles [*Seinfeld and Pandis, 1998*]. The results in Figure 5.12a show that either or both of these two mechanisms occur within 48 hours of photochemical processing. The possibility that OH-initiated oxidation on the hydrocarbon surfaces produces some semi-volatile organic compounds an volatilizes some of the particles [*Molina et al., 2004*] does not appear to be significant here as the particulate oxygenated organics do not show a downward trend with

decreasing particulate hydrocarbons. However, it is possible that this mechanism offset an increase in organic mass.

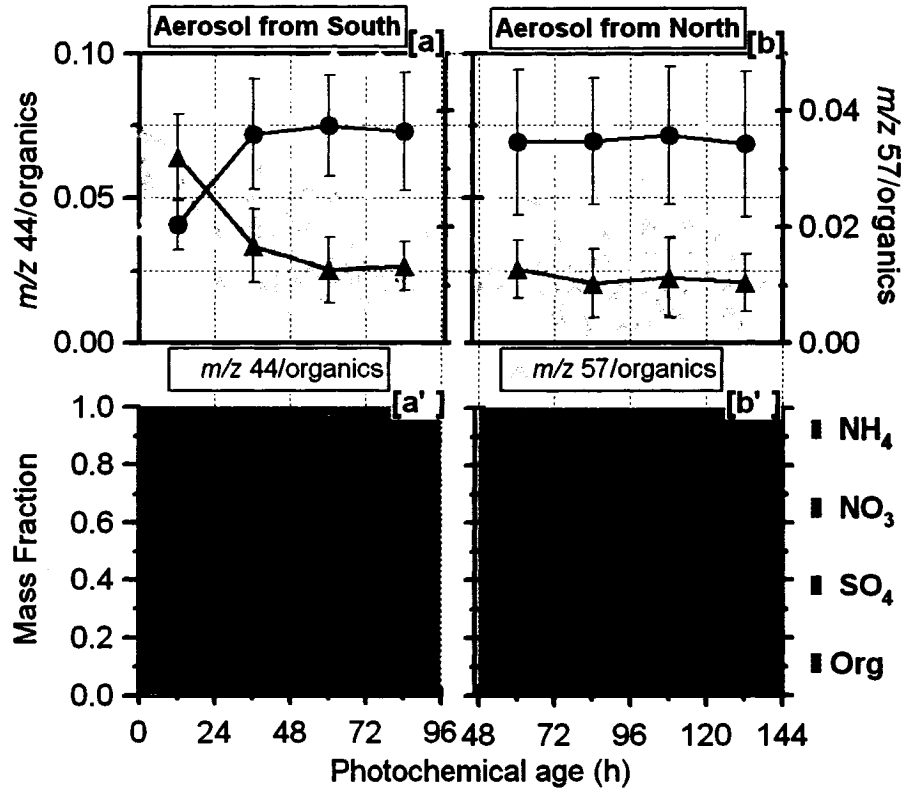

Figure 5.12 Evolution of particulate oxygenated organic fraction and hydrocarbon-like organic fraction (as represented by *m/z* 44/organics and *m/z* 57/organics, respectively) in the AMS measurements as a function of photochemical age of air mass for (a) the aerosol from the south, and (b) the aerosol from the north. The large blue dots and red triangles, connected with lines, represent the average value of *m/z* 44/organics and *m/z* 57/organics, respectively, for each 24 h time bins of the photochemical age, and the vertical bars represent one standard deviation for the each interval. Panels (a') and (b') show the average chemical composition for the aerosols from the south and the north, respectively, for the same photochemical age intervals.

The chemical composition of the particulate matter may provide insights for atmospheric evolution of particulate oxygenated organics and hydrocarbons. It is important to consider that the trend is controlled by the composition and the internal structure of the particles. Figure 5.12a' shows the average composition of the submicron particles for a given photochemical age interval. While the total organic mass concentrations remain almost unchanged, the sulfate mass concentrations clearly increase while nitrate

decreases with increasing photochemical age. The initially higher nitrate is consistent with locally formed ammonium nitrate resulting from the presence of higher levels of NH_3 [*Rupakheti et al., 2005*]. As available ammonium preferably remains in the form of ammonium sulfates in the presence of sulfate, and ammonium sulfate remains partitioned in the particulate-phase [*Seinfeld and Pandis, 1998*], the higher levels of sulfate are unfavorable for the partitioning of nitrate to the particle-phase. Thus, particulate ammonium nitrate forms locally and gradually decreases with increasing atmospheric processing, i.e., with increasing photochemical age, and particulate sulfate increases.

One can raise an interesting question here. Is the increasing sulfate fraction in particles impeding further oxygenation of organics? Figure 5.12b show the change in the oxygenated organic and hydrocarbon-like organic fractions with increasing photochemical age for the aerosol from the north. Figure12.5b' shows the corresponding particulate chemical composition. There is no significant change in average values of the particulate the oxygenated organic and hydrocarbon-like organic fractions with increasing photochemical age up to 140 hours. However, there is a huge change in the sulfate and nitrate fractions.

Basically, Figures 5.12a and 12.5b represent air masses originated in the different source regions with various degrees of photochemical processing, and approaching the sampling site from two different directions. However, these figures suggest that the composition of the aerosol from the south (mostly pollution aerosols) gradually approaches the composition of the aerosol from the north (clean or background air). Figure 5.13 shows the evolution of particulate oxygenated organic fraction and hydrocarbon-like organic fraction, as well as aerosol composition with increasing photochemical age of air mass for the entire period i.e. when aerosols from the South and the north combined. The particulate hydrocarbon fraction decreases most rapidly over the first 24 hours of photochemical processing, and thereafter remains relatively constant. The oxygenated fraction increases rapidly during the first 48 hours, thereafter shows no change in the average. There is an enormous change in nitrate and sulfate fractions. The relatively constant total organic mass concentrations may indicate that the oxidation of primary

particulate hydrocarbons is more significant than the condensation of secondary organic from the gas phase. However, it is not possible to indicate whether biogenic sources were responsible for change in *m/z* 44, in fact there must be some contribution when air masses carried aerosols from southern USA where biogenic sources are prevalent, together with aged anthropogenic m/z 57 contributing to m/z 44 over time.

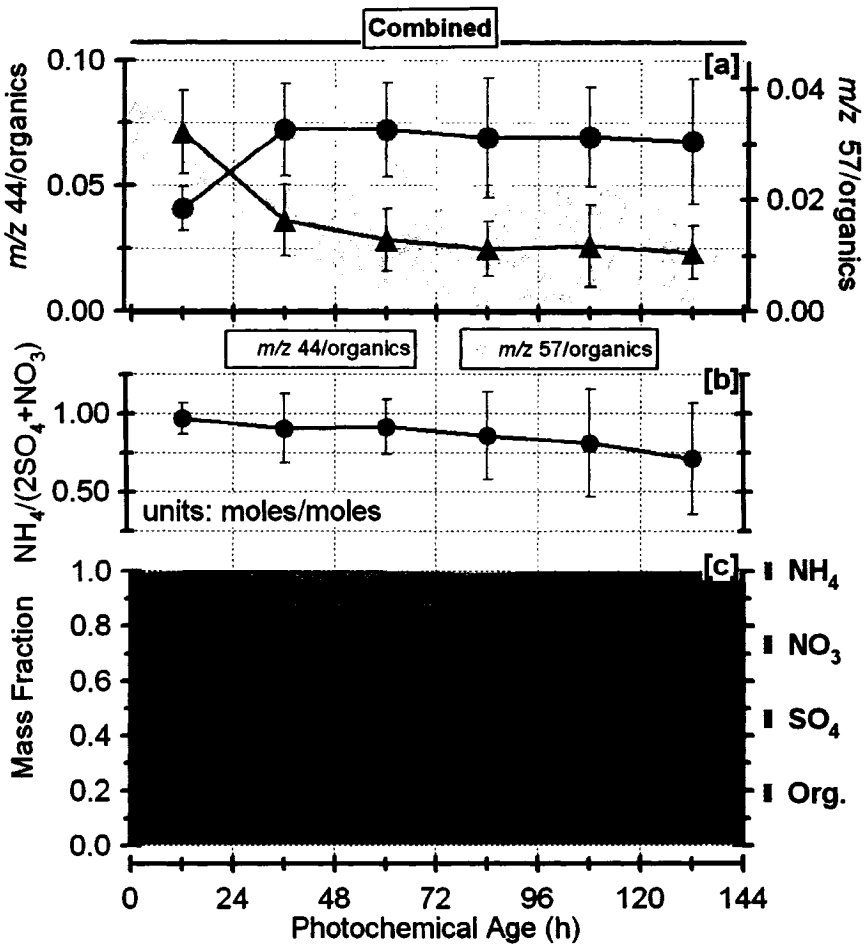

Figure 5.13 Evolution of aerosol composition with photochemical age of air mass, (a) change in particulate oxygenated organic fraction and hydrocarbon-like organic fraction as a function of photochemical age for the entire period i.e. polluted and periods combined. The large blue dots and red triangles, connected with lines, represent the average value of *m/z* 44/organics and *m/z* 57/organics, respectively, for each 24 h time bins of the photochemical age, and the vertical bars represent one standard deviation, (d) change in average ratios of molar concentrations of measured ammonium to sulfate and nitrate, this ratio is used as measure of particle acidity, for same photochemical age intervals, (e) the average particulate chemical composition for the same intervals.

One of the hypotheses to explain the absence of continued oxidation of organics after about 24 hours is that the coating of the organic particles by sulfates results in a core-shell structure that prevents organics in the core from further oxidation. The outer shell of sulfate may also inhibit condensation of gas-phase secondary organics. Although AMS measurements do not provide conclusive information on mixing states of various species, the similarity in the mass distributions indicates that organics and inorganics are likely internally mixed in the aged aerosols.

It is also possible that the gas-phase reactive hydrocarbons are used up after some time and there are no more gas-phase species to be partitioned in to the particle-phase. However, the mixing ratios of several reactive and short-lived hydrocarbons such as ethylbenzene, n-butane and toluene among other are still available in the air mass with photochemical age of more than 100 hours. The other possible explanations include the change in OH uptake during oxidation, increase in oxidation with increasing size [*Robinson et al., 2006*] or particle may be inhomogeneous either due to kinetic (slow diffusion) thermodynamic constraints [*Maria et al., 2004*]. Concentration gradients are observed in ambient particles collected on substrates, with evidence that carbonyl-containing compounds favor the particle surface [*Maria et al., 2004*].

Another likely explanation for the change in organic composition with photochemical age is the change in aerosol fraction with increasing photochemical age that may indicate the distance from the measurement site. This would imply that the variation in the particulate oxygenated organics and hydrocarbons indicate that the more anthropogenic sources are distributed closer to the site than the biogenic sources. Thus, the biogenic organics had enough time for oxygenation before reaching the site. In order to explore it further, and estimate the distances traveled by the air masses we need to run trajectory models with Lagrangian setting, such as FLEXPART model. HYSPLIT model is unable to estimate the distances. This was beyond the scope of this study.

The average ratios of the molar concentrations of measured ammonium to nitrate and sulfate, which is a measure of aerosol acidity, [i.e., acidity = $NH_4^+ / (2SO_4^{--} + NO_3^-)$] for

different photochemical time bins are shown in Figure 5.13b. The average ratios are 0.96, 0.90, 0.89, 0.85, 0.81 and 0.70 for the photochemical ages in range of 0-24 h, 24-48 h, 48-72 h, 72-96 h, 96-120 h and 120-144 h, respectively. This ratio is an approximate indicator for the acidity of the aerosol, since the AMS does not detect refractory components in the particles, and sulfates and nitrates associated with organic compounds are included in the ratio while organic acids are not. The molar ratios suggest that the particles became more acidic with increasing photochemical processing, consistent with the increase in sulfate at the expense of nitrate. No corresponding enhancement in total organics or oxygenated organics was observed, suggesting that the acid-catalyzed secondary organic aerosol formation [*Jang et al., 2002; Liggio et al., 2005*] was not important at least after 48 hours of photochemical processing during this study.

Thus, the most likely explanation for the evolution of oxygenated organics with photochemical age is that the condensation of sulfate on organic aerosol particles either retards the continued oxidation of hydrocarbons in the particles or inhibits absorption of condensable secondary organics from the gas-phase. After two photochemical day of emission, the ability of organics to act as efficient cloud condensation nuclei (CCN) is mostly likely determined by the presence of the sulfate coating on these particles.

Finally, these results are for a period when biogenic emissions were relatively low, especially in the north; a different picture may be obtained for a period when such emissions are higher.

Chapter **6**

Conclusions

6.1 Conclusions

Atmospheric sampling was conducted from March 27-May 8, 2003 at the Centre for Atmospheric Research Experiments (CARE), a rural site near Egbert in an agricultural setting, approximately 70 km to the north of the city of Toronto. The springtime measurements of atmospheric aerosol at a rural site in Southern Ontario, Canada provided more detail of the physical properties and chemical composition of atmospheric aerosol. The aerosol chemical composition measured simultaneously with number distributions, various gas-phase species and meteorological parameters provided a unique data set suitable for investigating the physical and chemical properties of aerosols under various atmospheric conditions and air mass histories, for example, aerosol in relatively clean air from the north and polluted air from the south. The physical properties and chemical composition of the rural aerosol were contrasted, whenever appropriate, with the same of the urban aerosol measured at Toronto. The urban measurements were conducted from August 20 to September 25, 2003 (~ 37 days) at the University of Toronto in downtown Toronto. The aim of this study was to increase our knowledge of the aerosol characteristics and the processes governing the aerosol mass and chemistry at a rural site in eastern North America. The main results are briefly presented here.

6.1.1 Mass Closure: Performance of the AMS

The aerosol mass spectrometer (AMS) [*Jayne et al., 2000*] was deployed at both sites. The AMS provided online the quantitative information on the mass concentrations of non-refractory species (compounds that volatilize below 500°C) in submicron aerosols and their mass distributions as a function of vacuum aerodynamic diameter (D_{va}). The performance of the AMS was evaluated through the intercomparison of AMS

measurements with the co-located aerosol instrumentation. The AMS measurements were compared with the intercomparison of the AMS measurements with semicontinuous instruments (TEOM $PM_{2.5}$, SMPS+APS, R&P nitrate monitor) as well as time-integrated filter measurements. The intercomparison showed that the AMS measurements agreed reasonably well with various semi-continuous measurements as well as time-integrated filter measurements, provided the cut-off size of those instruments were considered. Mass closure among the various measurements was explained on the basis of the relative size of particles sampled by various techniques. The presence of particles larger than about 600 nm D_{va}, which the AMS samples with reduced efficiency, can explain much of the discrepancies between AMS measurements and other instruments. Sometimes, the presence of refractory material also led to discrepancies. The number distribution measurements helped distinguish the periods with the higher concentrations of larger particles, and to explain the discrepancies. These intercomparisons have confirmed the ability of the AMS as a powerful tool to measure quantitatively the mass concentrations of the non-refractory fractions of submicron particulate mass and their mass distributions in near-real-time.

Besides the performance of the AMS, this study has demonstrated and confirmed the inability of the TEOM to report $PM_{2.5}$ correctly during nitrate events. A significant amount of semi-volatile species such as ammonium nitrate was evaporated in the TEOM measurements during nitrate events. The evaporative loss of semi-volatile species has been reported in other studies as well [*Allen et al., 1997*]. Such evaporative loss can be a concern when using the TEOM to monitor $PM_{2.5}$, in particular, in areas where other semivolatile species contribute significantly to the particulate matter. The R&P particulate nitrate monitor was also suspected of evaporative loss of semi-volatile species.

6.1.2 Rural and Urban Aerosol

The springtime measurements at Egbert and [early] fall measurements at Toronto provided exceptionally detailed information on atmospheric aerosol chemical composition that was measured with the aerosol mass spectrometer (AMS). One of the important measurements during both campaigns was the measurements of particulate

organic material. The organic material dominated urban aerosol composition throughout the sampling period, except during a regional smog episode when sulfate was prominent particulate component. The rural aerosol contained mainly secondary components (ammonium, sulfate, nitrate and some organics). Higher mass concentrations events at Egbert were due primarily to high nitrate mass concentrations that were frequently observed when the site was exposed to urban emissions advected from the south.

The AMS derived mass size distributions for the rural aerosol showed that the inorganic species had mass modal vacuum aerodynamic diameters around 400 - 500 nm. The total organics normally exhibited one mode at 425 nm coincident with inorganics and occasionally a second mode at about 100 nm, more noticeable when urban-industrial air masses from the south affected the site. Nitrate mass distributions resembled that of total organics during the pollution events, implying that the small organic particles provided surfaces for the condensation of nitric acid. The small organic mode was well correlated with gas-phase non-methane hydrocarbons such as ethylbenzene, toluene and propene, suggesting that the likely sources of small organic particles were combustion related emissions. Sulfate exhibited a bimodal mass distribution with a small mode around 150 nm when the air trajectories passed over the Sudbury region to the northwest of the site. For the urban aerosol, ammonium, nitrate and sulfate had single modes around 350 - 400 nm and total organic material had two modes at around 400 nm and 150 nm, with a significant amount of organic mass in the small mode. The smaller particles contained preferentially higher levels of hydrocarbons, and some oxygenated organics were present in the larger mode. In contrast, the aerosol particles at the rural site were aged particles most of the time, and composed of highly oxygenated short-chained organics.

6.1.3 Diurnal Patterns of Aerosol Components

The 15-min averaged continuous measurements of aerosol chemical composition with the AMS and meteorological data provided an unprecedented opportunity to study the diurnal variations of various aerosol components, and to inference about the origin of various particulate species. The nitrate mass concentrations exhibited a diurnal variation with higher concentrations during dark hours and minimum in the afternoon at both sites.

Its diurnal pattern qualitatively follow the diurnal variations of ambient temperature and relative humidity, suggesting that the lower temperatures and higher relative humidities in the early morning hours favor formation of ammonium nitrate and its partition from the gas-phase. This suggests that nitrate (ammonium nitrate) formation was relatively local. Sulfate and total organics mass concentrations at Egbert showed evidence of photochemical processing with higher levels of sulfate and oxygenated organics in the afternoon. Ammonium and total organics did not exhibit clear diurnal patterns.

6.1.4 Origins of Particle Nitrate, Organics and Sulfate

The data set was classified into two groups, aerosols from the south and the north, based on the local winds direction, air mass back trajectories and gas-phase NO mixing ratios, as described in Chapter 5. During the pollution events associated with the southerly air trajectories that passed over urban centers, nitrate was the prominent aerosol component flowed generally by total organic material and sulfate. Formation of high nitrate mass concentrations was of great interest. The nighttime accumulation mode nitrate at Egbert can be attributed to the formation of particulate nitrate, either locally at the site or at upwind locations and transported to the site, under appropriate environmental conditions (lower temperature and higher relative humidity), as well as the availability of gaseous NH_3 from agricultural activities and oxides of nitrates from urban emissions. As the pre-existing small organic particles provided high surface areas, it is most likely that gas-phase HNO_3 condensed on those particles, and hence the mass distribution of particulate nitrate resembled that of total organics during nitrate events. Because a number of gas-phase reactive nitrogen species such as NO_x and HNO_3 were not measured during this study, it limited severely the further analysis of the significance of various mechanisms of the formation of particulate nitrate, as described in chapters 4 and 5.

The relatively clean periods were associated with air masses from the north. During such periods, there were at least three events with high sulfate mass concentrations, the events were short-lived though, during which the air trajectories had passed directly over the Sudbury region, the area with nickel smelters noted for with high SO_2 emissions. There was a gradual increase in particulate organic mass concentrations during the periods with

aerosol from the north. This gradual increase in organics may be associated with increases in biogenic emissions. Biogenic organic emissions from trees, grass and soil may have been enhanced by increases in ambient temperature, solar radiation, loss of snow cover on the ground, and possibly decomposition of organic materials on the ground. The melting snow on the ground provides water, and thus modulates the emissions from the soil of the aerosol precursors from decomposition of organic material [*Bigg, 2001*].

6.1.5 Evolution of Aerosol Components with Photochemical Age

Atmospheric evolution of aerosol composition, in particular the oxygenated organic fraction and hydrocarbon fraction as a function of photochemical age of air mass arriving at CARE, was analyzed. The photochemical age was estimated from the observed gas-phase mixing ratios of toluene and benzene [*de Gouw et al., 2005; McFiggans et al., 2005; Roberts et al., 1984*]. The data set was classified into tow classes; aerosol from the south and aerosol from the north, and the evolution of aerosol composition and sizes with increasing photochemical age was studied. This study demonstrated that the size and composition of particulate organic material changes when aerosols undergo a significant atmospheric processing. The exposure of aerosols to an oxidizing environment while moving away from the sources controls the size and composition of organic aerosols, such as the fraction of oxygenated organics and unoxidized hydrocarbon organics in the particles; the latter tends to be more water-insoluble. The hydrocarbons tend to be higher in freshly emitted organic particles, preferably particles smaller than about 200 nm in vacuum aerodynamic diameters, whereas the more aged aerosols show presence of more oxygenated organics.

For the aerosols from the south, the organic composition evolves with photochemical age in such a way that the particulate hydrocarbon fraction decreases most rapidly over the first 24 hours of photochemical processing, and thereafter remains relatively constant. In contrast, the oxygenated fraction increases rapidly during the first 48 hours, but thereafter shows no change on average. For aerosols from the north with photochemical age in the range of 48 h to 144 h, those two fractions do not exhibit the same pattern as in the

aerosols from the south. The pollution aerosols from the south rather gradually approach the composition of the aerosols from the north. This allowed to two cases to be combined. The mass fraction of nitrate decreases continuously with photochemical age, while the mass fraction of sulfate increases. This indicates first that nitrate formation is relatively local, second that the condensation of sulfates onto the organic particles may impede the increase in oxygenated organic fraction. The change in aerosol fraction with increasing photochemical age may also indicate the distance from the measurement site, implying that the variation in the particulate oxygenated organics and hydrocarbons indicate that the more anthropogenic sources are distributed closer to the site than the biogenic sources. Thus, biogenic organics had enough time for oxygenation before reaching the site. Thus, if the photochemical ages estimated in this study are representative, the change in organic and inorganic fractions imply that within 2 day of photochemical age, and perhaps even less time, the ability of these particles to act as cloud condensation nuclei (CCN) may be controlled by inorganic species such as the sulfates.

6.2 Outlook for Future

A number of gas-phase species such as NO_x, HNO_3, HONO, NO_3, and PAN were not measured during the sampling at Egbert. The lack of those species limited the analysis of the importance of various mechanisms of particulate nitrate formation.

There were several suspected particle nucleation events. It was difficult to further analyze those events due to lack of gas-phase SO_2 data.

The particulate organic material was measured with the AMS only. The particulate organic material measured with the AMS provided unprecedented information on the composition and potential sources of organic material. However, there were no other independent measurements of particulate organics during this study to compare with the AMS measurements. Measurement of volatile organic compounds (VOCs) that can be used as tracer for biogenic, biomass burning, automobiles, meat cooking etc. should be

employed in future to identify the presence of biogenic organics, and possibly assess the relative contribution of the sources.

Measurements of the size-segregated chemical composition with the MOUDI (Micro-Orifice Uniform Deposition Impactor) can provide important information on the mass distribution of various species in supermicron, as well as submicron particles. The MOUDI data can provide important insights on the partitions of various aerosol components into submicron and supermicron sizes. Therefore, in order to gain further insights into the particulate composition at this rural site, the aforesaid measurements should be incorporated in future campaigns.

References

Ackerman, A.S., O.B. Toon, D.E. Stevens, A. J. Heymsfield, V. Ramanathan, and E.J. Welton (2000). Reduction of Tropical Cloudiness by Soot. *Science,* 288:1042– 1047.

Albrecht, B. (1989). Aerosols, Cloud Microphysics and Fractional Cloudiness. *Science,* 245:1227-1230.

Alfarra, M.R., H. Coe, J.D. Allan, K.N. Bower, H. Boudries, M.R. Canagaratana, J.L. Jimenez, J.T. Jayne, A.A. Garforth, S.M. Li, and D.R. Worsnop (2004). Characterization of Urban and Regional Organic Aerosols in the Lower Fraser Valley Using Two Aerodyne Aerosol Mass Spectrometers. *Atmos. Environ.* 38:5745-5758.

Allan, J.D., J.L. Jimenez, P.I. Williams, M.R. Alfarra, K.N. Bower, J.T. Jayne, H. Coe, and D.R. Worsnop (2003a). Quantitative Sampling Using an Aerodyne Aerosol Mass Spectrometer, 1, Techniques of Data Interpretation and Error Analysis. *J. Geophys. Res.* 108 (D3):4090, doi:10.1029/2002JD002358.

Allan, J.D., M.R. Alfarra, K.N. Bower, P.I. Williams, M. W. Gallagher, J.L. Jimenez, A.G. McDonald, E. Nemitz, M.R. Canagaratana, J.T. Jayne, H. Coe and D.R. Worsnop (2003b). Quantitative Sampling Using An Aerodyne Aerosol Mass Spectrometer, 2, Measurements of Fine Particulate Chemical Composition in Two U.K. Cities. *J. Geophys. Res.* 108(D3):4091, doi:10.1029/2002JD00235.

Allan, J.D., H. Coe, K.N. Bower, M.R. Alfarra, A.E. Delia, J.L. Jimenez, A.M. Middlebrook, F. Drewnick, T.B. Onasch, M.R. Canagaratana, J.T. Jayne, and D.R. Worsnop (2004a). A Generalized Method for the Extraction of Chemically Resolved Mass Spectra from Aerodyne Aerosol Mass Spectrometer Data. *J. Aerosol Science* 35(7):909-922, DOI: 10.1016/j.jaerosci.2004.02.007.

Allan, J.D., K.N. Bower, H. Coe, H. Boudries, J.T. Jayne, M.R. Canagaratana, D.B. Millet, A.H. Goldstein, P.K. Quinn, R.J. Weber, and D.R. Worsnop (2004b). Submicron Aerosol Composition at Trinidad Head, California during ITCT 2K2, Its Relationship with Gas Phase Volatile Organics Carbon and Assessment of Instrument Performance. *J. Geophys. Res.* 109(D23), D23S24, doi:10.1029/2003JD004208.

Allen, G., C. Sioutas, P. Koutrakis, R. Reiss, F.W Lurmann, and P.T. Roberts (1997). Evaluation of the TEOM Method for Measurement of Ambient Particulate Mass in Urban Areas. *J. Air & Waste Manage. Assoc.* 47:682-689.

Andreae, M.O. (2001). The Dark Side of Aerosols. *Nature,* 409:671-672.

Andreae, M.O., and P.J. Crutzen (1997). Atmospheric Aerosols: Biogeochemical Sources and Role in Atmospheric Chemistry. *Science*, 276, 1052-1058.

Andrea, M.O., C.D. Jones, and P.M. Cox (2005). Strong Present-day Aerosol Cooling Implies a Hot Future. *Nature*, 435: 1187-1190.

Atkinson, R. et al., (2004). Evaluated Kinetic and Photochemical Data for Atmospheric Chemistry: I. Gas Phase Reactions of O_x, HO_x, NO_x, SO_x Species. *Atmos. Chem. Phys.*, 4:1461-1731.

Baron, P.A., and K. Willeke (2001). Aerosol Fundamentals, in Aerosol Measurement Principles, Techniques and Applications, 2nd Edition, P. A. Baron and K. Willeke (eds.), Wiley Interscience, Toronto.

Bigg, E.K. (2001). The Aerosol in a Boreal Forest in Spring. *Tellus*, 53B:510-519.

Brickell, P.C., J.W. Bottenheim, F. Froude, and Z. Jiang (2003). Continuous In-Situ NMHC Measurements in Rural Ontario, Canada. *Eos Trans. AGU* 84(46), Fall Meeting, Suppl., A31D-0070, San Francisco, December.

Brook, J. and T. Dann (1999). Contribution of Nitrate and Carbonaceous Species to PM_{10} and $PM_{2.5}$ Observed in Canadian Cities. *J. Air & Waste Manage. Asso.*, 49:193-199.

Broekhuizen, K. R. Y.-W. Chang, W. R. Leaitch, S.-M. Li, and J. P. D. Abbatt (2005) Closure between measured and modeled cloud condensation nuclei (CCN) using size-resolved aerosol compositions in downtown Toronto. *Atmos. Chem. Phys. Discuss.*, 5:6263–6293.

Buset, K.C., G.J. Evans, W.R. Leaitch, J.R. Brook, and D. Toom-Sauntry (2005). Use of Advanced Receptor Modeling for Analysis of an Intensive 5-Week Aerosol Sampling Campaign. submitted to *Atmos. Environ.*

Charlson, R.J., S.E. Schwartz, J.M. Hales, R.D. Cess, J.A. Coakley, J.E. Hansen, and D.J. Hoffmann (1992). Climate Forcing by Anthropogenic Aerosols. *Science* 255: 423–430.

Chýlek, P., and J. Wong (1995). Effect of Absorbing Aerosol on Global Radiation Budget. *Geophys. Res. Lett.* 22:929– 931.

Davidson, C.I., R.F. Phalen, and P.A. Solomon (2005). Airborne Particulate Matter and Human Health: A Review. *Aerosol Sci. Technol.* 39 (8):739-749.

de Gouw, J.A., A.M. Middlebrook, C. Warneke, P.D. Goldan, W.C. Kuster, J.M. Roberts, F.C. Fehsenfeld, D.R. Worsnop, M.R. Canagaratna, A.A.P. Pszenny,W.C. Keene, M. Marchewka, S.B. Bertman, and T.S. Bates (2004). The Budget of Organic Carbon in a Polluted Atmosphere: Results from the New England Air Quality Study in 2002. *J. Geophys. Res.,* 110, D16305, doi:10.1029/2004JD005623.

DeCarlo, P.F., J.G. Slowik, D.R. Worsnop, P. Davidovits, and J.L. Jimenez (2004). Particle Morphology and Density Characterization by Combined Mobility and Aerodynamic Diameter Measurements. Part 1: Theory. *Aerosol Sci. Technol.*, 28:1185-1205.

Decesari, S., M.C. Facchini, M. Mircea, F. Cavalli, and S. Fuzzi (2003). Solubility Properties of Surfactants in Atmospheric Aerosol and Cloud/Fog Water Samples. *J. Geophys. Res.,* 108, 4685, doi: 10.1029/2003JD003566.

Decesari, S., M.C. Facchini, S. Fuzzi, and E. Tagliavini (2000). Characterization of Water-soluble Organic Compounds in Atmospheric Aerosol: A New Approach, *J. Geophys. Res.* 105:1481-1489.

Dockery, D.W., C.A. Pope, X.P. Xu, J.D. Spengler, J.H. Ware, M.E. Fay, B.G. Ferris, and F.E. Speizer (1993). An Association between Air-Pollution and Mortality in Six United States Cities. *New England J. Medicine* 329(24):1753-1759.

Donaldson, K., X. Y. Li, and W. MacNee (1998). Ultrafine (nanometer) Particle-mediated Lung Injury. *J. Aerosol Sci.,* 29:553-560.

Draxler, R.R, and G.D. Rolph (2000). HYSPLIT (HYbrid Single Particle Lagrangian Integrated Trajectories) Model (V 4). *http://www.arl.noaa.gov/ready/hysplit4.html,* NOAA Air Resource Laboratory, Silver Spring, MD, USA.

Dreher, K., R. Jaskot, J. Richards, J. Lehmann, D. Winsett, A. Hoffman, D. Costa (1996). Acute Pulmonary Toxicity of Size Fractionated Ambient Air Particulate Matter. *Am. J. Respir. Crit. Care Med.,* 153:A15.

Drewnick, F, J.J Schwab, J.T. Jayne, M.R. Canagaratana, D.R. Worsnop, and K.L. Demerjian (2004). Measurement of Ambient Aerosols During the PMTACS-NY2001

Using an Aerosol Mass Spectrometer Part I: Mass Concentrations. *Aerosol Sci. Technol.* 38(S1):92-103, doi:10.1080/02786820390229507.

Ehhalt, D.H., F. Rohrer, A. Wahner, M. J. Prather, and D.R. Blake (1998). On the Use of Hydrocarbons for the Determination of Tropospheric OH Concentrations. *J. Geophys. Res.*, 103:18981-18997.

Facchini, M.C., M. Mircea, S. Fuzzi, and R.J. Charlson (1999). Cloud Albedo Enhancement by Surface-active Organic Solutes in Growing Droplets. *Nature,* 401:257-259.

Finlayson-Pitts, B. J. (1993). Comments on "Indication of Photochemical Histories of Pacific Air Masses from Measurements of Atmospheric Trace Species at Point Arena, California", by Parish et al., *J. Geophys. Res.*, 98:14991-14994.

Finlayson-Pitts, B. J., and J. N. Pitts (2000). Chemistry of the Upper and Lower Atmosphere: Theory, Experiments and Applications. Academic Press, San Diego.

Flagan, R. C. (2001). Electrical Techniques, in Aerosol Measurement: Principles, Techniques, and Applications, 2nd Edition, eds. P. A. Baron and K. Willeke, John Wiley, New York, 537–568.

Geyer, A., B. Alicke, S. Konard, T. Schmits, J. Stutz, and U. Platt (2001). Chemistry and Oxidation Capacity of the Nitrate Radical in the Continental Boundary Layer near Burlin. *J. Geophys. Res.*, 106:8013-8025.

Hansen, J., M. Sato, and R. Ruedy (1997). Radiative Forcing and Climate Response. *J. Geophys. Res.* 102:6831–6864.

Harrison, R.M., and J.X. Yin (2000). Particulate Matter in the Atmosphere: Which Particle Properties Are Important for Its Effects on Health? *Science of the Total Environment,* 249(1-3):85-101.

Heintz, F., U. Platt, H. Flentje, and R. Dubois (1996). Long-term Observation of Nitrate Radicals at the TOR Stations, Kap Arkona (Rügen). *J. Geophys. Res.* 101:22891–22910.

Huffman, J. A., J.T. Jayne, F. Drewnick, A.C. Aiken, T.B. Onasch, D.R. Worsnop, and J. L. Jimenez (2005). Design, Modeling, Optimization, and Experimental Tests of a Particle Beam Width Probe for the Aerodyne Aerosol Mass Spectrometer. *Aerosol Sci. Technol.*, 39(12):1143-1163, doi:10.1080/02786820500423782.

IPCC (Intergovernmental Panel on Climate Change) (2001). Climate Change 2001: The Scientific Basis, Contribution of Working Group I to the Third Assessment Report of the Intergovernmental Panel on Climate Change, J. T. Hougton et al., eds., Cambridge University Press, Cambridge, UK.

Jacob, D.J. (2000). Heterogeneous Chemistry and Tropospheric Ozone. *Atmos. Environ.*, 34:2131-2159.

Jaenicke, R. (1982). In "Chemistry of the Polluted and Unpolluted Troposphere", H.W. Georgii and W. Jaeschke (eds.), D. Reidel Publishing Co., pp 341-373.

Jang, M.S., N.M. Czoschke, S. Lee, and R.M. Kamens (2002). Heterogeneous Atmospheric Aerosol Production by Acid-catalyzed Particle-phase Reactions. *Science*, 298:814-817.

Jayne, J.T., D.C. Leard, X. Zhang, P. Davidovits, K.A. Smith, C.E. Kolb, and D.R. Worsnop (2000). Development of an Aerosol Mass Spectrometer for Size and Composition Analysis of Submicron Particles. *Aerosol Sci. Technol.* 33: 49-70.

Jimenez, J.L (2004). Aerosol Mass Spectrometry Part 2: Thermal Desorption Techniques, Tutorial no. 15, *23rd Annual Conference of American Association for Aerosol Research (AAAR),* Atlanta, Georgia, Oct.4-8, 2004

Jimenez, J.L., J.T. Jayne, Q. Shi, C.E. Kolb, D.R. Worsnop, I. Yourshaw, J.H. Seinfeld, R.C. Flagan, X. Zhang, K.A. Smith, J. Morris, and P. Davidovits (2003a). Ambient Aerosol Sampling Using the Aerodyne Aerosol Mass Spectrometer. *J. Geophys. Res.* 108 (D7):8425, doi:10.1029/2001JD001213.

Jimenez, J.L., R. Bahreini, D.R. Cocker III, H. Zhuang, V. Varutbangkul, R.C. Flagan, J.H. Seinfeld, C.D. O'Dowd, and T. Hoffmann (2003b). New Particle Formation From Photooxidation of Diiodomethane (CH_2I_2). *J. Geophys. Res.* 108(D10):4318, doi:10.1029/2002JD002452.

Kondo, Y., Y. Miyazaki, N. Takegawa, T. Miyakawa, R.J. Weber, J.L. Jimenez, Q. Zhang, and D.R. Worsnop (2006). Oxygenated and Water Soluble Organic Aerosols in Tokyo. *J. Geophys. Res.* (submitted).

Kotzick, R., and R. Niessner (1999). The Effects of Aging Processes on Critical Supersaturation Ratios of Ultrafine Carbon Aerosols, *Atmos. Environ.,* 33(17):2669-2677.

Kulmala, M. (2003). How Particles Nucleate and Grow. *Science, 302* (5647): 1000-1001.

Lesins, G., P. Chylek, and U. Lohmann (2002). A Study of Internal and External Mixing Scenarios and Its Effects on Aerosol Optical Properties and Direct Radiative Forcing. *J. Geophys. Res.* 107, doi:10.1029/2002JD000973.

Li, S.-M., L. A. Barrie, and D. Toom (1996). Seasonal variations of methanesulfonate, non-sea-salt sulfate, and sulfur dioxide at three sites in Canada. *J. Geophys. Res.,* 101, 4165-4174, doi:10.1029/95JD03000.

Liggio J., S.-M. Li, and R. McLaren (2005). Heterogeneous Reactions of Glyoxal on Particulate Matter: Identification of Acetals and Sulfate Esters. *Environ. Sci. Technol.*, 39(6): 1532-1541, doi:10.1021/es048375y.

Lim, H.J., A.G. Carlton, and B.J. Turpin (2005). Isoprene Forms Secondary Organic Aerosol through Cloud Processing: Model Simulation. *Environ. Sci. Technol.*, 39: 4441-4446.

Liu, P., P.J. Ziemann, D.B. Kittelson, and P.H. McMurry (1995a). Generating Particle Beams of Controlled Dimensions and Divergence: I. Theory of Particle Motion in Aerodynamic Lenses and Nozzle Expansions. *Aerosol Sci. Technol.* 22:293-313.

Liu, P., P.J. Ziemann, D.B. Kittelson, and P.H. McMurry (1995b). Generating Particle Beams of Controlled Dimensions and Divergence: II. Experimental Evaluation of Particle Motion in Aerodynamic Lenses and Nozzle Expansions. *Aerosol Sci. Technol.* 22:314-324

Lohmann, U., and J. Feichter (1997). Impacts of Sulfate Aerosol on Albedo and Lifetime of Clouds: A Sensitivity Study with the ECHAM GCM. *J. Geophys. Res.* 102:13685-13700.

Lohmann, U., and J. Feichter (2005). Global Indirect Aerosol Effects: A Review. *Atmos. Chem. Phys.* 5:715-737.

Lohmann, U., and C. Leck (2005). Importance of Submicron Surface Active Organic Aerosols for Pristine Arctic Clouds. *Tellus,* 57B: 261-268.

Lohmann, U., J. Feichter, C.C. Chung, and J.E. Penner (1999). Predicting the Number of Cloud Droplets on the ECHAM GCM. *J. Geophys. Res.*, 104, 9169-9198.

Lohmann, U., J. Feichter, J.E. Penner, and W.R. Leaitch (2000). Indirect Effects of Sulfate and Carbonaceous Aerosols: A Mechanistic Treatment. *J. Geophys. Res.* 105:12193-12206.

Lohmann, U., K. Broekhuizen, R. Leaitch, N. Shantz, and J. Abbatt (2004). How Efficient is Cloud Droplet Formation of Organic Aerosols? *Geophys. Res. Lett.* 31, doi:10.10292003GL018999.

Martin, R.V., D.J. Jacob, and R.M. Yantosca (2003). Global and Regional Decreases in Tropospheric Oxidants from Photochemical Effects of Aerosols. *J. Geophys. Res.* 108 (D3), 4097, doi:10.1029/2002JD002622.

Macfarlane, R., M. Campbell, and S.V. Basrur (2000). Toronto's Air: Let's Make it Healthy. Health Promotion and Environmental Protection Office, Toronto Public Health.

McFiggans, G., M. R. Alfarra, J. Allan, K. Bower, H. Coe, M. Cubison, D. Topping, P. Williams, S. Decesari, C. Facchini, and S. Fuzzy. Simplification of the Representation of the Organic Component of Atmospheric Particulates. *Farady Discuss.*, 130: 341-362, 2005.

McKeen, S.A., and S.C. Liu (1993). Hydrocarbon Ratios and Photochemical History of Air Masses. *Geophys. Res. Lett., 20*:2363-2366.

McKeen, S.A., S.C. Liu, E.-Y. Hsie, X. Lin, J.D. Bradshaw, S. Smyth, G.L. Gregory, and D.R. Blake (1996). Hydrocarbon Ratios During PEM-West A: A Model Perspective, *J. Geophys. Res.* 101: 2087-2109.

McLaren, R., R.A. Salmon, J. Liggio, K.L. Hayden, K.G. Anlauf, and W.R. Leaitch (2004). Nighttime Chemistry at a Rural Site in the Lower Fraser Valley. *Atmos. Environ.* 38:5837-5848.

McMurry, P.H. (2000). A Review of Atmospheric Aerosol Measurements. *Atmos. Environ.* 34:1959-1999.

Middlebrook, A. M., D.M. Murphy, and D.S. Thomson (1998). Observations of Organic Material in Individual Marine Particles at Cape Grim during the First Aerosol Characterization Experiment (ACE1). *J. Geophys. Res.* 103(D13): 16475-16483.

Molina, M.J. (1991). Heterogeneous Chemistry on Polar Stratospheric Clouds. *Atmos. Environ.* 25A: 2535-2537.

Molina, M.J., A.V. Ivanov, S. Trakhenberg, and L.T. Molina (2004). Atmospheric Evolution of Organic Aerosol. *Geophys. Res. Lett.*, 31, L22104m, doi: 10.1029/2004GL020910.

Moshammer, H., and M. Neuberger (2003). The Active Surface of Suspended Particles as a Predictor af Lung Function and Pulmonary Symptoms in Austrian School Children, *Atmos. Environ.*, 27:1737-1744.

Murphy, D.M. (2005). Something in the Air. *Science*, 307:1888-1890.

Murphy, D.M., D.S. Thomson, and M.J. Maloney (1998). In-Situ Measurements of Organics, Meteorite Material, Mercury and Other Elements in Aerosols at 5 to 9 km. *Science*, 282:1664-1669.

Neuberger, M., M. Schimek, F. Horak Jr., H. Moshammer, M. Kundi, T. Frischer, B. Gomiscek, H. Puxbaum, H. Hauck, and AUPHEP-Team (2004). Acute Effects of Particulate Matter on Respiratory Diseases, Symptoms and Functions: Epidemiological Results of the Austrian Project on Health Effects of Particulate Matter (AUPHEP), *Atmos. Eniron.*, 38:3971-3981.

Novakov, T. and J.E. Penner (1993). Large Contribution of Organic Aerosols to Cloud Condensation Nuclei Concentrations. *Nature*, 365:823-826.

Novakov, T., D.A. Hegg, and P.V. Hobbs (1997). Airborne Measurements of Carbonaceous Aerosols on The East Coast of The United States. *J. Geophys. Res.*, 102:30023-30030, doi:10.1029/97JD02793.

O'Dowd, C.D., M.C. Facchina, F. Cavalli, D. Ceburnis, M. Mircea, S. Decesari, S. Fuzzi, Y.J. Yoon, and J.-P. Putaud (2004). Biogenically Driven Organic Contribution to Marine Aerosols. *Nature,* 431:676-680.

Orsini, D., Y. Ma, A. Sullivan, B. Sierau, K. Baumann, and R. Weber (2003). Refinements to the Particle-Into-liquid-Sampler (PILS) for Ground and Airborne Measurements of Water Soluble Aerosol Composition. *Atmos. Environ.* 37:1243-1259.

Patashnick, H., and E. G. Rupprecht (1991). Continuous PM_{10} Measurements Using the Tapered Element Oscillating Microbalance. *J. Air & Waste Manage. Assoc.* 41:1079-1083.

Peng, Y., U. Lohmann, R. Leaitch, C. Banic, and M. Couture (2002). The Cloud Albedo-Cloud Droplet Effective Radius Relationship for Clean and Polluted Clouds from RACE and FIRE.ACE. *J. Geophys. Res.* 107, doi:10.1029/2000JD000281.

Pengelly, L.D., and J. Sommerfreund (2004). Air Pollution-Related Burden of Illness in Toronto: 2004 Update. Environmental Protection Office, Toronto Public Health.

Peters, A., H.E. Wichmann, T. Tuch, J. Heinrich, and J. Heyder (1997). Respiratory Effects are Associated with the Number of Ultrafine Particles. *American J. Respiratory Critical Care Medicine*, 155:1376-1383.

Pope, C.A., R. T. Burnett, M. J. Thun, E. E. Calle, D. Krewski, K. Ito, and G.D. Thurston (2002). Lung Cancer, Cardio-pulmonary Mortality, and Long-term Exposure to Fine Particulate Air Pollution. *J. American Med. Assoc.*, 287:1132-1141.

Prather, K.A., T. Nordmeyer, and K. Salt (1994). Real-time Characterization of Individual Aerosol-particles Using Time-of-Flight Mass Spectrometry. *Anal., Chem.*, 66:1403-1407.

Quinn, P.K., T.S. Bates, T. Baynard, A.D. Clarke, T.B. Onasch, W. Wang, M.J. Rood, E. Andrews, J. Allan, C.M. Carrico, D. Coffman, and D. Worsnop (2005). Impact of Particulate Organic Matter on the Relative Humidity Dependence of Light Scattering: A Simplified Parameterization. *Geophys. Res. Lett.*, 32, L22809, doi:10.1029/2005GL024322.

Ramanathan, V., P.J. Crutzen, J.T. Kiehl, and D. Rosenfeld (2001). Atmospheric Aerosols, Climate, and the Hydrological Cycle. *Science*, 294:2119-2124.

Randles, C. A., L.M. Russell, and V. Ramaswamy (2004). Hygroscopic and Optical Properties of Organic Sea Salt Aerosol and Consequences for Climate Forcing. *J. Geophys. Res.* 31, L16108, doi:10.1029/2004GL020628.

Ravishankara, A.R. (1997). Heterogeneous and Multiphase Chemistry in the Troposphere. *Science*, 276: 1058-1065.

Roberts, J.M., F.C. Fehsenfeld, S.C. Liu, M.J. Bollinger, C. Hahn, D.L. Albritton, and R.E. Sievers (1984). Measurements of Aromatic Hydrocarbon Ratios and NO_x Concentrations in the Rural Troposphere: Estimates of Airmass Photochemical Age and NO_x Removal Rate. *Atmos. Environ.*, 18:2421-2432.

Rosenfeld, D. (2000). Suppression of Rain and Snow by Urban and Industrial Air Pollution. *Science,* 287:1793-1796.

Rupakheti, M., W.R. Leaitch, U. Lohmann, K. Hayden, P. Brickell, G. Lu, S.-M. Li, D. Toom-Sauntry, J.W. Bottenheim, J.R. Brook, R. Vet, J.T. Jayne, and D.R. Worsnop (2005). An Intensive Study of the Size and Composition of Submicron Atmospheric Aerosols at a Rural Site in Ontario, Canada. *Aerosol Sci. Technol.,* 39 (8):722-736, doi:10.1028/02786820500182420

Saxena, P., L.M. Hidlemann, P.H. McMurry, and J.H. Seinfeld (1995). Organics Alter Hygroscopic Behavior of Atmospheric Particles. *J. Geophys. Res.* 100(D9):18755-18770.

Schwartz, J. (1994). Air-Pollution and Daily Mortality - a Review and Meta Analysis. *Environ. Research,* 64:36-52.

Schwartz, J., D. W. Dockery, and L. M. Neas (1996). Is Daily Mortality Associated Specifically with Fine Particles? *J. Air and Waste Manage. Assoc.* 46:927-939.

Seinfeld, J. H., and S. N. Pandis (1998). Atmospheric Chemistry and Physics from Air Pollution to Climate Change. John Wiley and Sons Inc. USA.

Shantz, N.C., W.R. Leaitch, and P.F. Caffrey (2003). Effects of Organics of Low Solubility on the Growth Rate of Cloud Droplets. *J. Geophys. Res.* 108 (D5):4168, doi:10.1029/2002JD002540.

Shulman, M.L., M.C. Jacobson, R.J. Carlson, R.E. Synovec, and T.E. Yong (1996). Dissolution Behavior and Surface Tension Effects of Organic Compounds in Nucleating Cloud Droplets. *Geophys. Res. Lett.,* 23:277-280.

Smith, J.N, K.F. Moore, P.M. McMurry, and F.L. Eisele (2004). Atmospheric Measurements of Sub-20 nm Diameter Particle Cemical Composition by Thermal Desorption Chemical Ionization Mass Spectrometer, *Aerosol Sci. Technol,* 38:100-110.

Solomon, S., R.R. Garcia, F.S. Rowland, and D.J. Wuebbles (1986). On the Depletion of Antarctic Ozone. *Nature,* 321:755-758.

Solomon, S., R.W. Sanders, R.R. Garcia, and J.G. Keys (1993). Increased Chlorine dioxide over Antarctica Caused by Volcanic Aerosols from Mt. Pinatubo. *Nature,* 363:245-248.

Stolzenburg, M.R, and P.H. McMurry (1991). An Untrafine Aerosol Condensation Nucleus Counter. *Aerosol Sci. Technol.* 14:48-65.

Stolzenburg, M.R., and S.V. Hering (2000). Method for the Automated Measurement of Fine Particle Nitrate in the Atmosphere. *Environ. Sci. Technol.* 34(5):907-914.

Tan, P.V., G.J. Evans, J. Tsai, S. Owega, M. Fila, O. Malpica, J.R. Brook (2002). On-line Analysis of Urban Particulate Matter Focusing on Elevated Wintertime Aerosol Concentrations. *Environ. Sci. Technol.* 36: 3512-3518.

Thomson, D. S., M. E. Schein, and D. M. Murphy (2000). Particle Analysis by Laser Mass Spectrometry WB-57F Instrument Overview. *Aerosol Sci. Technol.* 33:153-169.

Thurston, G.D., K. Ito, C.G. Hayes, D.V. Bates, M. Lippmann (1996). Respiratory Hospital Admissions and Summertime Haze Air Pollution in Toronto, Ontario: Consideration of the Role of Acid Aerosols. *Environ. Res.*, 65: 271-290.

Twomey, S. A. (1974). Pollution and the Planetary Albedo. *Atmos. Environ.* 8:1251-1256.

Twomey, S. A. (1991). Aerosols, Clouds and Radiation. *Atmos. Environ.*, 25:2435-2442.

Vet, R. J., J.R. Brook, and T.F. Dann (2001). The Nature of $PM_{2.5}$ Mass, Composition and Precursors in Canada, in Precursor Contributions to Ambient Fine Particulate Matter in Canada, J.R. Brook et al., eds., Environment Canada.

Voisin, D., J.N. Smith, H. Sakurai, P.H. McMurry, and F.L. Eisele (2003). Thermal Desorption Chemical Ionization Mass Spectrometer for Ultrafine Chemical Composition, *Aerosol Sci. Technol.*, 37: 471-475.

Vrekoussis, M., E. Liakakou, N. Mihalopoulos, M. Kanakidou, P.J. Crutzen, and J. Lelieveld (2006). Formation of HNO_3 and NO_3- in the Anthropogenically-influenced Eastern Mediterranean Marine Boundary Layer. *Geophys. Res. Lett.*, 33, L05811, doi:10.1029/2005GL025069.

Weber, R. J., D. Orsini, Y. Duan, Y.N. Lee, P. J. Koltz, and F. Brechtel (2001). A Particle-into-Liquid Sampler for Rapid Measurement of Aerosol Bulk Chemical Composition. *Aerosol Sci. Technol.* 35:718-727.

Zappoli, S., A. Andracchio, S. Fuzzi, M. C. Facchini, A. Gelencsér, G. Kiss, Z. Krivácsy, Á. Molnár, E. Mészáros, H. -C. Hansson, K. Rosman and Y. Zebühr (1999). Inorganic,

Organic and Macromolecular Components of Fine Aerosol in Different Areas of Europe in Relation to Their Water Solubility. *Atmos. Environ.*, 33:2733-2743.

Zhang, Q., M.R. Canagaratana, J.T. Jayne, D.R. Worsnop, S.N. Pandis, and J.L. Jimenez (2004). Insights into the Chemistry of New Particle Formation and Growth Events in Pittsburg Based on Aerosol Mass Spectrometry. *Environ. Sci. Technol.*, 38:4797-4809.

Zhang, Q., M. R. Alfarra, D.R. Worsnop, J.D. Allan, H. Coe, M.R. Canagaratana, and J.L. Jimenez (2005a). Deconvolution and Quantification of Hydrocarbon-like and Oxygenated Organic Aerosols Based on Aerosol Mass Spectrometry. *Environ. Sci. Technol.*, 39:4938-4952.

Zhang, Q., D.R. Worsnop, M.R. Canagaratana, and J.L. Jimenez (2005b). Hydrocarbon-like and Oxygenated Organic Aerosols in Pittsburgh: Insight into Sources and Processes of Organic Aerosols. *Atmos. Chemi. Phys.* 5:3289-3311

Zhang, Q., M.R. Canagaratana, J.T. Jayne, D.R. Worsnop, and J.L. Jimenez (2005c). Time-and Size-resolved Chemical Composition of submicron particles in Pittsburgh: Implication for Aerosol Sources and Processes. *J. Geophys. Res.* 110, D07S09, doi:10.1029/2004JD004649.

Zhang, X., K.A. Smith, D.R. Worsnop, J.L. Jimenez, J.T. Jayne, and C.E. Kolb (2002). A Numerical Characterization of Particle Beam Collimation by an Aerodynamic Lens-Nozzle System Part 1, an Individual Lens or Nozzle. *Aerosol Sci. Technol.* 36:617-631.

Zimmer, A. (2002). The Influence of Metallurgy on the Formation of Welding Aerosols. *J. Environ. Monitor.*, 4:628-632.